MECHANICAL CHARACTERISATION, ANALYSIS AND MODELLING OF PARTICULATE NANOCOMPOSITES PRINTED USING PHOTOPOLYMER EXTRUSION TECHNIQUE

A THESIS SUBMITTED TO AUCKLAND UNIVERSITY OF TECHNOLOGY IN FULFILMENT OF THE REQUIREMENTS FOR THE DEGREE OF

DOCTOR OF PHILOSOPHY

By

Muhammad Asif

School of Engineering, Computer and Mathematical Sciences

May 2019

Attestation of authorship

I hereby declare that this submission is my own work and that, to the best of my knowledge and belief, it contains no material previously published or written by another person nor material which to a substantial extent has been accepted for the qualification of any other degree or diploma of a university or other institution of higher learning.

_____

Muhammad Asif

May, 2019

Acknowledgments

At the very outset, I would like to wish my deepest gratitude to my supervisors Dr Maziar Ramezani and Associate Professor Kean Chin Aw (University of Auckland) for their dedicated interest, understanding, patience and consistent encouragement during my PhD studies at Auckland University of Technology (AUT). Their epidemic passion and brainstorming discussions have been major driving factors during my candidature. They always showed faith in my abilities and have always been strong advocates for me.

I would also like to express my appreciation to National University of Sciences and Technology (NUST), Pakistan for granting me a fully funded PhD scholarship.

Many thanks to Dr Tim Giffney for his valuable suggestions and advice, the staff at Microfabrication Lab UoA, including Mr Danesh and Mr Emanuel for their technical support and help in fabrication of the parts.

Thanks to the staff at Engineering Workshop of AUT specially Mr Mark Masterton, for the help in conducting experiments and their technical support.

Thanks to Dr Kamran Khan and Dr Muhammad Ali Khan for their valuable suggestions and advise.

I also offer my profound thanks to my friends and colleagues in WZ 716. Further, I thank all my friends outside of AUT: Asim Anwar, Rizwan Butt, Mujadid Afzal, Arsland Rasheed, Fakhar Abbas and many others in making my time in New Zealand enjoyable.

Last but not the least, I would like to extend my thanks to my family members especially my parents, wife and brothers for their role in making me what I am today. My achievement could not have come to existence without their unflinching care and support.

Abstract

A new photopolymer extrusion 3D printing technique is proposed in this research. This hybrid 3D printer combines the strengths of two well established and commercial 3D printers i.e. fused deposition modelling (FDM) and UV assisted 3D printing (UV3DP). One of the distinct features of this novel technique is its two additional rotational axes, which are installed to print free-form and self-supported structures. A detailed and comprehensive study is carried out in this research on the mechanical characterisation, analysis and modelling of particulate nanocomposites printed using photopolymer extrusion technique.

Photopolymer resin is used as the base material in this technique. Generally, polymers are found to have low strength and stiffness. Nano sized fibres or particles are generally embedded in the polymer matrix to enhance their properties. Therefore, in order to improve the mechanical behaviour of the parts manufactured using photopolymer extrusion 3D printing technique, nano silica filler was added to the base material. Different concentrations of the silica filler were added and its effect on material viscosity, dimensional accuracy, strength and ductility have been studied. This part of the research outlined a suitable range of viscosities corresponding to different filler concentrations, provided plausible explanation on dimensional accuracy, reported significant improvement in mechanical properties of nanocomposite with the addition of the silica filler and demonstrated the capability of the proposed technique to print free-form and self-supported structures.

Interfacial adhesion, i.e. the bond between matrix and nanoparticles is one of the major contributors to the strong mechanical properties of the particle reinforced polymers. A comparison of the interfacial adhesion was drawn between 3D printed and casted samples. This part of the research outlined with the aid of scanning electron microscopy, why nanocomposites

printed using photopolymer extrusion technique have superior mechanical properties than casted samples.

Polymers are viscoelastic materials and they exhibit time dependent response. To study the time dependent mechanical response of the photopolymer used in the proposed technique, tensile tests at different strain rates were conducted. Silica filler was added to enhance the mechanical properties of the polymer. Quasi linear viscoelastic (QLV) model combining hyper and viscoelastic phenomena was used to model the rate dependent mechanical behaviour of the polymer and polymer reinforced composite with different concentrations of the filler. This part of the research outlined that the addition of the silica enhanced the mechanical properties of the polymer. It also outlined that higher filler content could lead to weak mechanical properties. Furthermore, it showed that QLV model with Yeoh's strain energy density function successfully captures the rate dependent stress-strain behaviour of the polymer and nanocomposite.

Finite element modelling (FEM) is a powerful tool and is commonly used to predict the behaviour of polymer nanocomposites. A FE model was developed by combining hyper and viscoelastic phenomena to investigate the effect of filler concentration on mechanical behaviour of the 3D printed particulate nanocomposite. The FE model with Yeoh's strain energy density function showed good agreement with experimental results. Finally, In order to study the mechanical behaviour of filler concentrations outside the reliable printing zone, empirical models were developed. These empirical models can predict the tensile strength of the nanocomposite based on filler concentration and the material viscosity.

The findings of this research give an insight into the mechanical characterisation and modelling of the 3D printed particulate nanocomposites using photopolymer extrusion technique.

LIST OF PUBLICATIONS FROM THIS RESEARCH

Journal Publications

- Asif, M., J.H. Lee, M.J. Lin-Yip, S. Chiang, A. Levaslot, T. Giffney, M. Ramezani and K.C. Aw, *A new photopolymer extrusion 5-axis 3D printer.* Additive Manufacturing, 2018. **23**: p. 355-361.
- Asif, M., M. Ramezani, K.A. Khan, M.A. Khan, and K.C. Aw, *Investigation of the strain-rate-dependent mechanical behavior of a photopolymer matrix composite with fumed nano-silica filler.* Polymer Engineering & Science, 2019. **59**(8): p. 1695-1700.
- Asif, M., M. Ramezani, K.A. Khan, M.A. Khan, and K.C. Aw, *Experimental and numerical study of the effect of silica filler on the tensile strength of a 3D-printed particulate nanocomposite.* Comptes Rendus Mécanique, 2019.
- Asif, M., M. Ramezani., K.C. Aw., *Effect of interfacial adhesion on tensile strength of 3D printed particulate nanocomposites*. IOP: Materials Science and Engineering (Vol 520, 012001)

Conference Presentations

- Asif, M., M. Ramezani., K.C. Aw., A new 3D printing technique using extrusion of photopolymer. *Twenty-fifth International Conference on Processing and Fabrication of Advanced Materials (PFAM-XXV)*, University of Auckland, January 22-25, 2017; Auckland, New Zealand.
- Asif, M., M. Ramezani., K.C. Aw., A new 3D printing technique using extrusion of photopolymer. *The 28th New Zealand Conference on Microscopy (MNZ),* Auckland University of Technology, January 31-3 February, 2017; Auckland, New Zealand.
- Asif, M., M. Ramezani., K.C. Aw., Effect of interfacial adhesion on tensile strength of 3D printed particulate nanocomposites. *4th International Conference on Mechanical, Manufacturing, Modelling and Mechatronics (IC4M),* February 22-24, 2019; Nice, France. (Won best presenter of the conference award).

Table of Contents

List of Tables

List of Figures

List of Symbols

Ra	Arithmetic average (for roughness profile)
$\boldsymbol{\sigma_c}$	Composite tensile strength
$\boldsymbol{\sigma}(t)$	Cauchy stress tensor
$\boldsymbol{F}$	Deformation gradient
$\bar{\mathrm{I}}_1$	First invariant of left Cauchy-Green strain tensor
$\boldsymbol{I}$	Identity tensor
μ	Instantaneous shear modulus
p	Lagrange multiplier
σ_m	Matrix tensile strength
φ	Volume fraction
γ_i	Relaxation coefficient
τ_i	Relaxation time
Rq	Root mean square (for roughness profile)
g_R	Shear relaxation modulus

Glossary

AM	Additive manufacturing
ASTM	American society of testing and materials
CAD	Computer aided design
DLP	Digital light processing
DIC	Digital image correlation
EBM	Electron beam melting
FDM	Fused deposition modelling
FEM	Finite element modelling
LMD	Laser metal deposition
PPE	Photopolymer extrusion
QLV	Quasi linear viscoelastic
RVE	Representative volume element
SLA	Stereolithography
STL	Standard triangulate language
SLS	Selective laser sintering
SLM	Selective laser melting
SEM	Scanning electron microscopy
SEDF	Strain energy density function
TWI	The welding institute
3DP	Three-dimensional printing
UV	Ultraviolet
UV3DP	Ultraviolet three-dimensional printing

CHAPTER 1: INTRODUCTION

1.1 Motivation and scope

At present, three dimension (3D) printing is widely used in different engineering fields (biomedical, mechanical, aerospace and many more). 3D printed objects are commonly used in various applications such as microsensors and actuators, fuel nozzles, scaffolds for cellular growth, home furniture and jewelry, to name a few [1]. Polymers are commonly used in 3D printing techniques due to characteristics like cost effectiveness, low weight and low processing time. Different 3D printing techniques have been used to manufacture polymers. Some are well established techniques such as stereolithography (SLA), fused deposition modelling (FDM), selective laser sintering (SLS), and inkjet printing; where some of the techniques are still in development stages.

Polymers are commonly found to have weak mechanical properties i.e. low tensile strength and Young's modulus. In order to improve their mechanical properties and expand their applications, inorganic particulate fillers ranging from micro/nano-silica, glass, Al_2O_3, $Mg(OH)_2$ and $CaCO_3$ particles, and carbon nanotubes are normally added. These fillers by introducing their rich mechanical behaviour enhance the physical and mechanical properties of the polymers. Particles can be mixed in polymers, whether they are in powder shape as for SLS or in liquid form as for SLA, or further to be extruded into printable filaments for FDM. The main purpose for 3D printing of particle reinforced composites is to increase the tensile strength, toughness and Young's modulus.

Even though the addition of micro/nano particles improves the mechanical properties of the polymer composites, when compared with the polymer composites manufactured with traditional techniques, majority of the 3D printed composites still found to have weak mechanical properties. Weak matrix-particle interfacial adhesion, non-homogenous dispersion,

and particle loading are some of the factors that contribute to the weak mechanical properties of 3D printed particulate-polymer composites.

Several complex 3D structures that include supported (layer-by-layer) and self-supported (helix), can be printed using most of the 3D printing techniques. However, manufacturing of 3D free form micro structures like helical geometries without the need of support material is still a big challenge [2-4]. The existence of support materials in 3D printing techniques have also been found to be disadvantageous as excessive material is required to hold the shape and rigidity of an object. The concept of adding additional rotational axes to the system to eliminate this problem has shown promising results, but systems still lack the capability to print complex structures without supports.

The aforementioned issues lead to the development of a new 3D printing technique which combines the strength of two well established commercial 3D printing techniques e.g. FDM and UV assisted 3D printing (UV3DP). This hybrid 3D printer uses liquid photopolymer and cures it using two UV laser diodes similar to UV3DP and extrudes the material in similar fashion to FDM. In addition, the proposed printer has two additional rotational axes which are installed to print complex free form and self-supported structures.

Therefore, in this research, a detailed investigation has been carried out in order to study, analyse, characterise and model the behaviour of the samples printed using the new photopolymer extrusion 3D printing technique.

1.2 Outline and objectives of the thesis

As the proposed method is a new 3D printing technique, mechanical characterisation, analysis and modelling of the parts manufactured using this technique are yet to be studied. Therefore, detailed experimentation and computer simulations were carried out in this research on the

parts manufactured using the proposed technique and its basic capability to print free form and self-supported structures using additional rotational axis was studied.

As part of these investigations, chapter 2 provides the literature review of the existing state of the art 3D printing techniques and different material used in the respective techniques. Chapter 2 also discusses 3D printing of filler reinforced polymer composites using existing 3D printing technologies. This chapter outlines from the literature certain limitations that the existing 3D printing techniques face in order to print polymer composites. It also provides a brief overview of the analytical and finite element (FE) methods used to model nanocomposites. The literature on the analytical modelling of nanocomposites indicates that existing models only predict effective stiffness and very little attention has been given to model the stress-strain relationship. In case of finite element method (FEM), majority of the work focused only on linear elastic properties of the nanocomposites. Little attention has been given to model the viscoelastic properties of the 3D printed particulate-polymer composites. It also indicates that most of the existing 3D printing techniques struggle to print free form and self-supported 3D structures; however, there are some 3D printers that are designed to cater this difficulty, but still these systems are unable to print free standing structures.

Chapter 3 provides the detailed experimental analysis by outlining the basic structure of the new 3D printing technique. Preliminary experimental study was conducted on old 3-axis printer to explore the range of filler concentrations, UV light intensity and other process parameters. Experimentation on 5-axis 3D printer was then formulated first by studying the effect of filler on material viscosity, which plays a crucial role for the smooth extrusion of the material. Different filler concentrations were added in the photopolymer and their viscosities were measured. A suitable range of viscosities was then proposed to effectively extrude the material. The effect of filler on dimensional accuracy was examined which provides plausible explanation on the difference between the printed and target dimensions. The effect of filler on

surface roughness was investigated by using optical profilometer and elaborated further with the help of scanning electron microscopy (SEM). The effect of filler on mechanical properties was also studied by conducting tensile and 3-point bending tests. Adding the filler enhanced the mechanical properties of the photopolymer and significant improvement in tensile as well as flexural strength was observed. Finally the basic capability to print free form and self-supported structures by utilising two rotational axes was successfully demonstrated, stair case and horizontal U shape objects were successfully printed, demonstrating the capability of this new technique of utilising 5-axis to print free standing structures.

Chapter 4 discusses the effect of filler on interfacial adhesion of the printed nanocomposite. A comparison of interfacial adhesion of printed and casted samples is drawn by conducting tensile tests and employing existing theoretical models yielding interfacial adhesion parameters. In addition, the chapter discusses that 3D printed samples have much stronger interfacial adhesion compared to cast samples and evaluates this finding by using scanning electron microscopy (SEM) to study the distribution of the filler on subsurface of the nanocomposite.

Chapter 5 investigates the strain rate dependent mechanical behaviour of the silica reinforced nanocomposite by conducting the tensile tests at different strain rates. It also outlines the effect of filler on mechanical properties, further it provides minimum amount of filler required to enhance the mechanical properties of the nanocomposite. Quasi linear viscoelastic (QLV) model combining hyper and viscoelastic phenomena has been employed which successfully captures the stress-strain relationship of the nanocomposite over the range of strain rates.

A numerical study was conducted in chapter 6 by FE modelling of the mechanical behaviour of the 3D printed nanocomposite based on hyper and viscoelastic phenomena. Tensile tests were conducted on three filler concentrations, stress relaxation tests were conducted to identify the viscoelastic properties. Computational model was found to have good agreement with

experimental results. To explore the mechanical properties of the filler concentrations outside the reliable printing zone, empirical models were developed. The empirical models can predict the tensile strength of the nanocomposite based on filler concentrations and material viscosity.

In the end, chapter 7 provides the conclusions of the thesis and suggests potential areas deserving further research and investigations.

CHAPTER 2: LITERATURE REVIEW

2.1 Additive manufacturing or 3D printing

Three dimension (3D) printing, also known as additive manufacturing, follows the principle of laying down successive layers of material (sheet material, powder or liquid) on top of each other by detecting the data from a CAD file [5, 6]. Every layer equals to a slice of a CAD model and they join together to make the final shape. In 1981 Hideo Kodama of Nagoya Municipal Industrial Research institute introduced this procedure after inventing manufacturing methods to create a 3D plastic model [7]. The process is much more advanced now a days and different 3D printers have been developed which are more sophisticated than the original machine. This has enabled the application of 3D printing technology in the fields such as aerospace, food industry, consumer products, education, manufacturing and medicine [8, 9].

3D printing techniques usually do not require the use of masks, moulds or dies to fabricate the 3D objects. However, a 3D CAD model is used in all 3D printing technologies, a .STL (Streolithography or Standard Triangulate Language or Standard Tessellation Language) file format is imported to the printer containing the coordinates of the vertices of triangulated sections for each surface of the CAD model. The .STL file can then be interpreted and converted into a G-Code (numerical programming language) by printer slicer software. A G-code contains the information on 2D horizontal cross sections, which prints 3D replicas of the input 3D CAD model in a layer by layer arrangement [10].

2.2 3D printing processes

The following sections outline the 3D printing processes and most common 3D printing technologies associated with each process.

2.2.1 Binder jetting

In this process, fabrication of objects is done by joining powdered materials through jet deposition of binding agents. Figure 2.1 shows the schematic of the binder jetting process. Materials used in binder jetting are polymers, ceramics, and metals. The technology which utilises this method is discussed below.

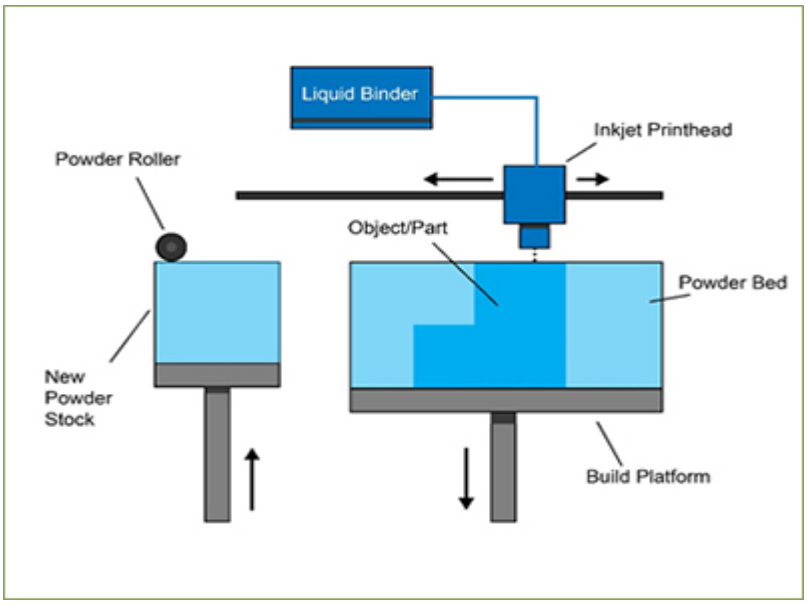

Figure 2.1. Schematic of binder jetting process [11]

2.2.1.1 Powder bed and inkjet head 3D printing (3DP)

This technique is based on powder processing; first powders are spread on the build platform and then selectively combined into the patterned layer by deposition of liquid binder through inkjet print head, which moves in x-y directions. The most important advantages of this technique are the material selection flexibility and room temperature processing environment. Theoretically, this technique can print any polymer materials in powder state.

2.2.2 Material jetting

In this process, fabrication of objects is done by setting down small droplets of filaments, which are later cured by exposure to UV light. Figure 2.2 shows the schematic of the material jetting process. Materials used in this technique are photopolymer and wax.

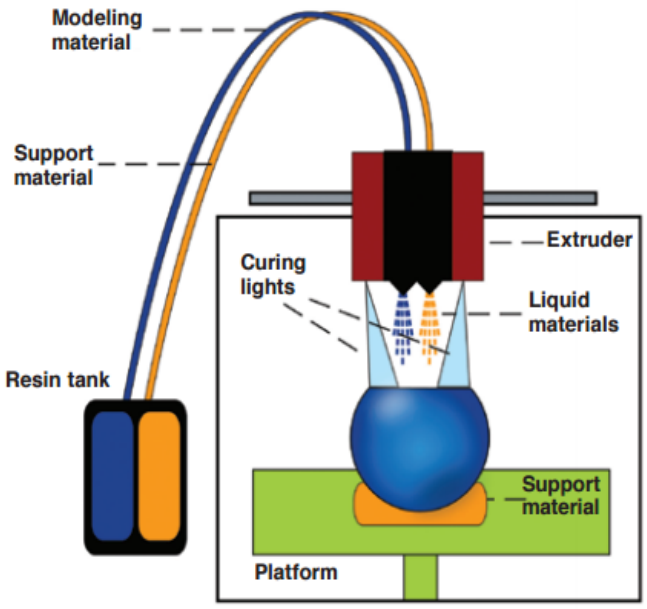

Figure 2.2. Schematic of material jetting process [12]

2.2.3 Direct energy deposition

In this process fabrication of objects is done by suing focused thermal energy for fusing material as it is deposited on substrate; materials used are powder and wire. Figure 2.3 shows the schematic of binder jetting process.

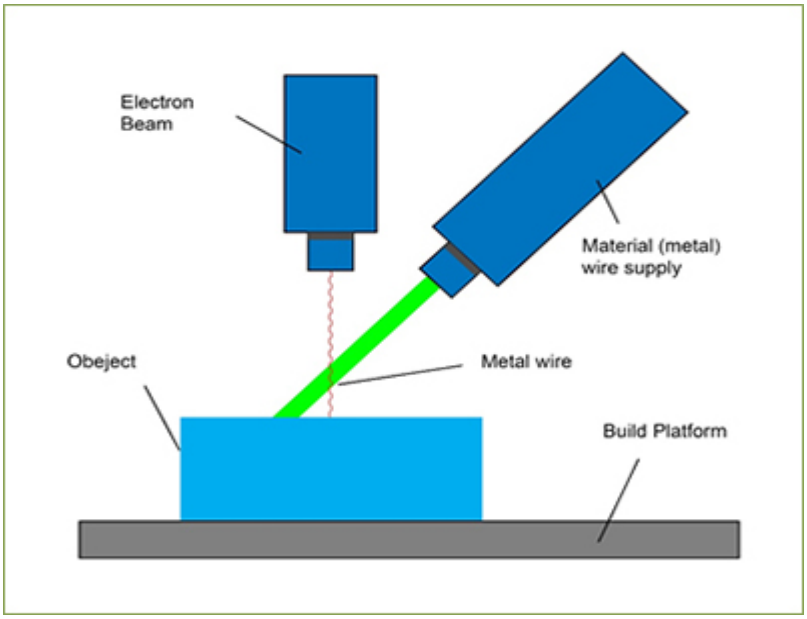

Figure 2.3. Schematic of direct energy deposition [11]

2.2.4 Material extrusion

The basic working principle of the material extrusion is to selectively dispense material through nozzle or orifice at discrete locations in build volume, material used are polymers. The technologies which utilise this method are discussed below.

2.2.4.1 Fused deposition modelling

FDM printer as shown in Figure 2.4 works by inserting thermoplastic filament into a hot extruder, which through the print head melts and extrudes the filament with a thickness depending on the software and hardware settings. Layer by layer format is used to deposit the melted thermoplastic in order to create 3D objects [10, 13].

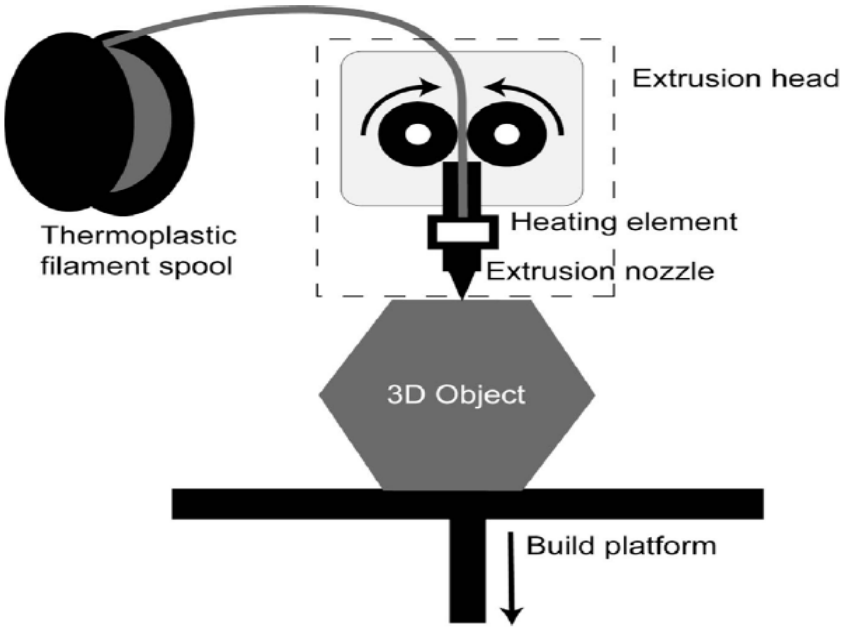

Figure 2.4. FDM printer [14]

After the deposition of first layer, in order to deposit the subsequent layer, build platform of the printer moves downward with the distance equal to the thickness of first layer. The process continues until the printing of the 3D object is completed [15].

Fused deposition modelling (FDM) is the most commonly used 3D printing technique for the manufacturing of polymer composites. ABS, PC and PLA are most commonly used

thermoplastics because of low melting temperatures. One of the common difficulties in printing composite material with FDM is that the material has to be in filament form in order to enable the extrusion process. Homogenous dispersion of reinforcements and removal of void formation during manufacturing of composite filaments is a challenging task. Another drawback of FDM printer is limitation of material used which is limited to thermoplastic polymers having sufficient melt viscosity. Advantages of FDM printers include high speed, low cost and simplicity [16].

2.2.4.2 3D plotting/direct-write

Smay et al [17] developed the direct-write technique which is an extrusion based system in which variety of inks can be patterned both in planar and 3D shapes having feature sizes as fine as 250 nm. In this technique, compressed air is used to push inks with controlled rheological properties using single nozzle having diameter in the range of 1 to 500 μm. This technique deposits inks at room temperature depending on ink rheology and nozzle diameter using controlled printing speed and pressure. A wide range of inks can be processed by direct-write assembly e.g. colloidal suspension and gels, polymer melts, nanoparticle-filled inks, and hydrogels. Figure 2.5 shows the schematic of the 3D plotting/direct write technique.

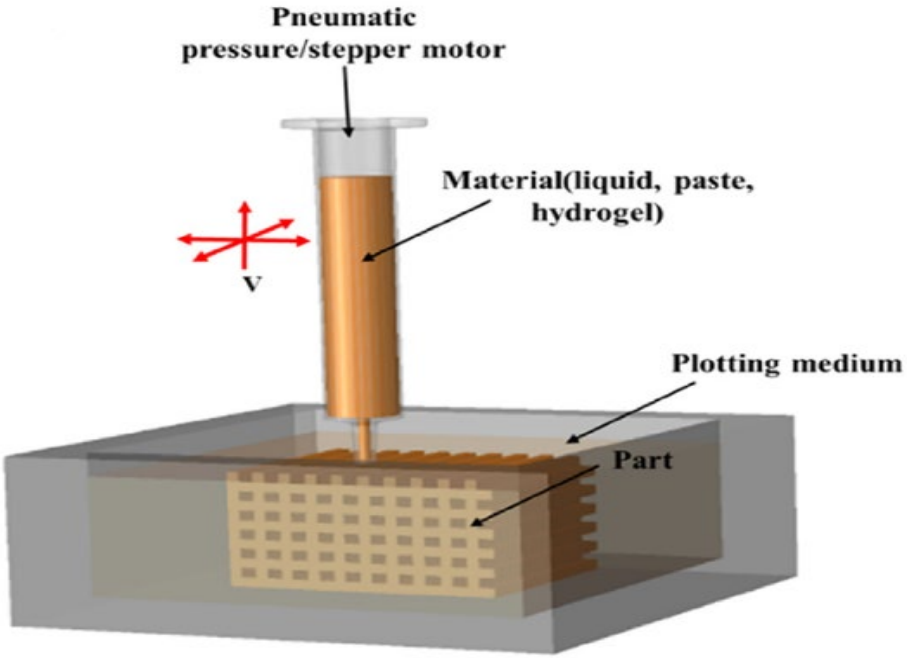

Figure 2.5. Schematic of 3D plotting/direct write technique [16]

Material flexibility is the key advantage of this technique. 3D plotting printers can easily load solutions, pastes and hydrogels.

2.2.5 Photo-polymerisation

Photo-polymerisation is an additive manufacturing process that follows the principle of selectively curing a liquid polymer by polymerisation process, which is initiated by a light source (most commonly UV light). Some of the most commonly used technologies which use this method are discussed below.

2.2.5.1 Stereolithography (SLA)

Stereolithography uses photopolymer liquid resin curable by ultraviolet (UV) light to print 3D objects as shown in Figure 2.6. It works by curing the liquid photopolymer using UV light layer by layer, while printed 3D object is slowly pulled down by build platform by a distance equal to the thickness of the first layer. One whole 2D cross section of the final 3D object is cured

by UV laser based on the input 3D CAD model by scanning the laser along the 2D cross section [10, 13, 18]. After a layer is cured, a resin loaded blade levels the surface of the resin in order to ensure a uniform layer of liquid before the next layer is cured.

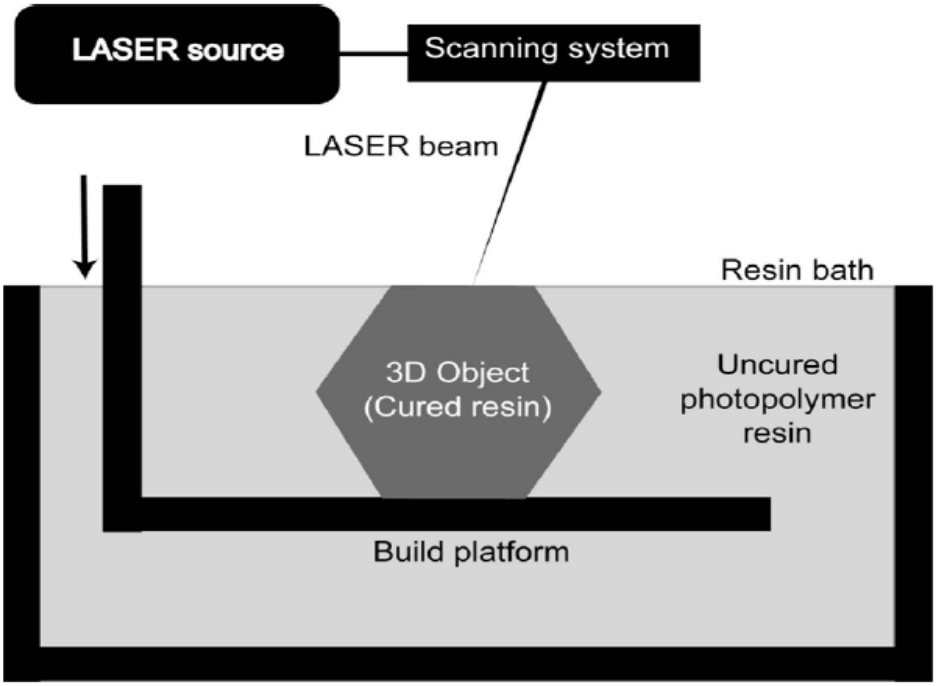

Figure 2.6. SLA Printer [14]

A relatively new subtype of SLA printer is the digital light processing (DLP) in which photo-polymerisation of liquid resins are carried out by using DLP projector light instead of scanned laser. The major differentiating factor between SLA and DLP 3D printing techniques is that DLP projector uses one single shot to cure on whole 2D cross section, whereas in SLA the laser has to be scanned across the entire 2D cross section. [10, 15].

Acrylic and epoxy resins are typical polymers used in SLA. In order to control the quality of the final printed part, it is critical to understand the curing reactions occurring during photo-polymerisation. Laser power intensity, duration of exposure to UV light and scan speed has some effects on curing time and printing resolution [19]. Depth of photo-polymerisation can be controlled by adding the UV absorbers and photo initiators to the resin [20].

2.2.5.2 UV – assisted 3D printing (UV-3DP)

The UV- 3DP technique is based on robotically-controlled micro-extrusion of a UV curable ink filament while the extrusion point is moved in three directions. Photo-polymerisation of uncured material occurs within seconds under UV exposure. Robot head contains the UV light emission set up which follows the extrusion point. Circular pattern of a set of six optical fibres as shown in Figure 2.7 delivers the UV light which is provided by two high intensity UV light emitting diodes of wavelength 356 nm near to the extrusion point at the tip of the extrusion micronozzle [21].

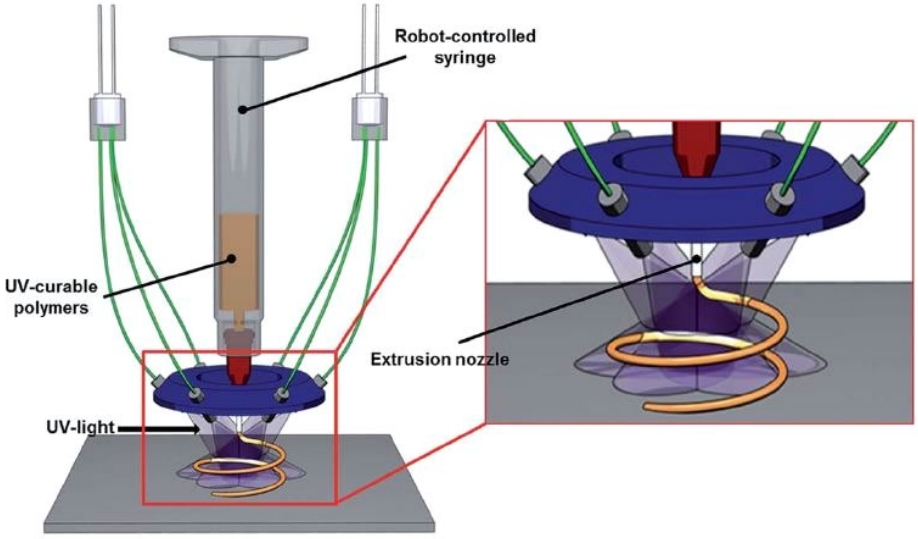

Figure 2.7. UV assisted 3D printing process [21]

2.2.5.3 Digital light processing (DLP)

DLP is a relatively new derivative of SLA technology, DLP utilises projector light instead of UV lasers to cure the photopolymer. The major difference between DLP and SLA is the entire 2D cross section is cured by DLP projector in a single shot, while in SLA laser scans across the 2D cross section. Figure 2.8 shows the schematic of the digital light processing technique.

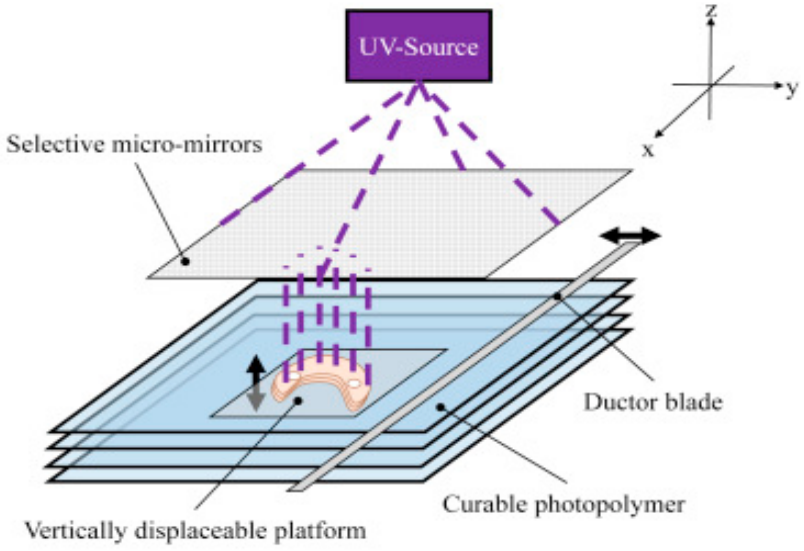

Figure 2.8. Schematic of digital light processing technique [22]

2.2.6 Powder bed fusion

Powder bed fusion is an additive manufacturing process which follows a principle of selectively fusing regions of a powder bed using thermal energy (laser or electron beam source). Some of the most commonly used technologies which use this method are discussed below.

2.2.6.1 Selective laser sintering (SLS)

A laser (normally a CO_2 laser) is utilised in laser sintering as shown in Figure 2.9 that selectively sinter bonds the powder in layer by layer arrangement in order to develop the 3D object [23, 24]. After the completion of laser sintering of one thin layer of powder, the next layer of powder is ready to be spread over and the build platform lowers at a distance equal to thickness of the first layer.

Even though theoretically SLS can process thermoplastic polymer in powder form, there is a limitation in the choice of materials in SLS process due to complex consolidation behaviour

and molecular diffusion during sintering [25]. Presently, polycaprolactone (PCL) and polyamide (PA) are commonly used laser sintering materials.

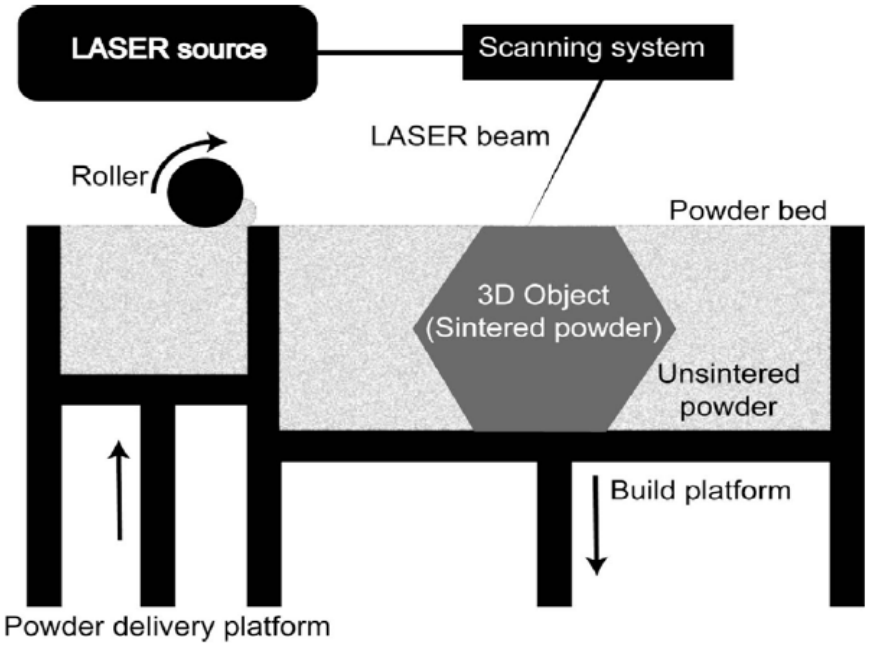

Figure 2.9. SLS printer [14]

2.2.6.2 Selective laser melting (SLM)

Selective laser melting's working principle is similar to SLS, apart from lasers having higher power to melt metal powders in an inert gas atmospheres [23]. Compared to SLS printing, SLM provides denser metal objects. Generally, parts manufactured by SLM have low porosity and high mechanical strength [26]. Figure 2.10 shows the schematic of SLM technique.

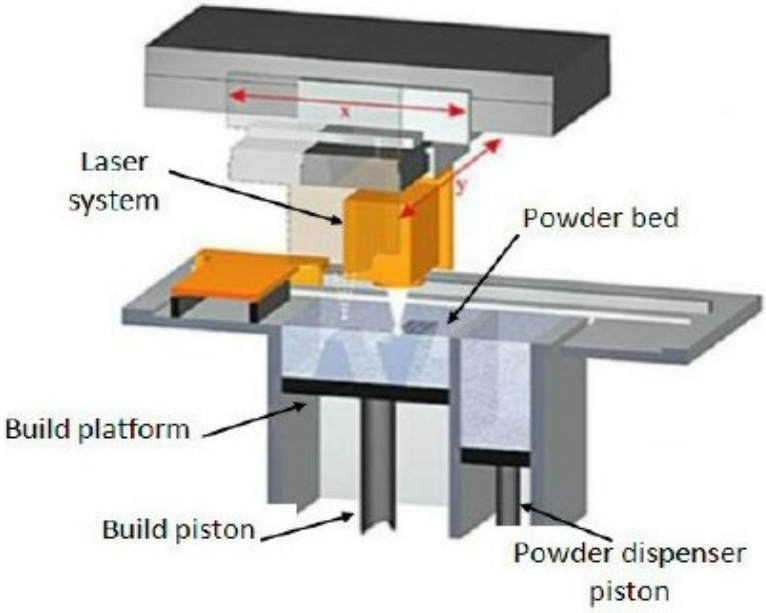

Figure 2.10. Schematic of selective laser melting technique [27]

2.2.6.3 Electron beam melting (EBM)

Another powder bed fusion technology that utilises high-power electron beam source rather than a laser source under vacuum is known as electron beam melting (EBM) [13, 23]. The electromagnetic coils are used to focus the electron beams and deflect them to desired spots using electromagnetic steering coils [28]. Figure 2.11 shows the schematic of EBM technique.

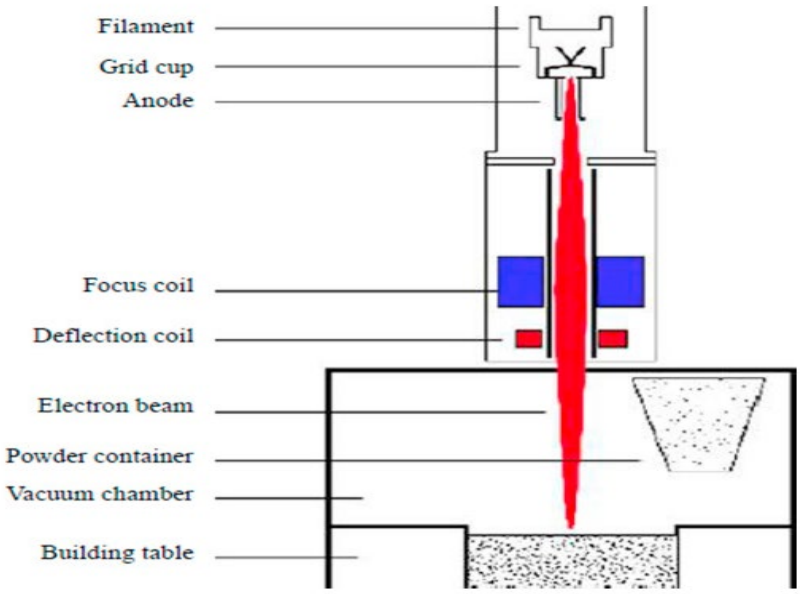

Figure 2.11. Schematic of electron beam melting technique [29]

2.2.7 Other techniques

A number of new techniques have been developed in the recent past, for example Polyjet which works by polymerisation, by depositing the droplets of photopolymer ink [30]; digital light processing (DLP) in which the entire surface of photopolymer is selectively polymerised with the help of projector light [31]; liquid deposition modelling (LDM), which is based on additive deposition of material layers directly from a solution in a volatile solvent [32]; and fibre encapsulation additive manufacturing (FEAM) in which a fibre and a matrix are co-deposited simultaneously within a single printer and the extruded flowable polymer matrix encapsulates the fibre. When compared with conventional 3D printing techniques, these techniques are less time consuming or have variety of material selection. However, these techniques have been adapted in few researches due to their complexity and high cost.

2.3 3D printing of polymers

Polymer materials having low melting point or in liquid state are commonly used in additive manufacturing industry due to the characteristics like low cost, light weight and shorter processing time. 3D printing technology can be used to process thermoplastic polymer materials such as acrylonitrile butadiene styrene (ABS) [33-35], polylactic acid (PLA) [33, 35, 36], polyamide (PA) [37] and polycarbonate (PC) as well as thermosetting polymer materials like epoxy resins. In order to complete the polymerisation process, epoxy resins require thermal or UV-assisted curing as they are reactive materials, and they initially show low viscosity, which increases as the curing proceeds [38-40]. Therefore, epoxy resins are ideally suited for heat or UV-assisted printing process. 3D printed polymers are used in different applications e.g. creating complex lightweight structures for aerospace industries [41], structural models for architectural industries [42], artefact replication or education in art fields [43] and printing of tissues and organs for medical field [8]. However, majority of 3D printed polymers are still used as conceptual prototypes, since 3D printed pure polymer products bear the disadvantage of weak strength and struggle to be used as efficient load bearing parts. These disadvantages lead to the limited use of 3D printed polymers in industrial applications.

3D printed polymer composites overcome these limitations using combination of matrix and reinforcements, so that enhanced structural properties not attainable by any of the constituents alone can be achieved. Polymer matrix composites are formed by the addition of particles, fibre or nanomaterials as reinforcements into polymers, which bear improved mechanical properties and excellent functionality. Traditional composite manufacturing techniques such as, moulding and machining, manufacture objects with complex geometries by removing material from a larger stock or sheet metals [44]. Even though using these methods, performance and manufacturing processes of composites are well controlled and understood, the capability to control the complex internal structure is limited. Additive manufacturing is able to manufacture

complex composite structures without generating typical waste. Computer aided design (CAD) precisely controls the size and geometry of the composites. Thus 3D printing of composites yields a very good combination of high performance products and process flexibility [16]. Addition of different materials for attaining required mechanical properties is a positive step to enhance the properties. Therefore, significant attention has been given to the development of the composite materials which are compatible to the available printers. Many studies in acquiring new printable particles, fibres or nanomaterials reinforced composites have been conducted [45-47]

Different 3D printing techniques have been used to manufacture polymer composites. Some of them are well-established techniques such as stereolithography (SLA), fused deposition modelling (FDM), selective laser sintering, and inkjet printing; whereas some of the techniques are still in development stages or in practice with small groups of researchers. Each technique has its own advantages and disadvantages in manufacturing composites materials.

2.4 Particle reinforced polymer composites

Particle reinforcements are commonly used to enhance the properties of polymer matrix due to their low cost. Particles are easy to mix in polymers, whether they are in powder shape as for SLS or in liquid form as for SLA, or further to be extruded into printable filaments for FDM. Different types of reinforcement particles can be used for enhancing the properties of 3D printed polymer matrix composites, such as improvement in tensile/storage modulus by the addition of glass beads [48] and iron and copper particles [49]; or improvement in wear resistance by addition of aluminium and aluminium oxide (Al_2O_3) [46]. FDM, SLS or SLA techniques were used to fabricate cuboid or cylinder shaped parts in these cases and improvement in the properties were observed.

Adding the particles in the polymers also helps to eliminate some obstacles in the printing process. For instance, one of the obstacles in FDM printing process is the deformation of the final printed parts, which is due to the thermal expansion of the polymer. Addition of metal particles into the polymer was found to be an effective solution to this obstacle [50]. When copper and iron particles are added, large reductions in the coefficient of thermal expansion was observed in ABS composite, thus reducing the distortion of the printed part. [50] A novel magnetically assisted 3D printing platform was developed by Kokkin's et al. [51] in which the orientation of particles can be controlled by incorporating magnetised alumina platelets into polymer matrix. The alignment of anisotropic particles helped to achieve the target properties in particular direction of the printed composite.

Although, the performance of the polymer composites is improved with the addition of reinforcements, in comparison with the polymer composites developed by traditional moulding methods, majority of the printed composites still found to have weak mechanical properties and struggle [16]. Several factors contribute to the weak mechanical strength of 3D printed particulate-polymer composites, e.g. non-homogenous dispersion, weak interfacial adhesion, particle loading, and presence of voids. How to avoid the occurrence of these factors to ensure strong mechanical properties requires a further significant research.

Homogenous dispersion of nanoparticles plays an important role to attain the desired properties of the composite by 3D printing technique. If the nanoparticles are dispersed homogenously throughout the matrix, the interfacial adhesion between the matrix and the nanoparticles will be very strong, and the externally applied load can be effectively transferred from the matrix to the nanoparticles. Hence, improved mechanical properties are achieved. If the particles are not dispersed homogenously, load cannot be transferred effectively from the matrix to the nanoparticles because of the weak interfacial adhesion and the strength of the composite cannot be any higher than the neat polymer. To eliminate agglomeration of nanoparticles and to ensure

improved interfacial adhesion between matrix and nanoparticles, a proper homogenisation technique should be employed. Some researchers have used the chemical surface treatment of nanoparticles [52] prior to printing and they reported significant improvement in the mechanical properties.

2.5 Nanocomposites

Nanocomposites are the type of composite materials in which matrix material is reinforced by nano sized filler materials in order to enhance the properties. Polymers are most commonly used as matrix material for nanocomposites. Nanomaterials have characteristic dimensions (e.g. grain size, diameter, aspect ratio) smaller than 100 nm.

Carbon nanotube [53], graphene [54], graphite [55], metal nanoparticle [56] and ceramic [57] as nanomaterials demonstrate unique mechanical, electrical and thermal properties. Thus, adding nanomaterials into polymers could lead to the development of high-performance functional composites.

Basically, there are three kinds of fillers in nanocomposites. They can be classified as cylinder-like nanofibres (nanotubes), flake-like (disk-like) platelets, (nanoclays, nanolayers) and spherical-like particulates as shown in Figure 2.12.

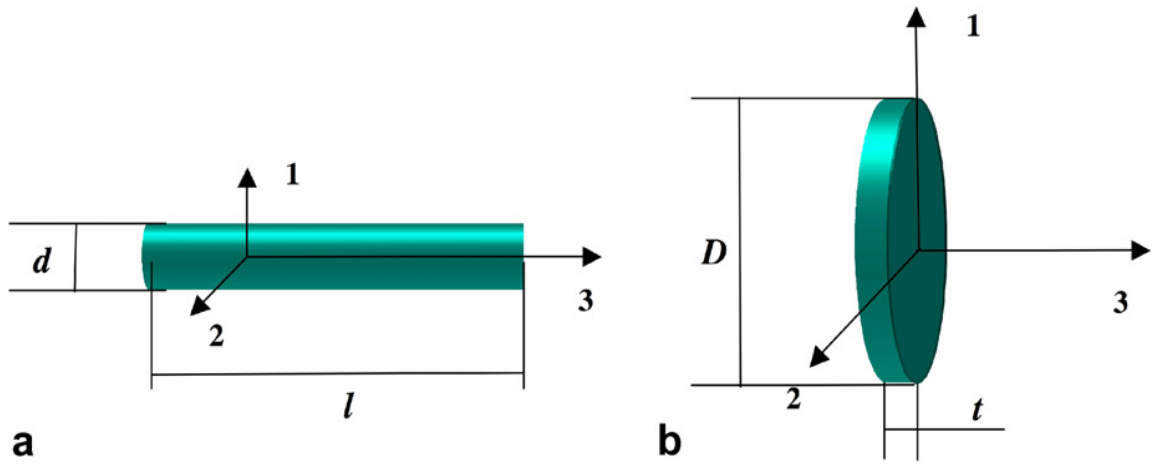

Figure 2.12. Schematic of (a) nanotube (b) nanoplatelet [58]

In case of nanocomposites reinforced with fibre, there are two categories which depends on the orientation of the fibres, i.e. aligned fibres and randomly oriented fibres as seen in Figure 2.13.

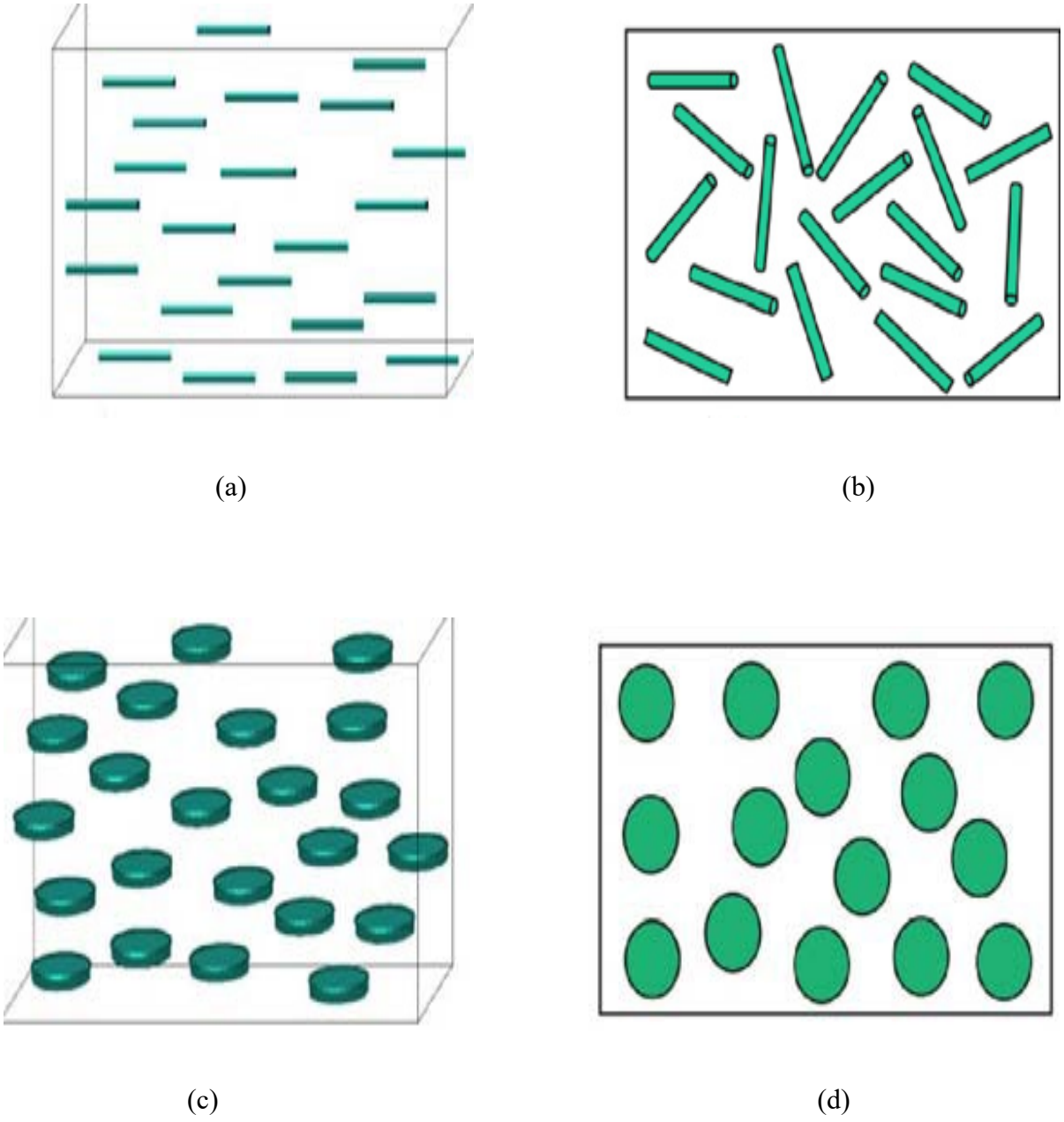

(a) (b)

(c) (d)

Figure 2.13 Nanocomposite containing (a) aligned fibres (b) randomly distributed fibre (c) aligned platelets (d) randomly oriented particulates [58]

There have been a number of attempts in which nanomaterials were used to enhance the mechanical properties of printed composite parts. Adding 5% nano-titanium dioxide (TiO_2) [59], 10% by weight of carbon nanofibre [60] or 10% by weight of multi-walled carbon nanotube [61] demonstrated a 13.2%, 39% and 7.5% improvement in tensile strength of printed nanocomposite compared to neat polymer parts respectively; however, a decrease in elongation and more brittle behaviour were observed in these cases. SLA fabricated graphene oxide/photopolymer composite was investigated by Lin et al. [62]. They reported a significant improvement in strength and ductility with 62.2% increase in tensile strength and a 12% increase in elongation with 0.2% of graphene oxide. In addition, an increase in thermal stability of printed nanocomposite was obtained by the addition of nano-TiO_2 [52] and nano-clay [63] into polymer matrix.

2.5.1 Modelling of nanocomposites

Even though applying continuum mechanics (including micro mechanics) to nano filler reinforced composites have been critically reviewed [64], many researchers have applied continuum mechanics to nanostructures and nanomaterials and have reported positive results and clarified certain issues [65, 66]. Micromechanics is a technique that identifies the properties of composite materials by studying the constituents of the composite materials. By identifying the properties of each constituent, micromechanical methods predict the mechanical behaviour of composite materials as a function of the properties of those constituents.

2.5.1.1 Analytical models

Several analytical models have been developed for studying and analysing the stiffness of the filler reinforced composite materials. Voigt [67] derived the equations for the effective modulus in fibre direction by assuming that the same uniform strain is applied to fibre and matrix in the fibre direction. Reuss [68] applied uniform stress on the fibre and matrix in the transverse direction and obtained the effective modulus in the transverse direction. Hashin and

Shtrikman [69, 70] worked on the macroscopical isotropy and quasi homogeneity of the composite, where shape of the filler is not the limiting factor, and used vibrational principles of elasticity to estimate the upper and lower bounds of the composite. Halpin and Tsai [71] got the equations for the estimation of elastic constants based on the work of Herman and Hill [72] for aligned fibre reinforced composite material. Mori and Tanaka [73] derived the analytical expressions to obtain elastic constants based on equivalent inclusion model of Eshelby [74].

Response of the composite is predicted by all micromechanics models based on volume fraction in addition to the individual properties of the matrix and inclusion phases and can typically account for orientation distribution and inclusion shape within the composite. Generally, similar results can be obtained from most established micromechanics models for the prediction of modulus at relatively low volume fractions, with these discrepancies becoming more evident at higher volume fractions and as the modulus of the inclusion decreases towards zero (in case of voids). While these micromechanics based models are able to predict the effective modulus of the material, they are unable to provide stress or strain results due to the effective medium averaging approach.

2.5.1.2 Finite element modelling (FEM)

Finite element method as a powerful numerical tool has been used to model mechanical behaviour of composite materials since early 1970s [75, 76]. Ever since, various finite element models have been developed to characterise different kinds of composite materials [77, 78]. A single unit cell of nanoparticle and polymer is considered as the simplest case for FEM [79, 80]. While other cases have also been considered with larger representative volume elements (RVEs) in which interaction of particles could be studied.

The representative volume element is generally considered as a volume of heterogeneous material that is adequately large to engulf all major heterogeneities of the composite's

microstructure, and to be statically representative of that composite material. The size of the RVE is of great importance in order for it to be representative. Different kinds of boundary conditions can be applied on RVE to calculate the effective properties of the composite. Figure 2.14 shows the RVEs consisting of randomly distributed identical spherical particles and periodically distributed identical particles, respectively.

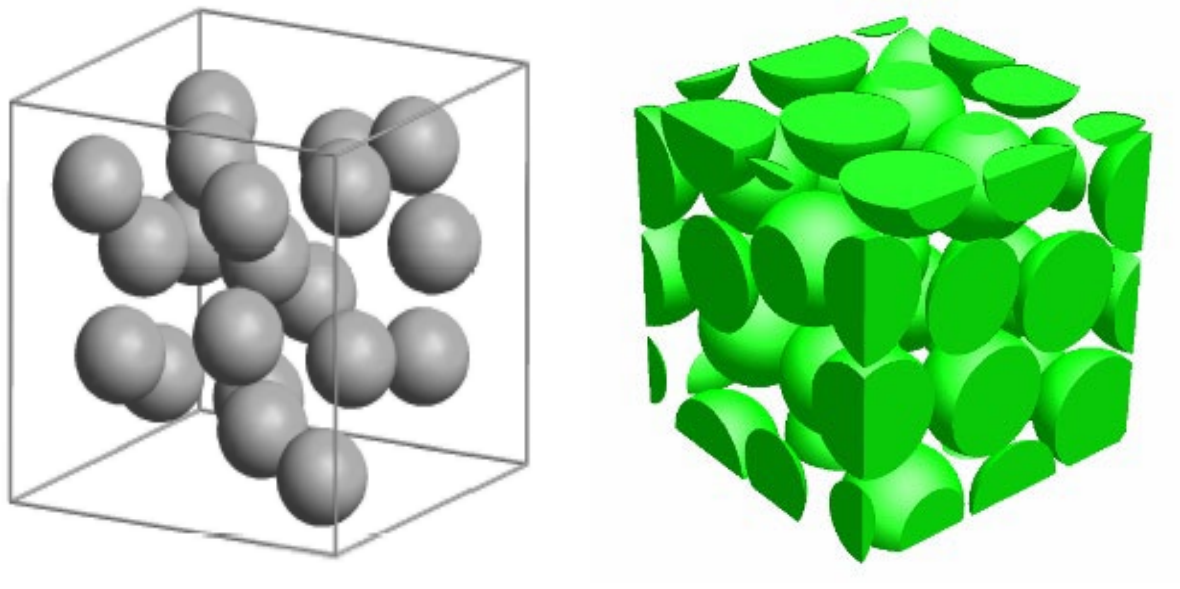

(a) (b)

Figure 2.14. (a) RVE consisting of randomly distributed identical spherical particles (b) RVE consisting of periodically distributed identical particles [81]

Li and Chou [82] further studied the RVE concept employed by Hyer [83] and Nemat-Nesser and Hori [84] for conventional fibre-reinforced composites at the microscale to nanoscale, and used three dimensional nanoscale RVE based on elasticity theory to predict the effective mechanical properties of CNT-based composites and solved it using finite element method. A single or multiple nanofiller(s) make up an RVE with surrounding matrix materials, together with proper boundary conditions that are applied to account for the effects of surrounding materials. It is used as a building block to assemble the composite. In a study conducted by

Zhang et al. [85], RVE method was used to study the mechanical behaviour with particular attention to the damage mechanisms of SiCp/Al composites. They developed a 3D microstructure finite element model predicting elasto-plastic response and fracture behaviour of 7% volume fraction SiCp/Al composite. Hua et al. [86] analysed the mechanical behaviour of TiO_2 nanoparticle reinforced resin based dental composites using a 3D nanoscale RVE. They characterised the effects of nanoparticle volume fraction, aspect ratio, stiffness and interphase zone between resin matrix and nanoparticle on bulk properties of the composite. Hua et al. [87] used nanoscale RVE to investigate the effect of interphase geometry and property on the mechanical behaviour of the silica-epoxy resin nanocomposite. They found that interphase modulus and interfacial bonding conditions have significant influence on effective stiffness of nanocomposites. After analysing the literature on FEM of nanocomposites, it is quite evident that until now, majority of the studies focused on linear elastic properties of the nanocomposites as functions of volume fractions, filler properties and in some cases filler orientation. The influence and effect of viscoelastic properties have been neglected.

2.6 Three dimensional printing of free form and self-supported structures

Many complex 3D features require support structures to hold the shape of an object during 3D printing process. The existence of these supports has been a major drawback for the technology as it increases production time, in terms of printing time as well as the time required for removal of the supports. Additional materials are required to build the supports, hence increasing the production cost. Due to the fact that the tool pathway is restricted by the printing sequence of layer by layer technique, printing capability is limited and complex shapes might not be feasible. The mechanical properties will also depend on the orientation of the slicing plane. Difference in strength of the materials along and in between the slice planes may cause errors in design calculation and prevent its use in potential applications.

One approach to eliminate the difficulty of printing complex free form and self-supported structures is the introduction of additional rotational axes to the system. At the moment there are very few 5-axis printers and they are still under development. Some of them are discussed below.

2.6.1 Optomec Inc. 5-axis printer

Optomec Inc. has developed a 3D printer that implements a 5 axes system to print electronics on complex 3D surfaces. It has a print envelope of 200mm ×300mm ×200mm, and has the capability to print features from 10 μm to 1 mm. Following the steps from Figure 2.15, the material in the liquid state is atomised and the particles are refined through a virtual impactor. Inert carrier gas is utilised to transfer the aerosol to the deposition head. In the end, the aerosol is deposited at a high velocity by focusing the aerosol with an annular sheath gas. The additional axes of the system enable the printer to access complex surfaces of an object. Despite utilising a 5 axes system, the printer is still limited to layer by layer techniques as the technology involves high velocity deposition, materials are volatile and hard to handle and sensitive to the environment [88].

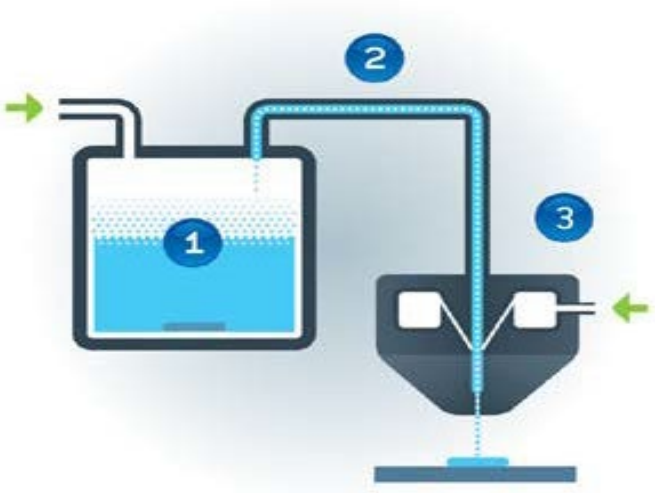

Figure 2.15. Aerosol jet process [88]

2.6.2 TWI 5-axis printer

Another 3D printer that utilises a 5-axis system has been developed by The Welding Institute (TWI) using laser metal deposition (LMD) technology. The principle of this technology is based on selective laser sintering and laser cladding. Two processes are considered in the project; laser metal deposition with powder (LMD-p) and with wire (LMD-w). Figure 2.16 (a) describes the concept of LMD-p. In this process, metal powder is used to clad conformal surfaces and to build up self-supporting 3D structures. The metal is injected through the nozzle and to the laser focal zone. It is then melted and re-solidified into fully dense metal parts. In comparison, as seen from Figure 2.16 (b), LMD-w uses wire from a continuous spool feeder [89]. The advantage of this system is that it is versatile to make a custom alloy by combining different materials. The toolpath is mapped in a 5-axis vector with deposition parameters to guide a 3-axis coaxial nozzle across a moving substrate manipulated by a 2-axis CNC rotary table. By utilising rotational axes, generation of rotational and helical structures are relatively easy. The technique deposits the material layer by layer and the rotary table acts like a potter's wheel in forming a clay pot. Figure 2.16 (c) shows an example of the printing process. The technology is mainly used for coating and repairing of complete products, combining different production methods and bridging of gaps. Since the materials used are metal powders, the technology shows extensive applications in the aerospace and automotive industries [90]. The use of a rotational axis significantly reduced production time, especially in generation of helical shapes. However, the technology is still a layer by layer method, and it is unavoidable to build a supporting platform that is difficult to disconnect due to strong bonding between welded components.

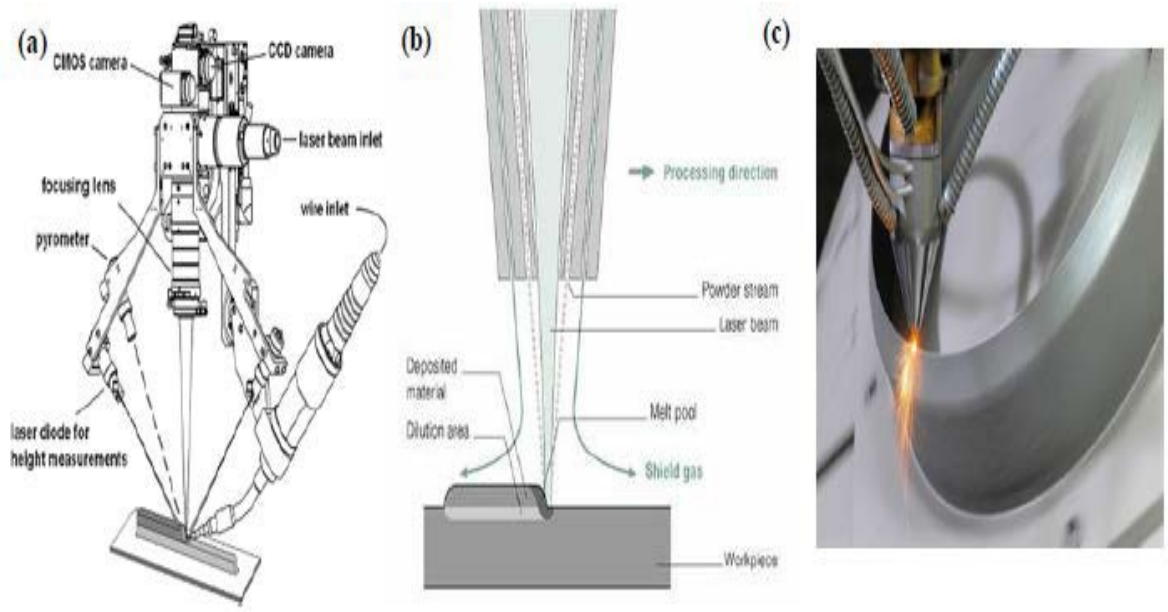

Figure 2.16. (a) Laser metal deposition with wire (LMD-w) concept (b) laser metal deposition with powder (LDM-p) (c) 5-ais manufacturing of the helicopter engine combustion casing [89]

2.6.3 FDM based 5-axis printer

The most recent research that integrates additional axes to a 3D printing system uses FDM technique and has been developed by the University of Oslo [91] As can be seen from Figure 2.17, the printer has a fixed XZ plane motion on the print head. Two rotational axes and the Y-axis are attached to the print bed. This enables the printing of overhanging structures without the need for support materials. Hence, it saves time to remove the support and also minimises the use of material to print. However, the additional degree of freedom is used here predominantly to have the capability to print smoother surfaces on curvature planes. With a fixed nozzle head, not only that it limits tool pathing while printing complex structures, but also gravitational factors are to be considered if the object is tilted during the printing process. Thermal degradation of the material also prevents its application for smart materials [91].

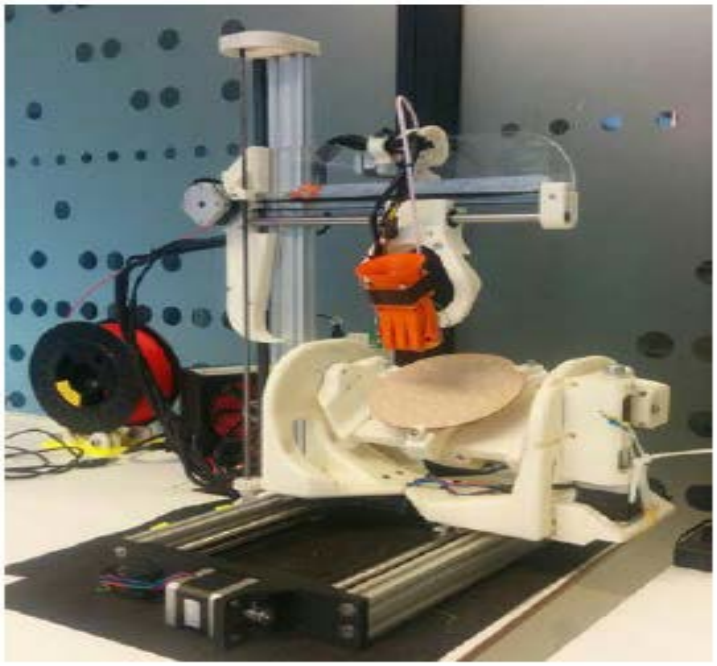

Figure 2.17. FDM based 5-axis printer [91]

2.7 Research gap

3D printing technique proposed in this study is relatively new and in depth study on mechanical characterisation of the photopolymer used as base material and reinforced with silica filler has not been characterised yet. Theoretical modelling i.e. capturing stress-strain behaviour of photopolymer and nanocomposite, and finite element modelling of the parts manufactured using the proposed technique have not been carried out either. The proposed technique has two additional rotational axes which makes it unique compared to existing 3D printing techniques, its capability to utilise those axes to print free-form and self-supported structures have not been demonstrated yet.

Therefore, in this thesis in order to study mechanical behaviour, theoretical and finite element modelling and testing the capability of proposed technique to print free-form and self-supported structures, following investigations will be carried out:

- In order to identify the suitable range of viscosities to print reliably, study on the effect of filler on material viscosity will be carried out.

- Silica is used as a filler and its effect on mechanical properties e.g. tensile strength and flexural strength, dimensional accuracy and surface roughness of 3D printed nanocomposite will be studied.
- The proposed technique's capability to print free-form and self-supported structures utilising additional rotational axes will be demonstrated.
- Interfacial adhesion which plays very important role in improving mechanical properties of the nanocomposites will be thoroughly investigated.
- Viscoelastic properties of the polymer and nanocomposite will be determined, minimum amount of filler required to enhance the mechanical properties of the nanocomposite will be proposed and existing theoretical models will be used to capture the stress-strain behaviour of the polymer and nanocomposite.
- Printing the nanocomposite with high filler concentration is difficult, in order to study the behaviour of the high filler concentrations bearing high viscosity, a finite element model will be developed. After validating the finite element model, empirical model will be developed which will predict the behaviour of filler concentrations bearing high viscosities.

2.8 Chapter summary

As discussed in section 2.3, majority of the 3D printed polymers still struggle to be used as conceptual prototypes since they bear the drawback of weak strength and not effective as load bearing parts. And as mentioned in section 2.4, to overcome these limitations, fillers are added to enhance the properties of the polymers. Even though these fillers diversify the mechanical properties of the polymers by introducing their rich mechanical behaviour, most of the polymer still found to have weak mechanical properties. There are several factors that lead to weak mechanical properties of 3D printed particulate-polymer composites, e.g. non-homogenous

dispersion, particle loading, weak matrix-particle interfacial adhesion, and presence of voids. An increase in filler content, may further complicate these factors.

As discussed in section 2.6 the existence of support materials in 3D printing techniques have also been found to be disadvantageous as excessive material is required to hold the shape of an object. The concept of adding additional rotational axes to the system to eliminate this problem has shown promising results, but systems still lack the capability to print complex structures without supports.

In order to address the limitations discussed in the literature review, there is a need to develop new 3D printing technologies, which are diverse enough to handle issues pertaining to the previous well-established techniques and methods. There is a need to develop a new technique, which enables the manufacturing of parts with improved mechanical properties and has the capability to print free form and self-supported structures. Therefore, a new photopolymer extrusion 5-axis 3D printing technique is proposed in this research which incorporates the strengths of FDM and UV3DP printers. This hybrid 3D printer extrudes photopolymer in a similar configuration to an FDM printer. By using an extrusion nozzle, photopolymer resin will be deposited on a build plate. The extruded photopolymer will then be cured solid on demand by exposure to ultraviolet light (UV) light. This developed new 3D printing technique not only allows the traditional layer upon layer printing, but is capable of printing free form and self-supported 3D structures with the approach of implementing additional degrees of freedom, i.e. 2 rotational axes to the system which will be unique compared with current printing systems.

As mentioned in section 1.2 of the chapter 1, the 3D printing technique proposed in this research is new and study on mechanical properties, analysis and modelling of the proposed technique has not been carried out yet. Therefore, in this thesis, detailed study on mechanical properties of the parts manufactured using this new technique, as well as theoretical and finite

element modelling have been carried out. Furthermore, the capability of the proposed printer utilising 5-axis to print free form and self-supported structures have been successfully demonstrated.

In the next chapter a comprehensive experimental study outlining basic structure of the photopolymer extrusion 5-axis printer is carried out. The chapter discusses the effect of filler on dimension accuracy, material viscosity, surface roughness and mechanical properties. It also outlines the capability of the proposed technique to print free-form and self-supported structures.

CHAPTER 3: A NEW PHOTOPOLYMER EXTRUSION 5-AXIS 3D PRINTER

3.1 Introduction

As discussed in previous chapters, 3D printing is a useful technique for manufacturing mechanical parts, with several advantages including freedom to fabricate intricate geometries, lack of material waste, and elimination of expensive tooling [92]. Particularly when the number of parts required is small, 3D printing techniques can help to avoid high setup costs, as well as reducing manufacturing time [93]. Although it might take up to several hours or even days to manufacture an object, this is still a short total time to obtain a physical product from a CAD file. Various 3D printing technologies such as fused deposition modelling (FDM) [94], stereolithography (SLA) [95], selective laser sintering (SLS) [96], and binder jet technique [97] have been developed. Each technique has different capabilities for the material(s), size, complexity, and geometry of the printed objects, as well as different ability to deposit support material layer-by-layer and print overhanging or bridging structures. As discussed in section 2.3 of the chapter 2, well established 3D printing techniques such as FDM, SLA, and SLS have certain limitations and challenges when it comes to printing polymer composites. Although printing of functional parts combining smart and conventional materials is a promising area, existing printers are not ideally suited to this, with FDM printers typically requiring high operating temperatures and SLA using a tank containing one single material. Additionally, multi-material 3D printing is increasingly desirable to allow functional parts combining materials of different mechanical properties, or even integrated sensors, to be produced [98, 99]. A technology well suited to multi material printing that avoids the high temperatures of FDM and single material bath of SLA is therefore desired.

As discussed in section 2.6 of chapter 2 that the construction of self-supporting [100] 3D freeform structures (e.g. a helix) without requiring support material remains a big challenge [101, 102]. Common 3D printers also require the deposition of additional "support" material to hold the shape of an object when printing overhang structures. The concept of adding additional rotational axes to the system to eliminate this problem has shown promising results, but such systems still lack the capability to print complex structures without supports. Ideally, a 3D printer should be able to produce parts of any desired geometry. In practice, it is challenging to produce overhanging or bridging structures due to the effect of gravity on the softened material (in FDM) or wiping action between layers (in SLA). Until now, this difficulty has been addressed by generating additional "support" material to prevent overhanging elements of the printed structure from sagging until it is solidified or cured. The requirement for these supports is a significant drawback due to the increased production time and material wastage. Removing support material after curing may be difficult (e.g. internal supports in a tube or cavity) or leave damage or marks on the part surface. Methods to allow printing of complex structures without support are therefore desired. While FDM has sometimes been used to print free-from microstructures, this technique has some shortcomings: as the material is a thermoplastic, it can be softened by heat during the remainder of the printing process, with deformation of the extruded material during the cooling and hardening stage making it difficult to achieve accurate geometry without support material [103]. Photopolymer extrusion is a more promising technique for fabricating freeform structures e.g. by ultraviolet light assisted 3D printing (UV-3DP) [103] and direct-print photo-polymerisation [104]. Both of these examples use a syringe driver to extrude the material, with the drawback of small reservoir size meaning that this method is effective for small test parts only. In addition, these photopolymer extrusion techniques have a conventional 3-axis layout. Even using photopolymer extrusion, it is difficult to print complex free-form structures with a 3-axis machine.

5-axis printing has advantages for printing complex structures. As discussed in chapter 2 sections 2.6.1, 2.6.2 and 2.6.3 that there are some 5-axis printers which are developed, these systems are under development and still struggle to print complex free form and self-supported structures. A move from 3-axis to 5-axis printing has another potential advantage. Existing 3D printers usually produce objects in a strict layer by layer fashion. While this substantially simplifies tool path generation, the mechanical properties of printed structures may depend on the orientation of the slicing plane [97]. In particular, a part that has been printed layer by layer is likely to have different strength along and between the slice planes. Combined with appropriate tool path generation, a 5-axis printer could deposit material in a wider range of directions allowing for the strength of a part in various directions to be customised. Whereas, the method of using additional axes to the system is increasing nowadays, these axes are all rotational axes to allow either the tools or build platform to accommodate the movements in the space. By using this method, complex free-from and self-supported 3D structures can be printed more accurately and in less time.

To overcome the limitations discussed above and short comings of the existing printers outlined in chapter 2, there is a need to develop new 3D printing methods that combine the strengths of existing techniques and fully realise printing of free-form, self-supported 3D structures. A printing technique where deposited material can be instantly cured so as to be self-supporting, and a machine layout that allows complex extrusion paths, must be combined in one device. Printing of macroscopic objects with a high level of detail will also require a material extrusion system that can precisely control the deposited volume independent of the total size of the part (unlike a syringe driver). Ideally, deposition of a range of materials will be possible, without requiring feed materials to be diluted with a solvent (that would otherwise reduce the speed and efficiency of producing bulk objects).

Therefore, a new photopolymer extrusion 5-axis 3D printing technique is proposed, which combines the strength of FDM and UV3DP and has three translational axes and two rotational axes. In this chapter, a detailed experimentation to study the effect of filler on mechanical properties and dimensional accuracy of the parts printed using the novel 3D printing technique and basic capability of this novel technique to print free form and self-supported structures have been demonstrated. Results presented in this chapter outline the operational procedure of the proposed new technique, mechanical properties of the parts manufactured, suitable filler concentration based on viscosity and its ability to print free standing structures.

3.2 Methods and materials

Our proposed system is a hybrid of FDM and UV assisted 3D printing technologies, which combines FDM-style extrusion from a nozzle with UV curing, and implements 5 axis movement for printing of complex structures. The combination of photopolymer extrusion with the integration of two additional rotational axes on the extruder allows various free-form and self-supported 3D structures to be printed easily. With these additional two degrees of freedom, the extruder can maintain the proper angle relationship between the extrusion nozzle and the deposited material even while following a complex motion path, improving the ability of our system to print true free-form and self-supported structures. A positive displacement peristaltic pump is applied to precisely control the amount of material extruded. This approach has the advantage that the precision at which the volume of deposited material can be controlled does not depend on the amount of material in the reservoir.

This hybrid 3D printer extrudes photopolymer in a similar manner to a FDM printer. Photopolymer resin is deposited from an extrusion nozzle that is attached to a 5-axis motion system. The extruded photopolymer can then be cured solid soon after leaving the nozzle upon exposure to ultraviolet (UV) light from UV laser diodes that move with the printing nozzle. Two rotational axes (A, B) along with the Cartesian axes (X, Y, Z) allow freeform printing in

addition to conventional layer by layer printing. As this printing technique does not require a material bath, works at low temperature, and can print more viscous materials than an inkjet printing head, it is suitable for future printing of multi material structures.

To customise the properties of the deposited material during printing and the mechanical properties of the finished part after curing, fillers were added into the photopolymer resin. The effect of adding different concentrations of fumed silica as filler on the viscosity of the deposited liquid and the strength and dimensional accuracy of the finished parts is investigated to provide a starting point for producing mechanical parts using the developed technique.

Prior to moving to the novel 5-axis photopolymer extrusion 3D printer, some preliminary experimentations were carried out on 3-axis photopolymer extrusion 3D printer which has the same printing methodology expect the curing source which was UV light. Details of the preliminary experimental procedure carried out on 3 axis printer are discussed in the following sections

3.3 3-axis photopolymer extrusion 3D printer with UV light as curing source

3.3.1 Preliminary experimentation

In the beginning, a 3 axis 3D printer using UV light as curing source was used as shown in Figure 3.1. In order to set the foundation for a shift from 3-axis printer to 5 axis printer, initial parameter optimisation, adequate filler concentration determination and mechanical tests were conducted on the samples printed using the 3-axis machine. An open source software (Repetier – Host) was used to control the printing process and fluid delivery.

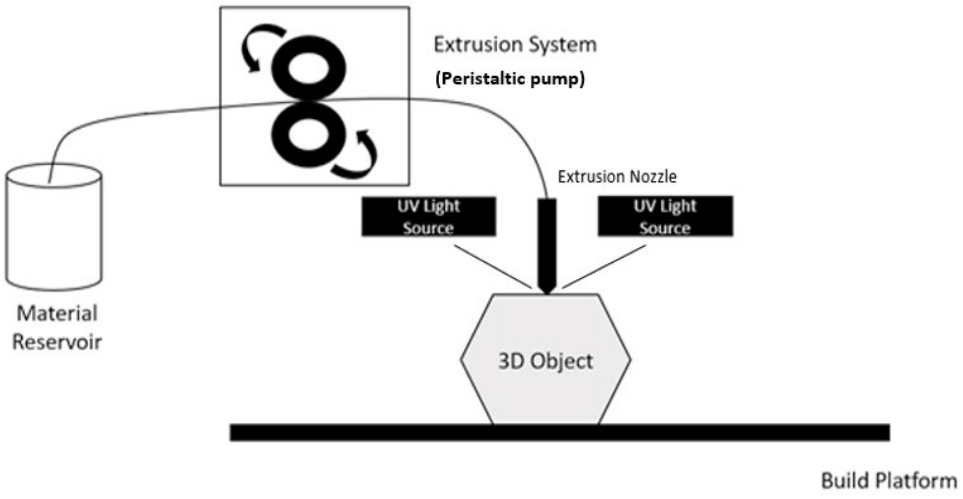

Figure 3.1. Schematic of 3-axis photopolymer extrusion 3D printer

The parameters initially studied, that influenced the printing process were printing speed which can be split into two parts infill speed and outline speed, extrusion factor which defines how quickly resin can be extruded and UV light intensity which control how fast resin can be cured. Fumed silica was used as reinforcement filler. In order to determine the adequate range of filler concertation, resin blends with 6%, 8.2%, 9.5%, 11% and 12% (percentage of silica by weight) were mixed. After mixing the resin it was held under vacuum for 1.5 hours to eliminate air bubbles. Using different combinations of parameters, dog-bone samples following the ASTM standard (D638) type V were printed. Resin blends with 6% and 12% filler concentrations would not print because of very low and very high viscosities, respectively, hence these two concentrations were ruled out.

Preliminary test results showed that 8.2% filler had disproportionate dimensions as shown in Figure 3.2 (a) with tensile strength of 18 MPa. Samples with 9.5% resulted in more conformed dimensions than 8.2% as shown in Figure 3.2 (b) with more improved tensile strength of 22

MPa. Samples with 11% filler had better representation of required shape than 8.2% as illustrated in Figure 3.2 (c), but when compared with 9.5% it had weaker tensile strength.

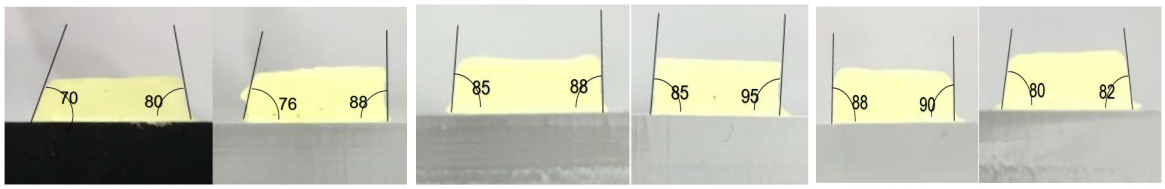

(a) (b) (c)

Figure 3.2. (a) Vertical dimensions for 8.2% (b) vertical dimension for 9.5% (c) vertical dimensions for 11%

Since 9.5% filler had better overall representation of required shape and better tensile strength it was used in all subsequent prints to examine the effect of other print variables such as outline speed/infill speed, extrusion factor and UV light intensity. Different combinations of the variables were also used in order to achieve better surface finish and good mechanical properties with relatively shorter print time. Tensile and 3-point bending tests were conducted on the printed samples to determine the mechanical strength of the printed samples.

Different samples were printed at different speeds, extrusion factors and UV light intensities, in order to determine the best printing variables combination. Here, five different variables settings were used to print the dog bone samples. Three samples were printed for each setting, of which two samples were used for tensile test and one for 3-point bending test.

Table 3.1 shows the five settings of the three print variables (outline/infill speed, extrusion factor and UV light intensity) used to print the samples.

Table 3.1. Print setting with different print variables

Setting No	**Outline Speed/Infill Speed (mm/s)**	**Extrusion Factor**	**Light Intensity (Watts)**
1	25/15	2.0	1.0
2	30/30	2.5	1.0
3	30/20	2.5	1.0
4	20/15	1.5	0.8
5	20/15	2.0	1.0

The printed samples with the above settings are shown in Figure 3.3.

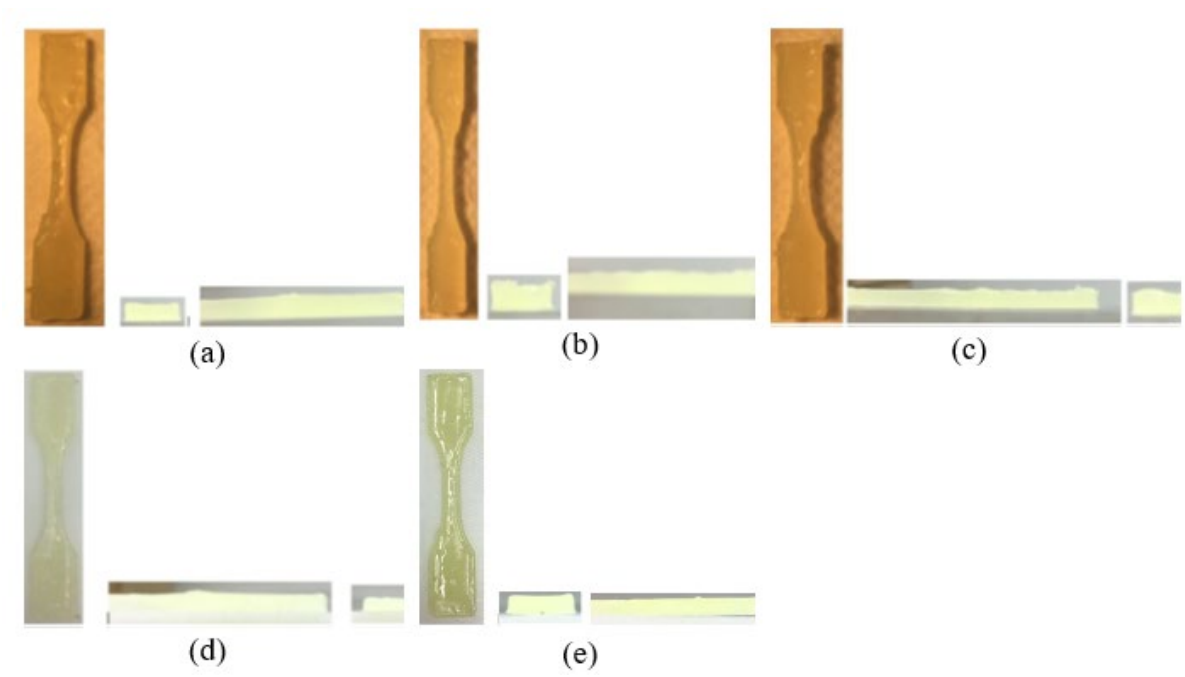

Figure 3.3 The top and side views of the printed samples of setting number (a) 1 (b) 2 (c) 3 (d) 4 (e) 4

Table 3.2 summarises the five settings, with the worst case mechanical testing results, together with measurement on the closeness of the printed samples to the required dimensions and the printing time.

Table 3.2. Overview of parameters, tensile and 3-point test results

Setting No	Filler	Outline speed/infill speed (mm/s)	Extrusion factor	UV Light (W)	Tensile strength (MPa)	Tensile Test breakage extension (mm)	3 - point bending Test (Force, N/ deflection	Printed/ actual dimensions ratio (L, W1, W2, W3, t) (mm)	Surface finish	Printing time (min)
1	9.5%	25/15	2	1	19	1.3	25.66/7.59	1.01,1.04,1.13,1.04,1.1	Medium	15
2	9.5%	30/30	2.5	1	25	2.4	51/6.08	0.995,1.03,1.12,1.03,1.02	Rough	10
3	9.5%	30/20	2.5	1	21	1.85	39.33/5.49	1.01,1.01,1.07,1.05,1.13	Rough	12
4	9.5%	20/15	1.5	0.8	16	3	20/8.53	1.001,1.08,1.24,1.07,0.87	Smooth	17
5	9.5%	20/15	2	1	26.5	3.2	41.66/5	0.998,1.05,1.18,1.05,1.02	Smooth	17

The results showed that printing with setting combinations 4 and 5 had the best average surface finish and settings 2 and 3 had the worst surface finish. However, settings 4 and 5 have lower printing speed and settings 2 and 3 have higher printing speed, which confirm the fact that lower printing speed has better surface finish. As this was the preliminary experimental stage, observation of the surface finish was based on the visual inspection of the specimen.

Also settings 4 and 5 share the same printing speed; however, the extrusion factor is the major difference between the two settings. Higher extrusion factor results in higher tensile strength

and higher bending load. More amount of material is extruded in case of higher extrusion factor, thus in order to reach the same curing speed, higher UV light intensity is required.

The lowest UV light intensity of 0.8 Watt was used in setting 4 which resulted in a significant drop in tensile strength and bending load and was more stretchable before failure. This indicates that the 9.5% photopolymer resin required at least 1Watt of UV light intensity to have sufficient cross-linking in the resin for mechanical strength.

The following sections outline operational procedure and experimental analysis including mechanical tests, suitable filler concentration based on viscosity and capability of using 5-axis to print free form and self-supported structures using 5-axis photopolymer extrusion 3D printer which utilises UV laser as curing source and has two additional rotational axes.

3.4 A New photopolymer extrusion 5-axes printer

Figure 3.4 shows the 5-axis photopolymer extrusion (PPE) printing technique. The entire 3D printing system includes the UV curing system based on two UV laser diodes, an extrusion system consisting of the stationary peristaltic pump, flexible tubing, and the extrusion nozzle, and a platform with 3 linear motions (X, Y and Z) and 2 rotary motions (A and B).

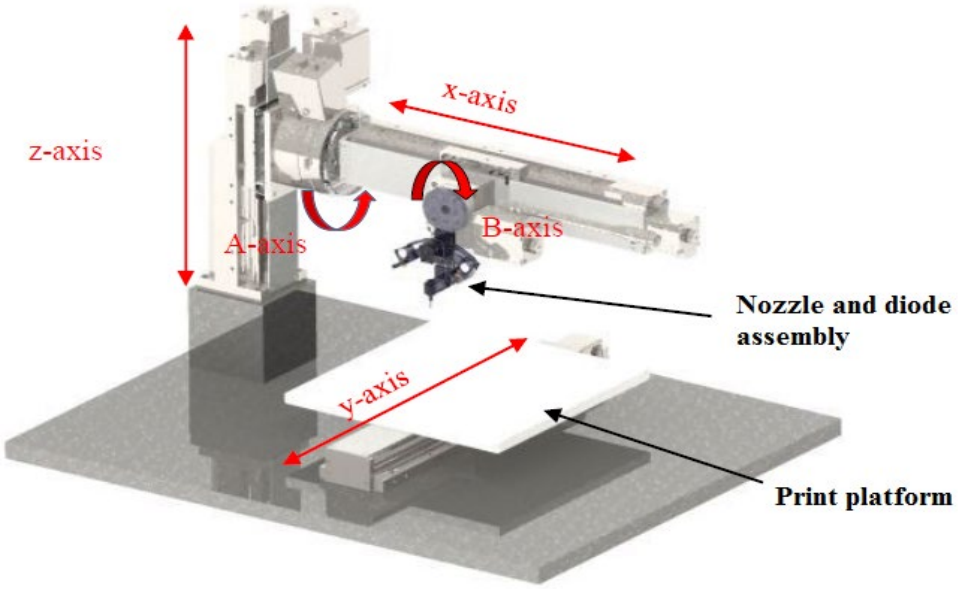

Figure 3.4 A schematic of the 5-axes photopolymer extrusion printer

Figure 3.5 shows a picture of the PPE printer showing the 5-axes and a close-up of the nozzle with laser diodes mounted on each side.

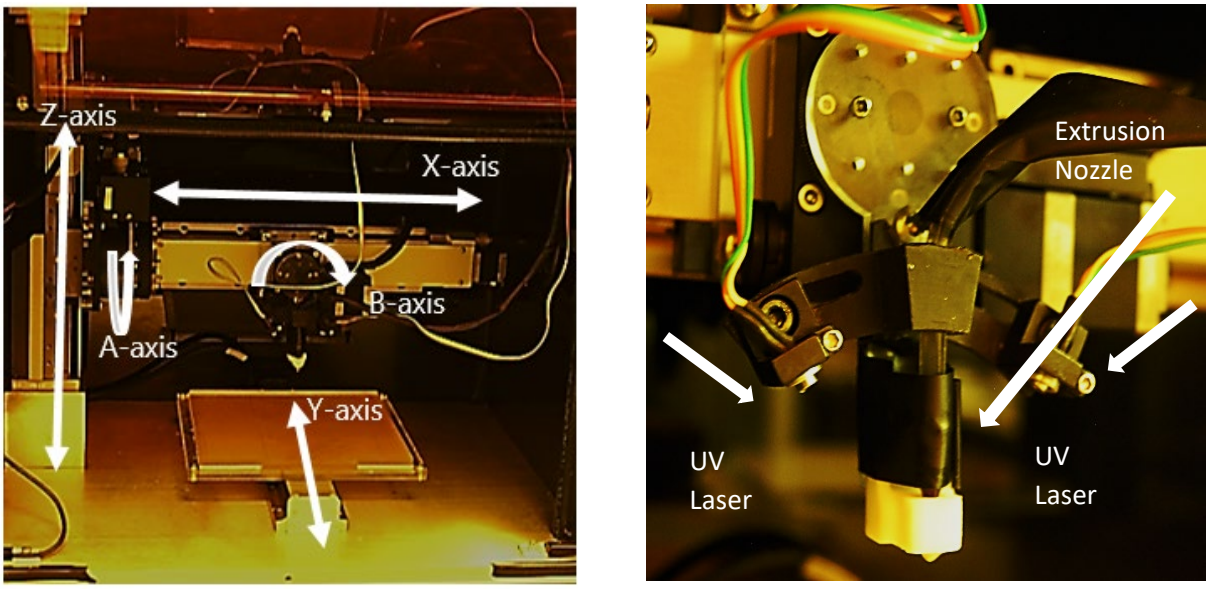

(a) (b)

Figure 3.5. (a) 5-axes PPE printer (b) UV laser and extrusion nozzle

All axes can be controlled simultaneously for continuous adjustment of the nozzle angle and position while printing complex objects. Most importantly, the 2 additional rotational axes are implemented by mounting rotational motors on the built platform. These 2 additional rotational axes (A and B) provide better printing of free-form and free standing objects (for example a helical object). By having more degrees of freedom, the extrusion nozzle has the ability to move in a more complex path providing the ability to print much more complex objects.

As the aim of the system is to print complex free standing and free-form structures, the extrusion system must be capable of delivering a precise amount of fluid in small quantities and have sufficient power to push the viscous fluid through the nozzle. Deposition should be done through a small nozzle tip to control its output, a 21 gauge (0.51 mm) nozzle is used in this study. A pair of peristaltic pumps as shown in Figure 3.6 is used to deliver the photopolymer blend from a reservoir to an extrusion nozzle. In comparison to the common

use of syringe drivers [104, 105], the size of the material reservoir is not related to the smallest volume increment that can be dispensed enabling multi-scale printing. An Arduino microcontroller [106] and the open source host software Pronterface [107] control the machine. The entire equipment is enclosed in a UV-opaque case to prevent unwanted curing of the resin from ambient white light, and protect the operator from laser radiation.

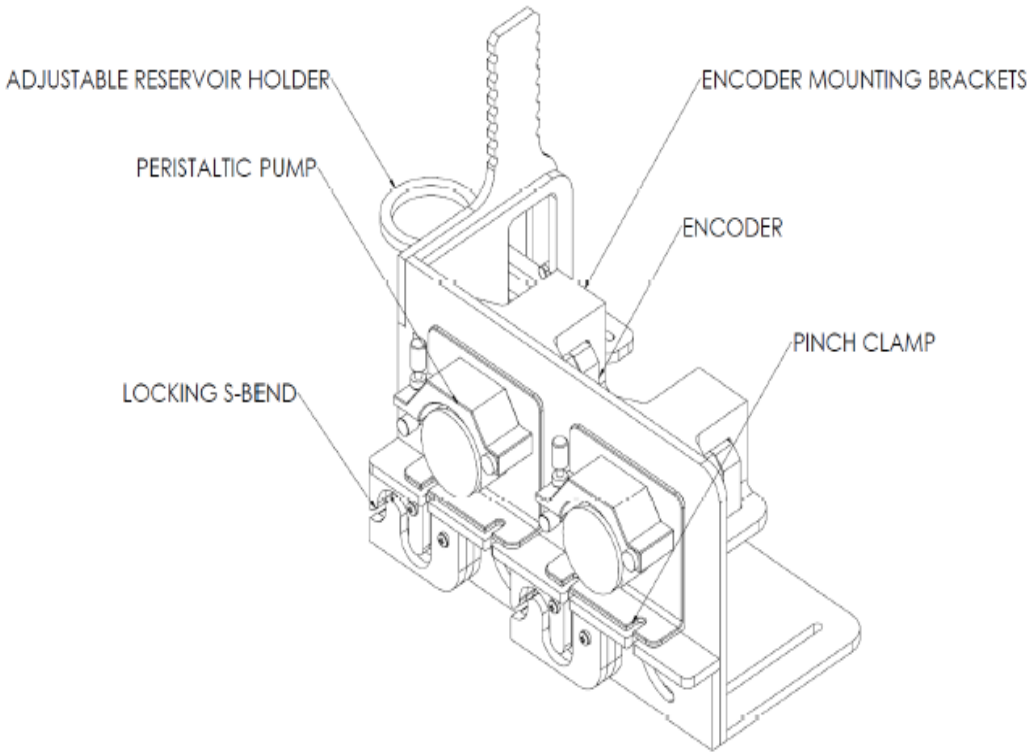

Figure 3.6 Extrusion system assembly including peristaltic pump

3.4.1 Integrated slicer and print communication software

The modified Marlin firmware communicates with the printer communication programme called Printrun [107] shown in Figure 3.7. It is an integrated software with slicer utility, Slic3r, and it consists of a command window to send G-code (Pronsole), G-code command entry with graphical user interface (Pronterface) and graphical model viewer.

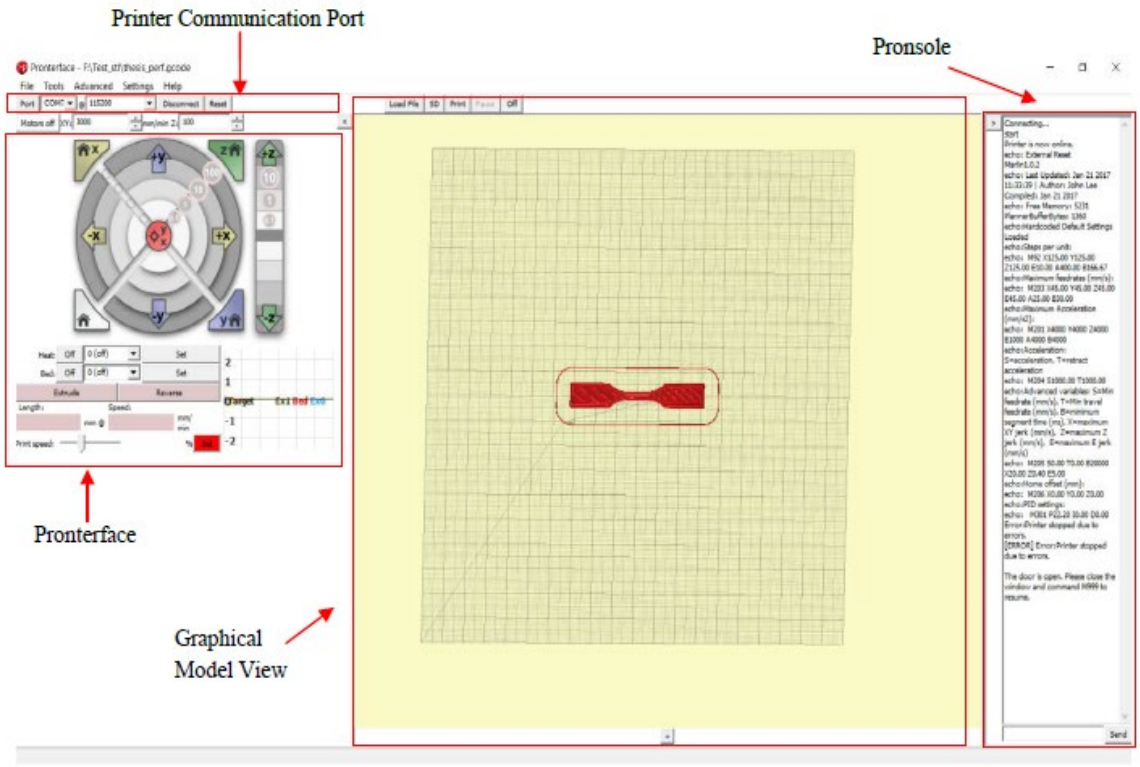

Figure 3.7. Printer communication programme

Printrun is chosen as user communication interface due to its capability to send commands directly to the printer. This gives flexibility to handle the variables, codes and to troubleshoot errors with ease without modifying the embedded software. Errors such as triggering endstops of translational axes and detection of door open will be reported by the Pronsole.

The software also gives a graphical model view that shows the print path in real time. The imported G-code file can be accessed from the console for monitoring and editing. It also estimates the time taken for the object to be printed. The software communicates with the designed 3D printer with a default baudrate of 115200. The connection can be controlled on printer communication port as seen in Figure 3.7. Another useful feature that Printrun utilises is Pronterface, which provides a graphical user interface to control the translational axes and extrusion of materials manually.

Printrun is integrated with a slicer program, Sli3er that generates G code by importing a stl file formatted CAD model. It slices the model into several layers so that the print undergoes a layer upon layer process. The program allows the user to manipulate the print settings and to optimise the printing process. As seen on Figure 3.8, a model is imported in stl file format. It is divided into 4 main sections: plater, print settings, filament settings, and printer settings. The plater allows the user to arrange and transform the objects freely.

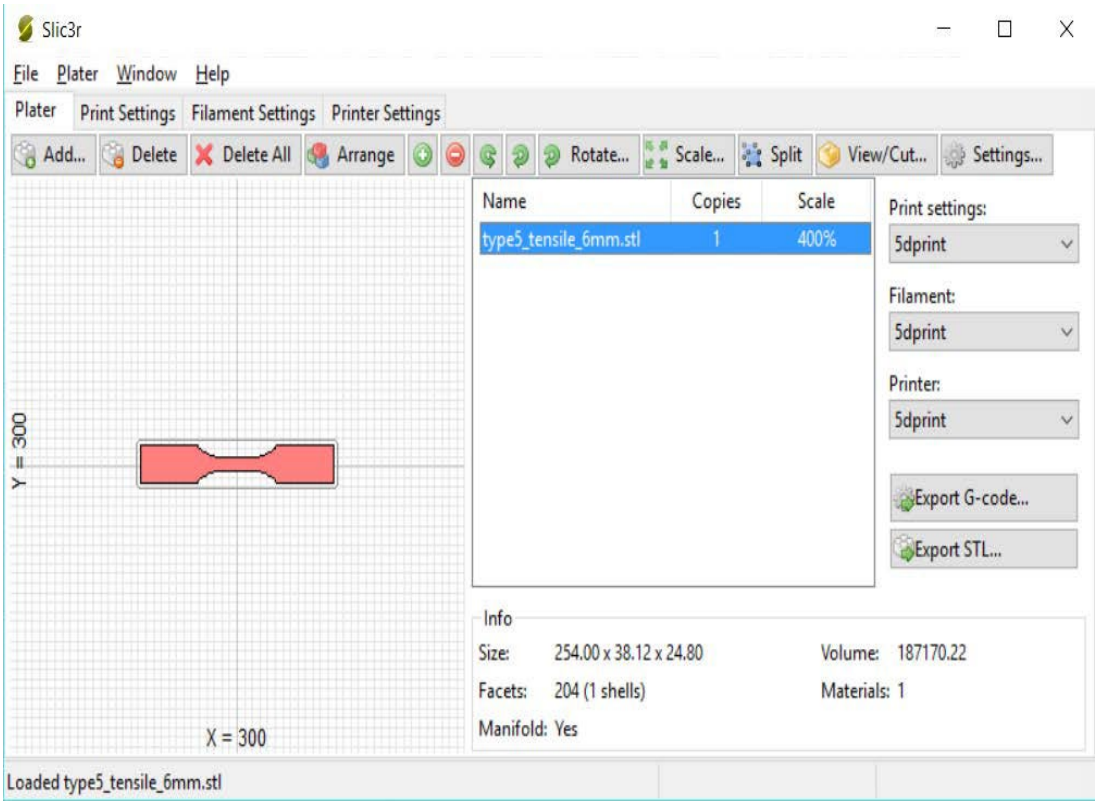

Figure 3.8. Slicer programme

Print settings give options to change several variables that influence time taken and quality of the printed object. They are divided into following sections: layers and perimeters, infill, speed, skirt and brim, and support material.

3.4.2 UV curing system

The UV curing system uses two UV laser diodes as shown in Figure 3.9 (a) placed around the extrusion head to provide even curing of the extruded photopolymer. The purpose of using UV laser as curing source is to focus on the deposited polymer without affecting surrounding material. The lasers have an output power of 40 mW with a wavelength of 405 nm (Thorlabs DL5146-101S) [108] which can rapidly cure the resin. The laser beams have an elliptical profile with beam divergence of 8 degrees in the narrow axis of the ellipse and perpendicular divergence of 19 degrees in the long axis of ellipse as shown in the Figure 3.9 (b).

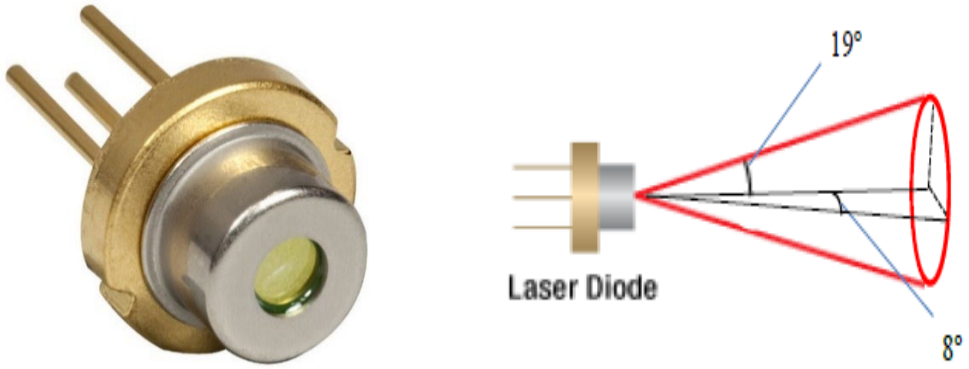

(a) (b)

Figure 3.9. (a) UV laser diode (b) laser elliptical profile

A holder unit is designed to hold up to 2 lasers; i.e. one laser on each side of the nozzle head Figure 3.10. The holder unit is directly mounted on B-axial rotary stage and can easily be removed for maintenance and troubleshooting. The unit is made of mainly acrylic as it is light weighted, easily manufactured and replaceable if problem arises.

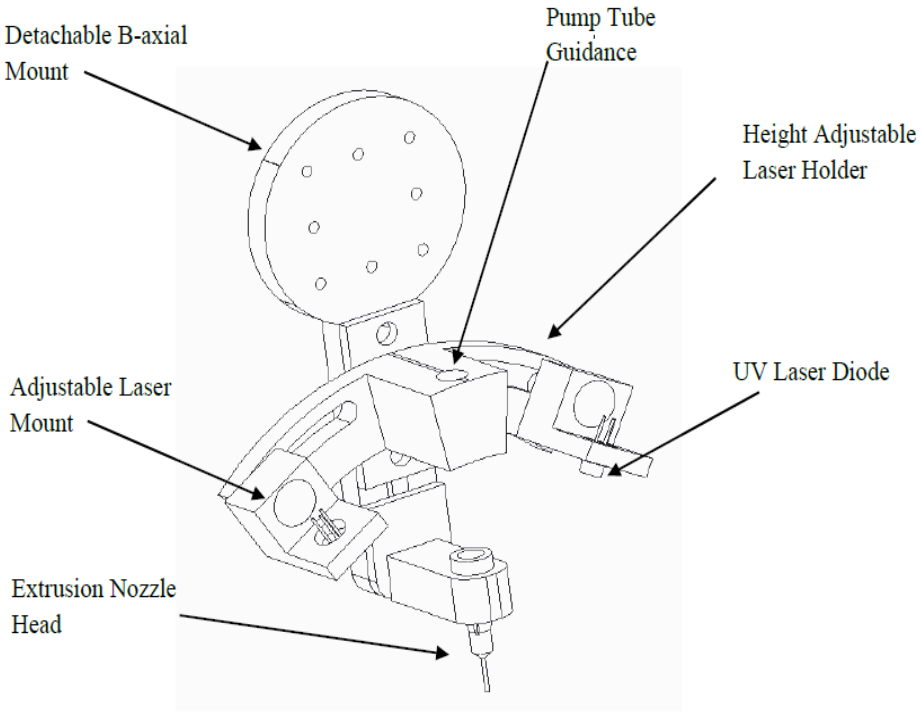

Figure 3.10. Holder unit

3.5 Preparation of UV curable resin

The photopolymer resin (UV Dome 58) being extruded was commercially procured from Whitehall Technical Services Ltd, Auckland, New Zealand. It is based on a proprietary epoxy acrylate that is designed to be cured with UV exposure at 405 nm. Fillers due to their high stiffness can be used to diversify and improve mechanical properties [109]. In this study, fumed silica is added to the resin. The fumed silica is used to control the fluid viscosity and may be useful for increasing the mechanical properties [109]. Fumed silica has nanoparticles with a very large surface area and a low bulk density. Before mixing, it is in the form of a white powder. The powder is very lightweight and insoluble with water. With adequate homogenisation, it is possible to mix the fumed silica particles with other components of the resin. Adding silica changes the rheological behaviour of the resin, adjusting the viscosity of the fluid [110]. As shown in Figure 3.11, the fumed silica nanoparticles have a spherical shape with diameters ranging approximately between 25 to 30 nm. The particles make up long chains

or form agglomerates. The diameter of agglomerates depends on the interaction conditions when the particles are mixed with the resin.

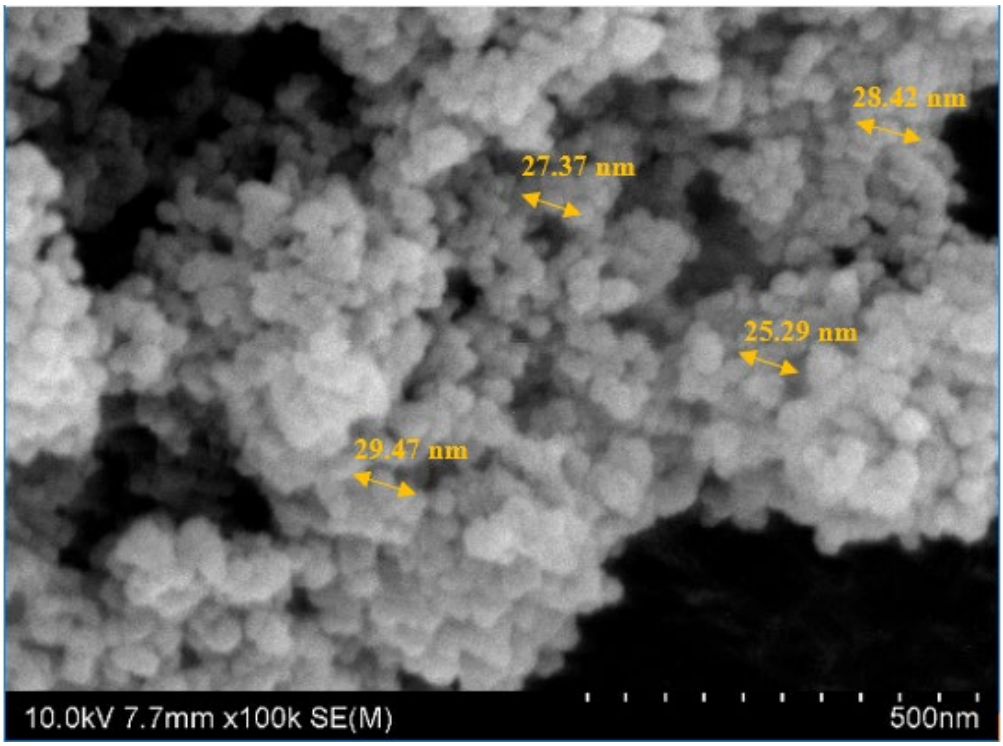

Figure 3.11. SEM image of the fumed silica nanoparticles

To investigate the mechanical properties of printed parts, samples were prepared with different concentrations of the silica filler (by weight) mixed into the resin. Mixtures were prepared the same day to have samples with the same aging and were prepared inside a room with UV-free illumination to avoid premature curing. A total of 100 g of mixture was made for each concentration, for instance for a mixture with 2% filler by weight, 98 g of the resin was mixed with 2.0 g of fumed silica. After a slow manual stirring for 5-10 minutes with a thin spatula, the mixture was treated with an ultrasonic homogeniser. The Sonics and Materials Inc ultrasonic homogeniser [111] was applied for 2 periods of 1 minute at 20 kHz of ultrasound frequency and 130 W of intensity. Finally, to remove air bubbles from the mixture, the samples were degassed in a vacuum oven for 45 minutes at 65 $^{\circ}$C.

3.6 Results and discussion

The key parameters for the material (such as filler concentration) and printing process (such as extrusion rate) were investigated to observe their effects on the dimensional accuracy and mechanical strength of the printed objects.

3.6.1 Effect of filler on material viscosity

In order to obtain smooth extrusion, the viscosity of the resin must lie within a certain range. If the viscosity of the resin is low, it is likely to spread due to gravity before it can be cured by the UV laser, but if the viscosity is high, it will be difficult to extrude the resin through the nozzle. Therefore, the resin viscosity was measured with different filler concentrations using a rheometer and their printability was observed.

Resins with 2%, 4%, 6%, 8%, 10%, and 12% of fumed silica by weight were prepared as per section 2.2. The dynamic viscosity of each concentration was measured using a rheometer (Brookfield Ltd DV3T Extra)

The rheometer drives a spindle immersed in the fluid to be tested, through a calibrated spring. The user gives a constant rotational speed value (rpm) to the spindle and the fluid, inside a stationary cylinder container. The viscous drag created by the rotational force (or moment force or torque: τ) against the spindle is measured by the spring system.

In order to accurately measure the viscosity of the resins with the concentrations of fumed silica mentioned above, a 64 gauge spindle as shown in Figure 3.12 was used. For each sample, the revolution speed was adjusted to achieve a torque close to the midpoint (50%) of the sensor range. The rheometer then calculates a viscosity value based on the spindle, speed, and measured torque. Table 3.3 lists the parameters used and the measured viscosities.

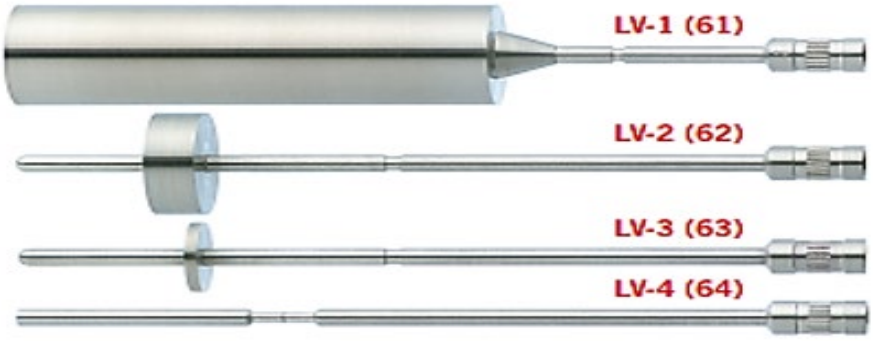

Figure 3.12 Different spindles used to calculate viscosity

Table 3.3. Rheometer parameters and measured viscosities

Filler Concentration (%)	**Spindle**	**Speed (rpm)**	**Torque (%)**	**Time (s)**	**Viscosity (cP)**	**Viscosity (Pa.s)**
0	64	50	50.4	36	6048	6.05
2	64	40	50.3	35	7545	7.54
4	64	38	52.5	37	8289	8.29
6	64	35	58.1	58	9960	9.96
8	64	21	52	30	14860	14.9
9	64	18	50.7	33	16900	16.9
10	64	12	50	33	25000	25
11	64	10	59.5	41	35700	35.7
12	64	4	53.2	32	79800	79.8

Higher viscosity can cause difficulties during printing, resulting in inconsistent extrusion. Low viscosity results in material not being able to stay in shape while being cured by the pulsed UV beam. Therefore, defining an appropriate range of viscosities to precisely extrude the material from the deposition nozzle is very important. As shown in Figure 3.13, dynamic viscosity increases substantially with increasing percentage of filler. Fillers up to 6% were found to have low viscosity, while viscosity increased rapidly for filler concentrations greater than 9%. With the printer using a 21 gauge (0.5 mm) nozzle, only a narrow window of filler concentrations of 8%, 9% and 10% (corresponding to the dynamic viscosities of 15000 cP and 25000 cP) were found to be suitable to print reliably. However, 10% filler concentration still found to be a bit difficult to print. Therefore, in this chapter mechanical properties of 8% and 9% filler concentrations will be studied and analysed.

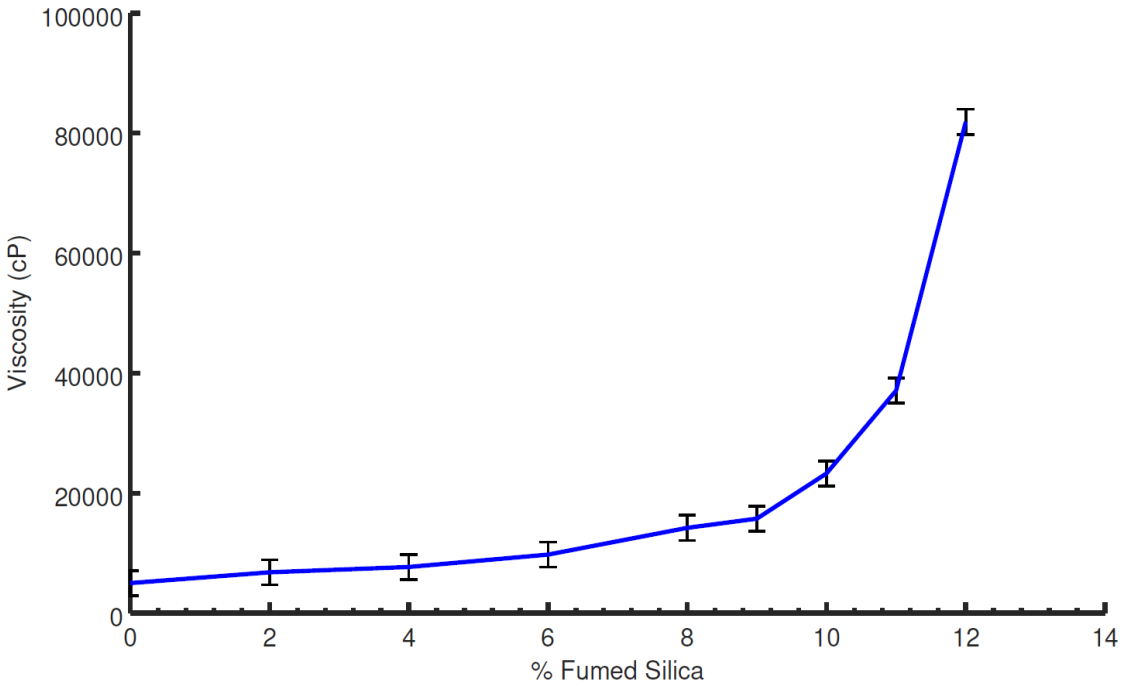

Figure 3.13. Effect of filler concentration on dynamic viscosity

3.6.2 Effect of filler on dimensional accuracy

The aim of dimensional accuracy measurement was to study the effect of filler on printed dimensions, ideally printed dimensions should closely resemble with CAD model dimensions.

In the present work, width (at two positions) and thickness of the printed samples were taken into account with CAD model as a reference. Figure 3.14 presents the average and deviation of the printed dimensions of width (at two positions) and thickness of samples printed with 8% and 9% filler concentrations. Three samples were printed and measured for each filler concentration. From Figure 3.14, the variation in the printed dimensions are slightly higher in 9% filler samples. The thickness of 9% filler sample is higher as the uncured material with this high filler percentage has higher viscosity; hence less spread out sideways than 8% filler samples. Higher filler concentration may lead to more deviated printed dimensions, as it is difficult to extrude from the deposition nozzle owing to its higher viscosity. The printed part could vary from the nominal dimension and obtaining a part with very high precision is often not possible.

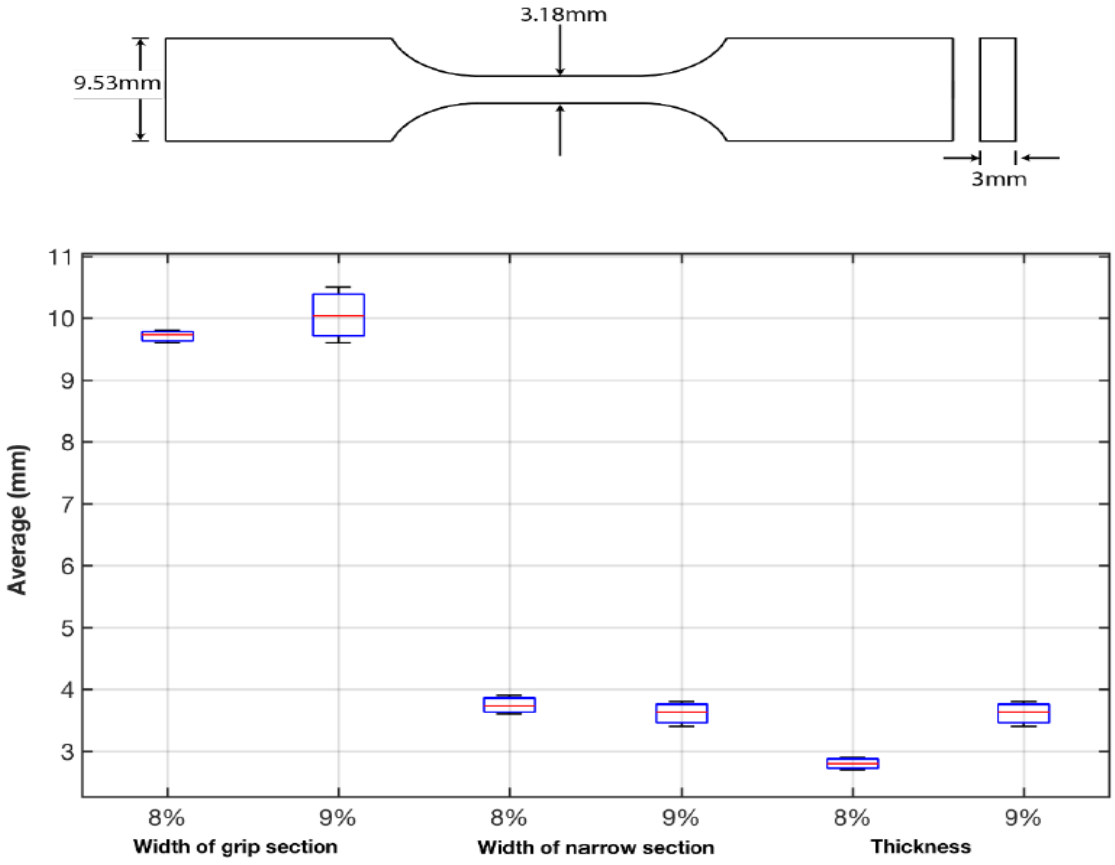

Figure 3.14. Comparison between designed and printed dimensions

3.6.3 Effect of filler on surface roughness

Effect of filler on surface roughness was analysed using the optical profilometer, this instrument measures the roughness of the surface in terms of Ra and Rq values. Optical profiliometer is a non-contact method with a confocal laser scanning microscope (CLSM). It generates the 3D images of the surface at a nano to micro range. Surface roughness tests were conducted on 8% and 9% filler concentrations, specimens were first coated as the profilometer works with reflection of photons. Figure 3.15 show the dog-bone specimen before and after coating.

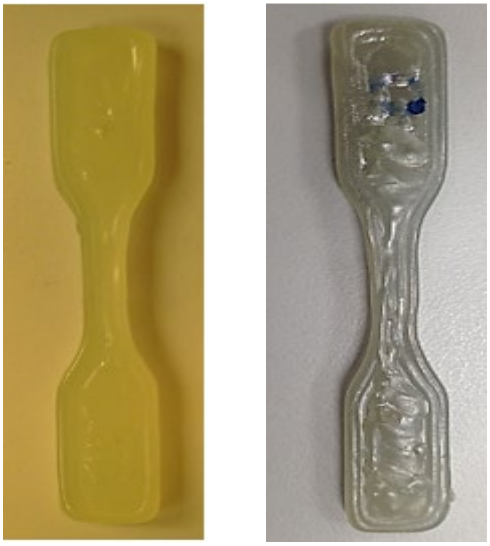

(a) (b)

Figure 3.15. Printed dog-bone specimen (a) before coating (b) after coating

Gage lengths of the samples with 8% and 9% filler concentrations were scanned as shown in Figure 3.16. Three different values of Ra and Rq (or RMS) were obtained on the scanned image and the average of these values was calculated.

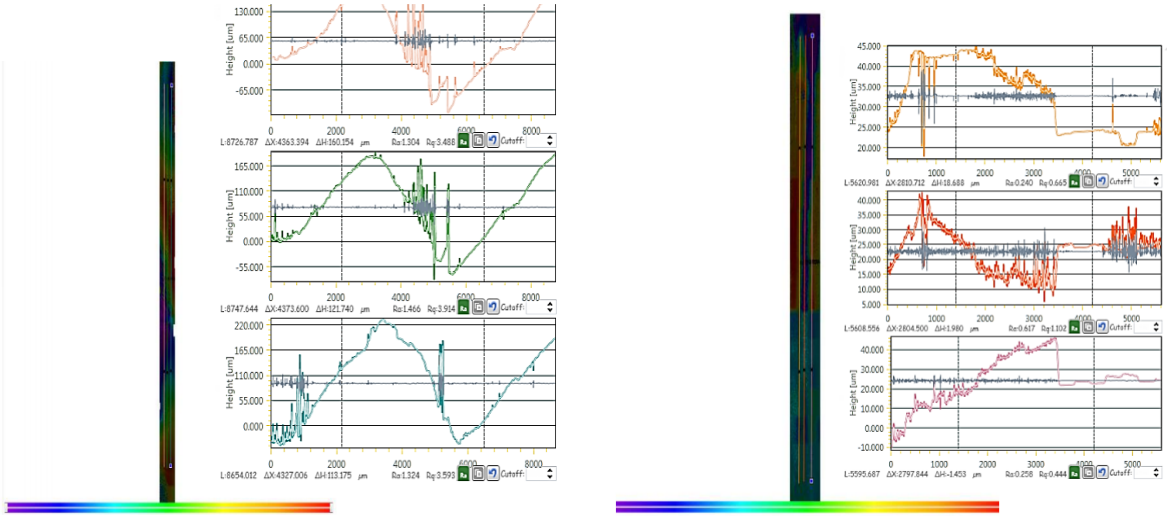

(a) (b)

Figure 3.16. Surface roughness measurement of (a) 8% filler concentration (b) 9% filler concentration

Table 3.4. Surface roughness parameters of 8% and 9% filler concentrations

Filler concentration	**Ra (µm)**	**Rq (µm)**
8%	1.304	3.488
	1.466	3.914
	1.324	3.593
Average	1.365	3.665
9%	0.24	0.665
	0.617	1.102
	0.258	0.444
Average	0.372	0.737

As it is evident from Table 3.4, Ra and Rq values of 9% filler concentration are lower than 8% filler concentration indicating 9% filler concentration has better surface roughness. This could

be due to lower viscosity of 8% filler compared to 9% filler as the filler with low viscosity tends to spread sideways which leads to uneven surface during printing. Scanning electron microscopy (SEM) was used to further analyse the surface of 8% and 9% filler concentrations before fracture. As evident from Figure 3.17, 9% filler concentration has smoother surface compared to 8% filler which confirms the findings of optical profilometer.

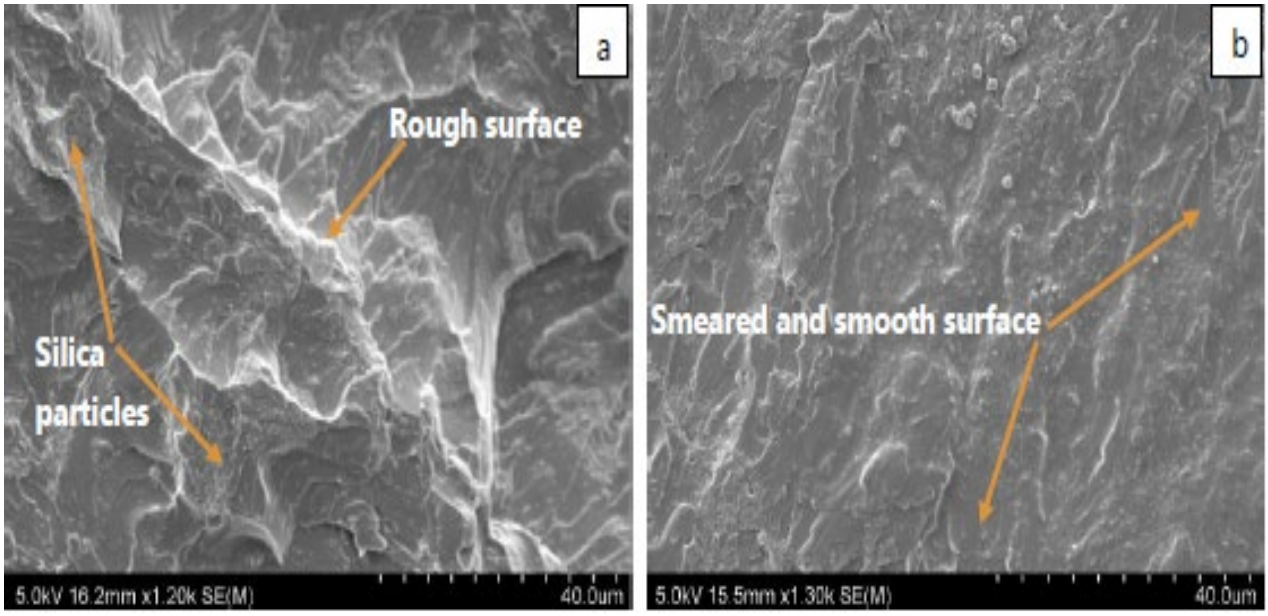

Figure 3.17. SEM image of (a) 8% filler concentration (b) 9% filler concentration

3.6.4 Effect of filler on mechanical properties

In order to test the strength and quality of the printed objects, dog-bone samples of specific dimensions (adopting ASTM D638 standard type V as shown in Figure 3.18) were 3D printed (see Figure 3.19). Table 3.5 represents the process parameters used to print 8% and 9% samples. Tensile and 3-point bending tests were conducted on these samples to characterise tensile strength, Young's modulus, strain at break and flexural strength.

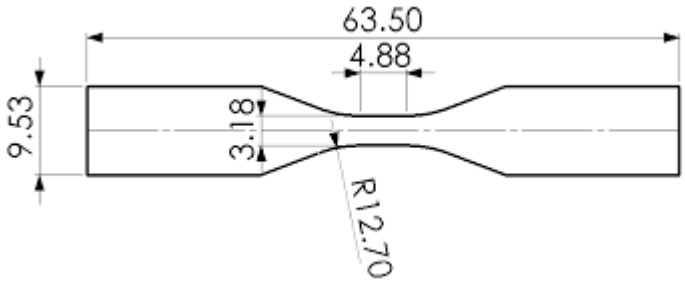

Figure 3.18. ASTM D638 type V specimen

Figure 3.19. 3D printed specimen

Table 3.5. Process parameters for 8% and 9% samples

Process parameters	**Variables**		
Print setting	Layers and perimeters	*Layer height (mm)*	3.22
		First layer height (mm)	0.20
	Infill	*Fill density (%)*	40
	Speed (print moves)	*Perimeters (mm/s)*	20
		Infill (mm/s)	40
	Overall time/sample	*(min)*	10
Filament setting	Filament	*diameter (mm)*	1
	Extrusion	*Extrusion multiplier*	0.0055

3.6.4.1 Tensile test

Improved mechanical properties e.g. tensile strength and Young's modulus may be achieved by optimising the filler loading due to increase in weight fraction or volume fraction leading to a continuous and uniform interface, which creates a strong polymer network [112]. A large amount of research has been conducted on different polymer nanocomposites in order to study the effect of weight fraction and volume fraction (%) on mechanical properties of polymer

nanocomposites [112-117]. In an attempt to understand the effect of weight fraction of silica nanoparticles on mechanical properties of epoxy, Liu et al. calibrated Young's modulus and tensile stress at different weight fractions [113]. They reported gradual increase in both Young's modulus and tensile strength with an increase in weight fraction of silica nanoparticles. Other studies have also been conducted on the effect of different weight fractions of silica nano-particles on tensile stress and Young's modulus of epoxy resin [112, 118]. They found that values of Young's modulus and yield stress of epoxy-silica nanocomposite at 20% weight fraction are 1.22 and 1.28 times the value of pure epoxy [118]. In order to study the effect of our chosen filler on mechanical properties of the nanocomposite, resins with 8 % and 9% silica nanoparticles were used. Six pieces for each concentration were printed. Tensile and flexural strengths were then determined from tensile and 3-point bending tests respectively.

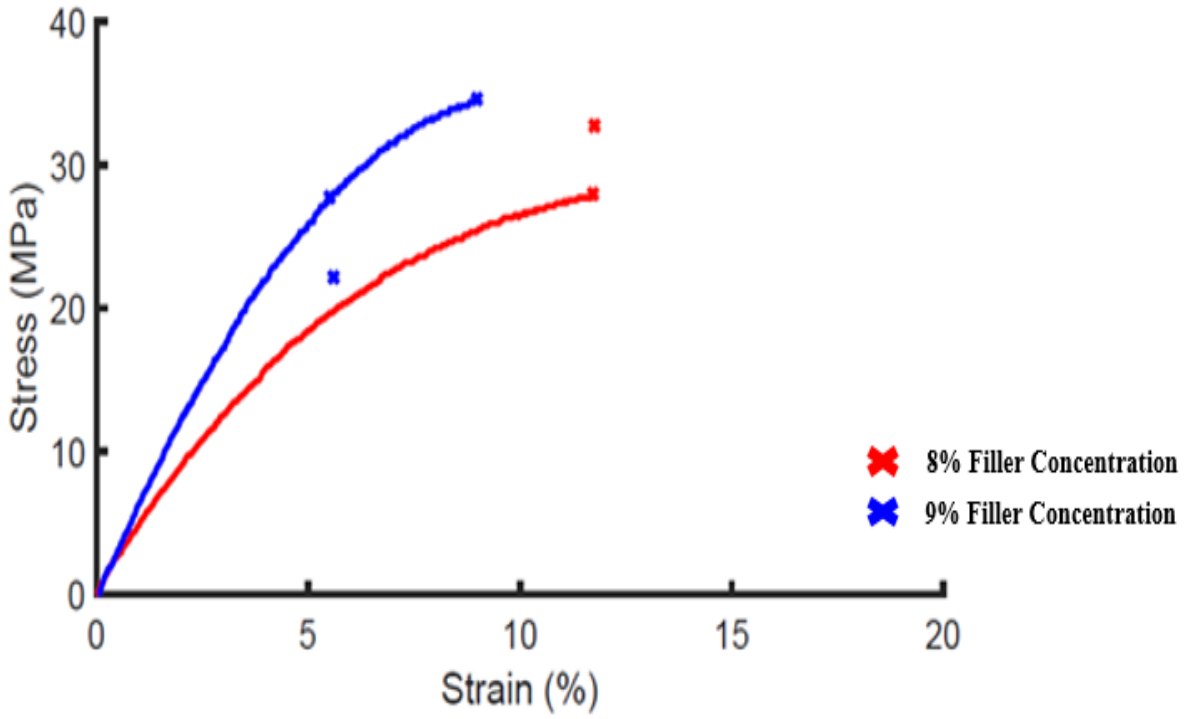

Figure 3.20 Tensile stress-strain diagram

Figure 3.20 shows the stress-strain diagram representative of 2 different filler concentrations. It is quite evident from the stress-strain diagram that samples printed by 8% filler have higher strain at break, while the samples printed with 9% filler have higher yield stress. Table 4 shows the tensile properties of samples with 8% and 9% filler concentrations. It indicates that higher filler percentage made the samples less elastic.

As shown in Table 3.6, a significant increase in the Young's modulus is observed with increasing the filler content, suggesting efficient transfer of stresses via interface and high interfacial stiffness. Effective stress transfer form matrix to nanoparticles is only possible when interfacial adhesion between the two is good, if the bond between the matrix and filler is weak, stress cannot be effectively transferred from matrix to nanoparticles which results in weak mechanical properties, therefore the effect of interfacial adhesion on tensile strength of 3D printed nanocomposites is discussed in detail in chapter 4.

Due to the high rigidity of silica nanoparticles, tensile strength and Young's modulus of the particulate nanocomposite is increased with increasing the filler content compared with the neat resin. It was found that the average tensile strength of 8% and 9% filler concentrations is 4.13 and 4.26 times and average Young's modulus is 6.68 and 8.13 times the value of neat resin, respectively. As the standard deviations shown in Table 3.6 are not high in comparison to the difference between the averages of the sample groups, the experimental results are reasonably low-variance.

Table 3.6. Tensile properties for 8% and 9% filler concentrations

Filler concentration (%)	Average ultimate tensile strength (MPa)	Standard deviation (UTS)	Average Young's modulus (MPa)	Standard deviation (Young's modulus)	Average yield (MPa)	Standard deviation (Yield)	Average strain at break (%)	Standard deviation (strain at break)
8	30.2	3.1	478.5	79.9	13.9	2.1	15.0	4.7
9	31.1	4.9	582.3	65.3	15.8	3.1	7.1	2.4

3.6.4.2 Flexural test

Researchers have reported the flexural properties of silica nanocomposites; e.g. Hsiao et al [119] reported flexural strength of ductile and brittle matrix epoxy-silica nanocomposite and observed linear increase in flexural strength with increase in particle loading.

A 3-point test was used to determine the flexural properties of the printed objects with 8% and 9% filler. Table 5 summarises the results of the 3-point tests. As listed in Table 3.7, the increase in flexural strength of nanocomposite compared with neat resin can be observed which is due to the reinforcement with silica nanoparticles. Both concentrations of 8% and 9% found to have nearly the same flexural strength. Again, it shows that higher percentage of filler makes the sample slightly more brittle.

Table 3.7. Flexural properties of 8% and 9% filler concentrations

Filler concentration (%)	Average F_{max} (N)	Standard deviation (F_{max})	Average max deflection before break (mm)	Standard deviation (Max deflection before break)	Average flexural strength (MPa)	Standard deviation (flexural strength)
8	16.3	0.8	8.5	2.1	18.8	1.4
9	14.6	0.8	7.9	1.3	18.4	1.0

3.7 Free-form and self-supported structures

The basic capability of printing free-from and self-supported structures using this 5-axes extrusion printer was demonstrated, including exploiting the two rotational axes A and B. Since there is no available translational algorithm to convert the CAD model into a free-from printing path, the printing of free-from and self-supported structures is controlled through manually generated G-code. As this is in the preliminary development stage, the demonstrated free-form structures will be limited.

Figure 3.21 shows the printing of a self-supporting staircase shape object. This is done by moving the x, y, z and B axes. Figure 3.21 shows how the fourth axis; i.e. the B-rotational axis is turned by 30° with respect to the z-axis, when the horizontal traces are being printed.

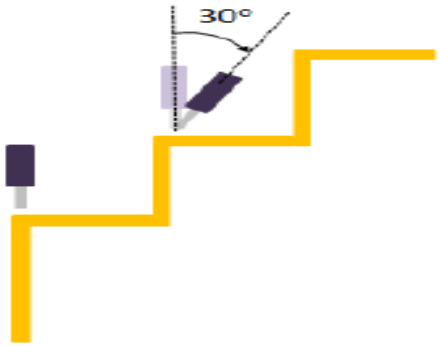

Figure 3.21. Diagram indicating nozzle orientation (B-axis) for printing vertical and horizontal sections of the staircase object

The staircase objects in Figure 3.22 show the progression of altered printing parameters. The printed staircase objects has the first step height of 20 mm, and subsequent steps are 10 mm tall. The difference between the models in Figure 3.22 (a), (b), and (c) are varying feed rates for motion in the z- and x-directions, as well as when rotating, and varying extrusion rates.

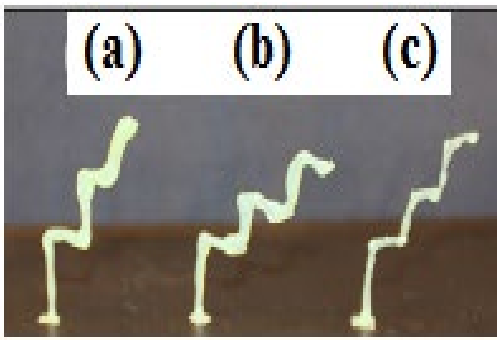

Figure 3.22. Staircase printed models (a) extrusion too high (b) slow rotation feed rate (c) smaller extrusion but faster feed rate

Table 3.8 shows that the printing parameters corresponding to Figure 16 (c) providing relatively better dimensional accuracy.

Table 3.8. Printing parameters for Figure 3.22 (c)

S.No	Printing Parameters	Value
1	Vertical Feed Rate	21 mm/min
2	Horizontal Feed Rate	19 mm/min
3	Extrusion	1.4 mm/min
4	Rotation Angle (B-Axis)	30°
5	Laser Angle	40°

Finally, to demonstrate the 5 axes capability of the printer to print a self-supporting and free form structure, a horizontal U-shape was printed as shown in Figure 3.23. This requires all the x, y, z, A and B axes to move. The nozzle has its B-axis tilted to 45° (along y-axis) with respect to the z-axis when it travels at the bend and then reduces slightly to 30° while tilting the A-axis to 10° (along x-axis) with respect to the z-axis as it travels to the right. As the nozzle travels along the U-bend, the B-axis is being tilted in steps to -30°. Then the nozzle will return the A-axis angle to 0° and B-axis to 45° when travelling to the left. Finally both A and B axes will

change to 0° to print the vertical trace. Blobs were formed during the printing process when the angle of A or B changes and to eliminate these blobs and ensure consistent diameter throughout the print, a better control of the polymer extrusion is required in the future. However, this preliminary demonstration has showed the capability of the 5-axis PPE printer to print free-form structures.

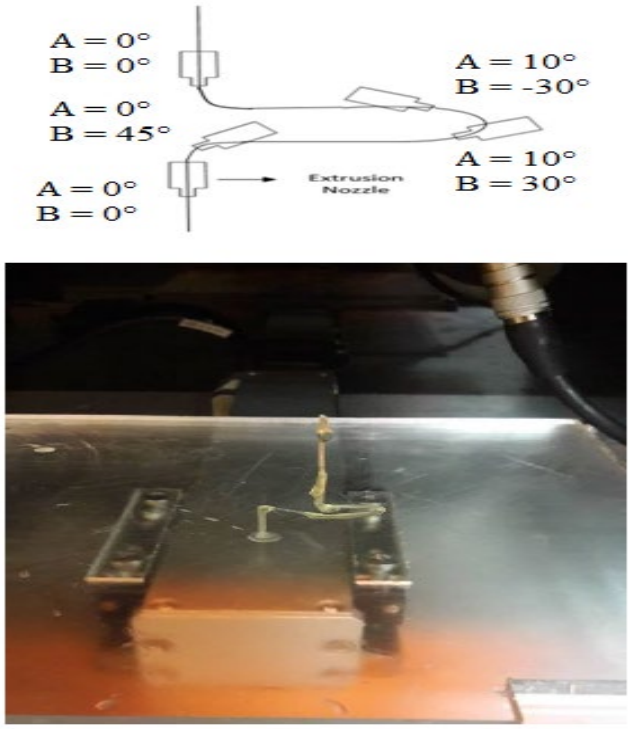

Figure 3.23. Free-form horizontal U-shape

3.8 Chapter summary

A 5-axis photopolymer extrusion 3D printer has been developed and tested. The system extrudes UV-curable resin through a nozzle moving in free space, while rapidly curing the deposited material using UV diode lasers. Because the nozzle can be rotated around two axes to approach a point in space from the desired angle, and the UV lasers cure the photopolymer resin quickly as it leaves the nozzle, the method is suitable for printing of freeform structures. To reinforce the resin, and achieve proper viscosity for proper extrusion, fumed silica is added to the uncured resin to form a composite. The fumed silica content helps ensure that the

extruded resin stays in form long enough to be cured through UV exposure without flowing as well as improves the mechanical properties of the photopolymer significantly. 8 % to 10% filler concentration was found to be suitable with the current nozzle size.

Dog bone samples were printed to investigate whether adding filler in the photopolymer have any effect on mechanical properties and dimensional accuracy of the printed parts. The strength of the fabricated parts was measured through tensile and flexural tests. It was found that silica filler significantly increased the tensile and flexural strength.

Although a system capable of printing self-supporting and free-form structures have been successfully demonstrated, future work will be required to improve the smoothness and accuracy of the printed objects. Also, automated software (comparable in function to the slicing software for conventional 3D printing) to generate and optimise the complex 5-axis printing path is required and an on-going research concern.

Interfacial adhesion i.e. effective stress transfer from matrix to nanoparticles plays a key role in the improvement of the mechanical properties, a detailed study on interfacial adhesion of the parts printed using photopolymer extrusion technique is discussed in next chapter.

CHAPTER 4: EFFECT OF INTERFACIAL ADHESION ON TENSILE STRENGTH OF PARTICULATE NANOCOMPOSITES PRINTED WITH PHOTOPOLYMER EXTRUSION TECHNIQUE

4.1 Introduction

To overcome the apparent limitations of polymers such as low stiffness, low yield and low strength inorganic particulate fillers such as micro/nano silica, Al_2O_3, $Mg(OH)_2$, $CaCO_3$ particles, glass and carbon nanotubes are commonly used in the manufacture of polymer composites. These fillers diversify the mechanical and physical properties of polymers by introducing their rich mechanical behaviour. By adding either micro or nano particles, Young' modulus or stiffness can be dramatically improved owing to higher stiffness of the micro or nano particles compared to polymer matrices [120-128]. Also, it is evident from chapter 3 sections 3.6.4.1 and 3.6.4.2 that adding nano silica filler significantly enhances the tensile and flexural properties of the photopolymer. However, strength is heavily dependent on the effective stress transfer between particles and matrix. If the bond between the matrix and particle is good, stress can be effectively transferred from the matrix to particles, and this leads to increase in the strength [120, 129-133]. However, for poorly bonded micro particles, strength is found to decrease with increase in filler content [121-123, 134-138].

The mechanical properties of polymer matrix nanocomposites rely on three main characteristics; i.e. particle size, matrix-particle adhesion and particle loading. Matrix – particle interface adhesion, plays an important role in enhancing the mechanical properties of polymer composites. For instance, tensile strength of glass bead filled polystyrene composites is dependent on matrix–particle adhesion and found to have increased with it [121]. Thus, coupling agents are used, which helps increasing particle-matrix adhesion resulting in higher strength [126, 139-142]. Rigid inorganic nanoparticles, for example, silica and calcium

carbonate, not only improve the toughness, but also enhance the tensile strength. However, interfacial adhesion between nanoparticles and matrix plays a key role in improving the mechanical properties. Jancar and Kucera [143, 144] found that weak adhesion between Polypropylene (PP) and $CaCO_3$ resulted in decrease in tensile strength with the increase of volume fraction of $CaCO_3$. It is quite evident that matrix-particle interfacial adhesion, particle size and particle loading affect mechanical properties of polymer matrix nanocomposites.

Significant amount of research were conducted on 3D printing of polymer matrix composites [145-148], which were also discussed in detail in chapter 2. These researchers have reported significant improvement in elastic modulus (up to 57 GPa in tension) [148] and the control of filler orientation and architecture [145], but the 3D printed particulate nanocomposites have not been comprehensively characterised and investigated in the context of interfacial adhesion. In addition, as mentioned in previous chapters, the printing technique proposed in this research is new and little has been done to study the interfacial adhesion of the samples printed using this technique. Therefore, in this chapter, we investigate the effect of interfacial adhesion on the mechanical properties of particulate nanocomposite printed using this novel printing technique. In order to demonstrate superior mechanical properties of 3D printed particulate nanocomposites a comparison is drawn from specimens with similar particulate nanocomposites, but instead were mould casted.

4.2 Background

4.2.1 Effect of matrix-particle interfacial adhesion on tensile strength

The strength of polymer matrix nanocomposites heavily depends on the effective stress transfer from matrix to the particles. When the matrix-particle bond is weak, the stress transfer at matrix-particle interface is inefficient. Defects in the form of debonding exists due to non-adherence of particle to matrix. Thus, the particles are unable to carry any externally applied

load and the decrease in composite strength is observed with increasing the particle content. However, for effectively bonded composites, the addition of particles will result in increased strength especially for high surface area nanoparticles [149].

In the case of the stress not able to be transferred from matrix to the filler, the strength of polymer-matrix nanocomposite is determined by the available effective region of load bearing matrix in the absence of filler [149]. Interfacial layer is unable to transfer stress and the strength of nanocomposite is dependent on effective load bearing cross sectional area portion $(1 - \varphi)$ as

$$\sigma_c = \sigma_m (1 - \varphi) \qquad (4.1)$$

where σ_c and σ_m are tensile strength of composite and matrix (base material) respectively. Considering φ as a power law function, Eq. (4.1) can be rewritten as:

$$\sigma_c = \sigma_m (1 - a\varphi^b) \qquad (4.2)$$

where φ is volume fraction and a and b are constants depending upon particle shape and arrangement in the composite.

Nicolais and Narkis [138] used Eq. (4.2) and presented a model to predict the tensile strength of nanocomposite reinforced with spherical filler as:

$$\sigma_c = \sigma_m (1 - a\varphi^{2/3}) \qquad (4.3)$$

When particles and matrix possess good adhesion, a small portion of the stress is transferred by the interfacial region, if the deformation of the matrix is very small. In this case, stress is effectively transferred and tensile strength is a combination of the matrix and filler properties. Therefore, parameter a in Eq. (4.3) becomes smaller than 1.21 indicating strong adhesion.

Another model presented by Kunori and Geil [150] associated the tensile strength of composite with parameter a, considering it as stress concentration factor as:

$$\sigma_R = exp\ (-a\varphi) \qquad (4.4)$$

where σ_R is relative tensile strength and expressed as(σ_c /σ_m). Higher values of parameter a indicate higher stress concentration.

A model developed by Pukanszky [130] relates the spontaneous formation of interphase in the nanocomposite considering variation of tensile strength as a function of composition [151]. The model can be written as:

$$\sigma_R = \sigma_m \frac{1-\varphi}{1+2.5\varphi} exp\ (B\varphi) \qquad (4.5)$$

Parameter B is expressed as the load carried by the dispersed phase based on its interaction, which can be considered as a measure of matrix-filler adhesion. The parameter B can be written as:

$$B = (1 + A\rho l) \ln (\frac{\sigma_i}{\sigma_m}) \qquad (4.6)$$

where A is surface area of particles, ρ is the density of particle, l and σ_i are thickness and strength of interphase, respectively.

4.3 Materials and methods

4.3.1 Preparation of UV curable resin

UV curable resin was prepared and mixed with fumed silica filler in accordance with the methodology discussed in section 3.5 of chapter 3.

4.3.2 Fabrication of 3D printed and casted samples

3D printed samples were fabricated using a new photopolymer 5-axis 3D printer as discussed in detail in section 3.4 of chapter 3. Dog-bone specimens of specific dimension as discussed in section 3.6.4 of chapter 3 were fabricated. In order to compare the mechanical properties of 3D printed samples, casted samples were prepared using a mould of the type V dog-bone specimen

as shown in Figure 4.1. UV curable resin prepared as discussed in section 3.5 of chapter 3 and was manually poured into the mould using a syringe and placed under UV light box for 3 minutes. Samples with 8%, 9% and 10% concentration of the filler prepared with two techniques; i.e. 3D printed and casting.

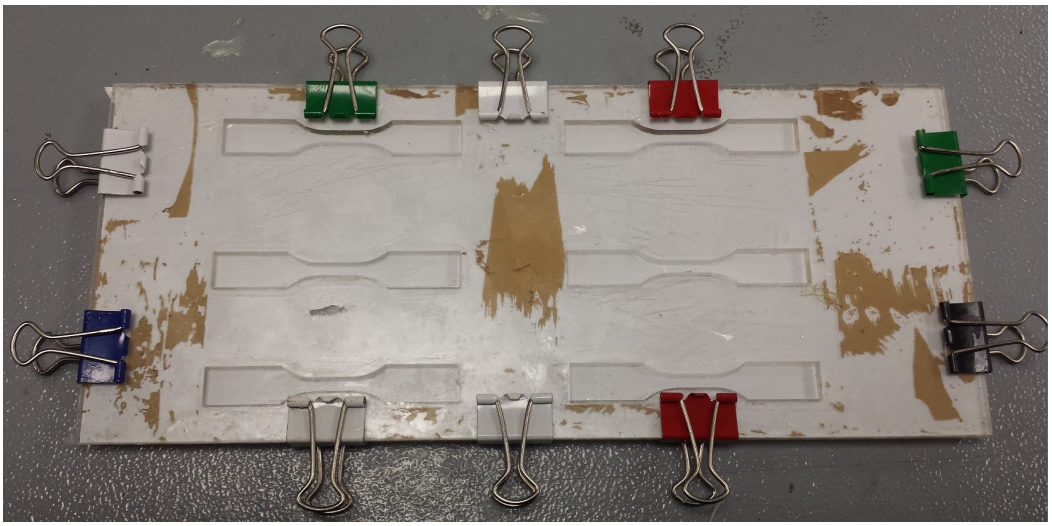

Figure 4.1. Mould used for fabricating casting samples

4.4 Experimental procedure

4.4.1 Tensile test

In order to characterise and compare the mechanical properties (e.g. tensile strength and Young's modulus) of 8%, 9% and 10% filler concentrations samples, tensile tests were conducted. Three dog-bone samples of each concentration of specific dimensions (following ASTM D638 standard type V) were fabricated in accordance with the methodologies discussed in section 4.3. Fillers of 8%, 9% and 10% concentrations were printed and casted as dog-bone samples. Results of the tensile tests are depicted in Table 4.1, and Figure 4.2 shows the printed and cast samples after the test. As the viscosity of the pure resin is too low

to be extruded through nozzle, pure resin samples were only casted and not printed for testing. Tensile testing shows that pure resin have an ultimate tensile strength of 12.87 MPa.

Table 4.1. Tensile properties of 8%, 9% and 10% 3D printed and casted samples

Tensile properties of 3D printed samples				**Tensile properties of casted samples**			
Filler concentration	**Sample**	**Ultimate tensile strength (MPa)**	**Young's modulus (MPa)**	**Filler concentration**	**Sample**	**Ultimate tensile strength (MPa)**	**Young's modulus (MPa)**
8%	a	32.5	535	8%	a	7.5	195.4
	b	28	422		b	12.0	250
	c	16.7	209		c	13.5	308
9%	a	22.2	507	9%	a	10.3	141.5
	b	34.6	617		b	19.3	256
	c	27.6	623		c	11.8	259
10%	a	28.5	443	10%	a	12.9	231
	b	23.6	386		b	9.9	184.4
	c	25.4	448		c	13.0	249

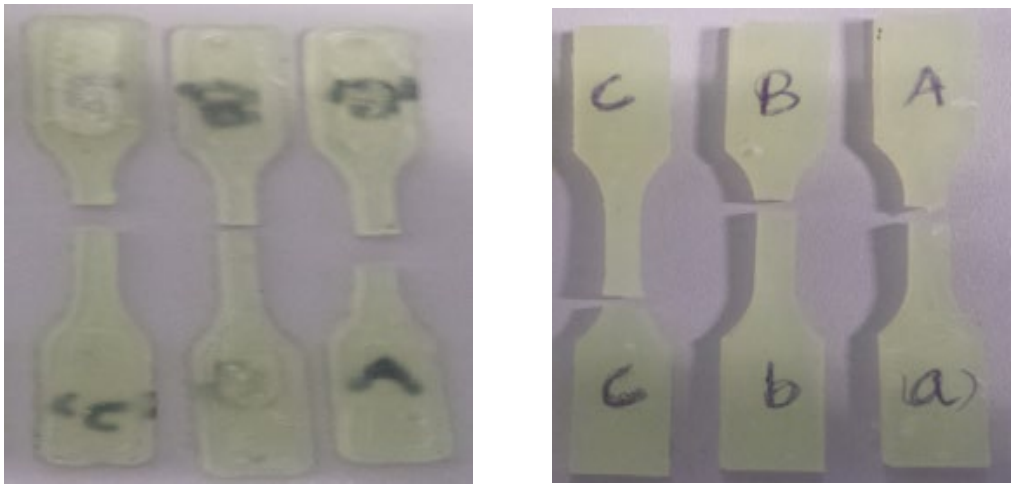

(a) (b)

Figure 4.2. (a) 3D printed specimen after tensile test (b) casted samples after tensile test

4.5 Results and discussion

4.5.1 Application of interfacial adhesion parameter models

3D printed and casted samples were fabricated and tested as discussed in sections 4.3 and 4.4. Nicolais and Narkis model Eq. (3), Kunori and Giel model Eq. (4) and Pukanszky Model Eq. (5) were applied to investigate and compare the interfacial adhesion parameters of 3D printed and casted samples. In order to convert the weight fraction into volume fraction, densities of filler (fumed silica) and UV dome 58 (polymer) are taken as 2.2 g/cm^3 and 1.1 g/cm^3 respectively. Volume fractions ($\boldsymbol{\varphi}$) of 0.041, 0.047 and 0.052 were calculated for 8%, 9% and 10% weight fractions, respectively. Figure 4.3 (a, b & c) represents the boxplots of the calculated interfacial adhesion parameters for 8%, 9% and 10% filler concentrations respectively based on Eq. (4.3), Eq. (4.4) and Eq. (4.5).

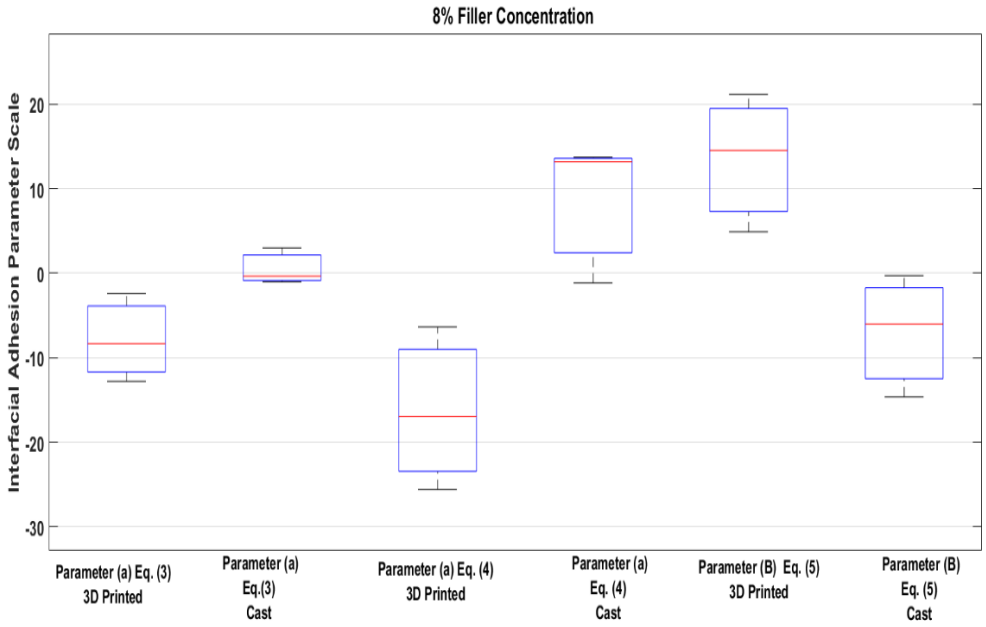
8% Filler Concentration
Interfacial Adhesion Parameter Scale
20
10
0
-10
-20
-30
Parameter (a) Eq. (3) 3D Printed
Parameter (a) Eq.(3) Cast
Parameter (a) Eq. (4) 3D Printed
Parameter (a) Eq. (4) Cast
Parameter (B) Eq. (5) 3D Printed
Parameter (B) Eq. (5) Cast

(a)

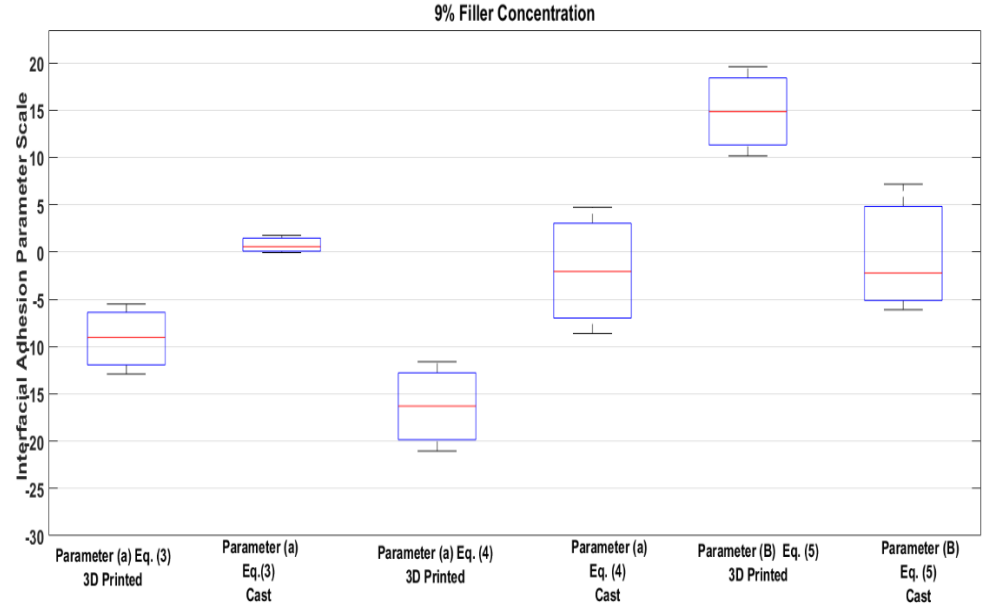
9% Filler Concentration
Interfacial Adhesion Parameter Scale
20
15
10
5
0
-5
-10
-15
-20
-25
-30
Parameter (a) Eq. (3) 3D Printed
Parameter (a) Eq.(3) Cast
Parameter (a) Eq. (4) 3D Printed
Parameter (a) Eq. (4) Cast
Parameter (B) Eq. (5) 3D Printed
Parameter (B) Eq. (5) Cast

(b)

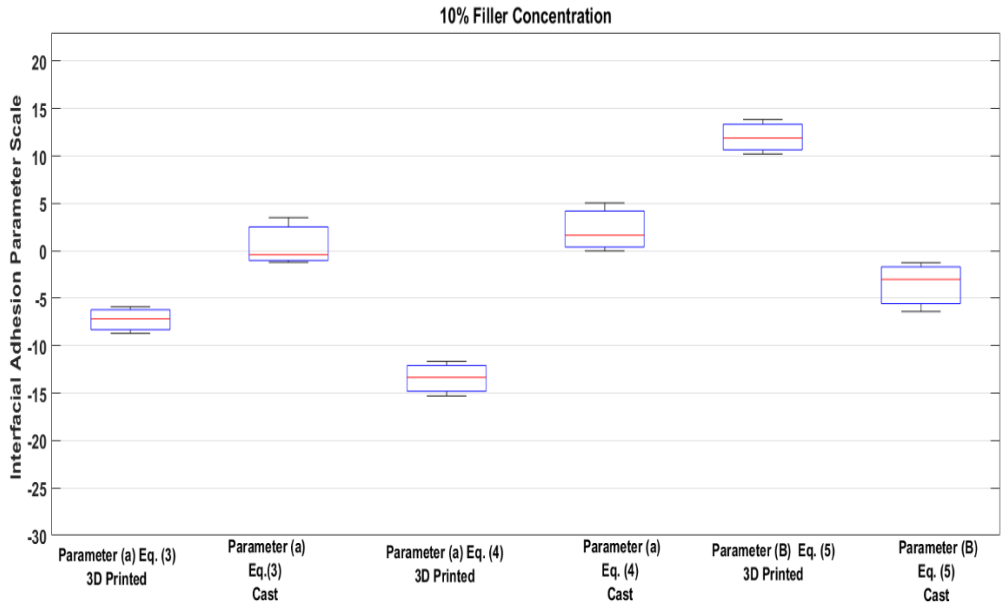

(c)

Figure 4.3. (a) 8% filler concentration boxplot (b) 9% filler concentration boxplot (c) 10% filler concentration boxplot

From Figure 4.3 (a, b & c), it can clearly be seen that all three models predict very strong interfacial adhesion for 3D printed samples, when seen on the scale defined by each model for perfect and weak adhesion. Casted samples exhibit weak interfacial adhesion as their interfacial adhesion parameters are weaker when compared with 3D printed samples. 3D printed samples for 8%, 9% and 10% filler concentrations exhibit much stronger bond between the filler and the matrix resulting in higher ultimate tensile strength. In order to further investigate this behaviour of 3D printed samples and to elaborate the reason behind stronger interfacial adhesion, scanning electron microscopy (SEM) was used to study the distribution of the filler at subsurface in both 3D printed and casted samples.

4.5.2 Scanning electron microscopy (SEM)

Figure 4.4 shows SEM images of the 3D printed and casted samples. It is evident from the SEM images that the distribution of the filler in the 3D printed samples is more homogenous

and the filler is well distributed throughout the image, compared to the casted sample where the distribution is not homogenous and areas that are absence of filler can be seen. This could be the reason why the casted samples have weak interfacial adhesion and non-homogenous distribution of filler resulted in weak bond between filler and matrix in casted samples. Homogenous distribution of filler in 3D printed samples results in a strong matrix–filler adhesion providing strong bond and ultimately higher interfacial adhesion and mechanical properties. For nanocomposites with weak matrix-filler adhesion, the particles cannot sustain any externally applied load and the strength of the composite cannot be any higher than that of neat resin.

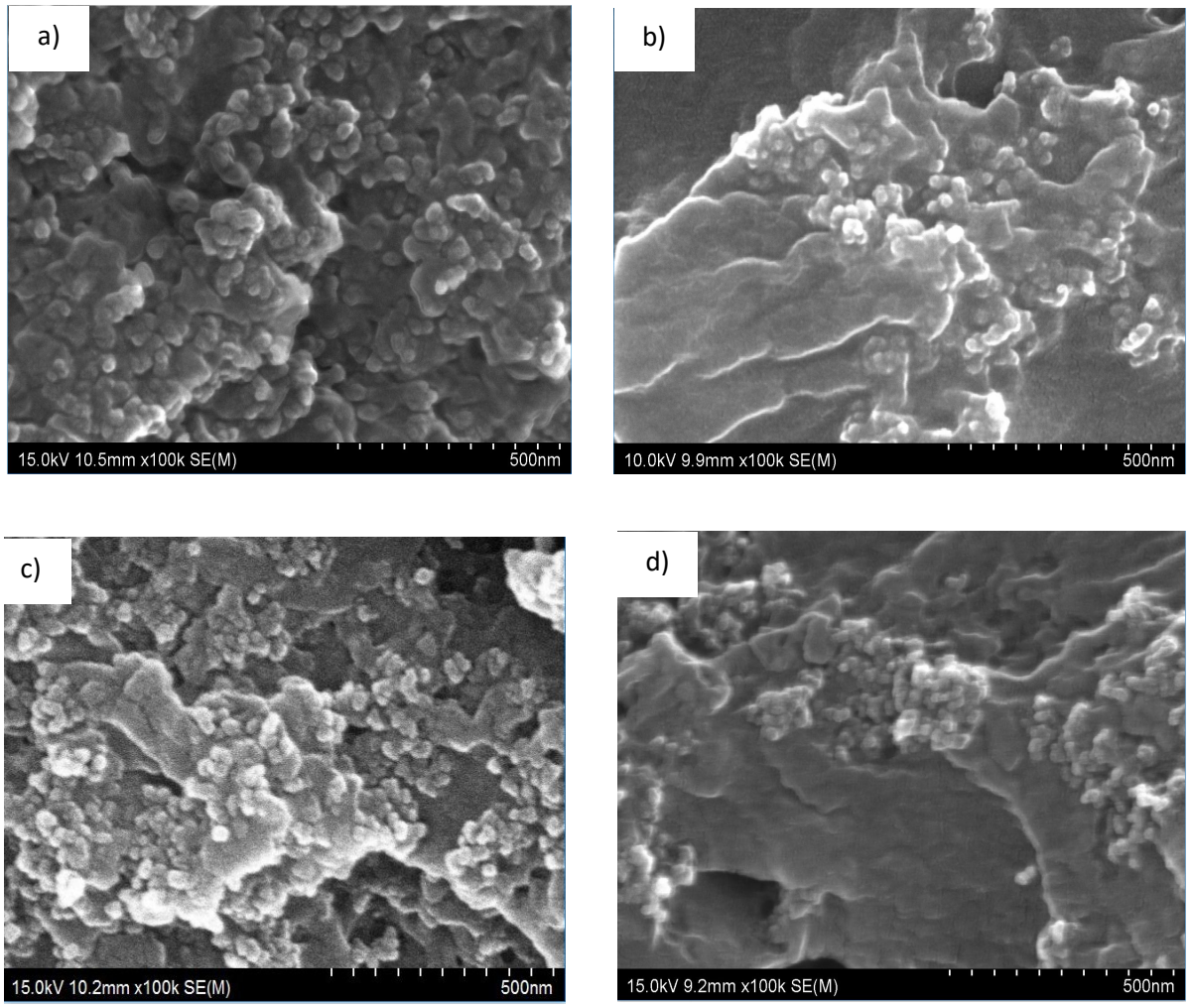

Figure 4.4.SEM images of (a) 8% 3D printed sample (b) 8% cast sample (c) 9% 3D printed sample (d) 9% cast sample

4.6 Chapter summary

In this chapter, interfacial adhesion parameters of 3D printed and casted samples were investigated with the aid of interfacial adhesion parameter models and SEM. Tensile tests were conducted on both 3D printed and casted samples in order to determine the tensile strength and Young's modulus. Measure of interfacial adhesion was obtained by applying existing theoretical models. After comparing the interfacial adhesion of 3D printed and casted samples, it was found that printed samples exhibit stronger interfacial adhesion. Casted samples on the other hand demonstrated weak interfacial adhesion. In order to further demonstrate this finding, SEM was used to study the distribution of the filler on the subsurface of 3D printed and casted samples. SEM revealed that the silica filler is homogenously distributed throughout the matrix in 3D printed samples where, in case of casted sample, non-homogenous distribution is observed. Homogenous distribution of filler is believed to create strong bonds between matrix and filler in 3D printed samples, which lead to superior mechanical properties.

In the next chapter, strain rate dependent mechanical behaviour of the photopolymer and photopolymer reinforced with nano silica filler will be studied. The chapter will investigate and validate the time dependent mechanical response using QLV model by combining hyper and viscoelastic phenomena. The viscoelastic properties of the photopolymer and nanocomposite will be determined.

CHAPTER 5: INVESTIGATION OF THE STRAIN-RATE DEPENDENT MECHANICAL BEHAVIOUR OF A PHOTOPOLYMER MATRIX COMPOSITE WITH FUMED NANO-SILICA FILLER

5.1 Introduction

Photopolymers are light sensitive polymeric materials, which change their chemical and physical properties when exposed to UV light. These photopolymers are commonly used in additive manufacturing processes such as Stereolithography (SLA) and Fused Deposition Modelling (FDM). Polymers commonly exhibit weak mechanical properties; for example low stiffness and low strength. In order to improve their mechanical properties and expand their applications, fillers such as micro/nano sized silica, carbon nanotubes, $CaCO_3$ and glass are added as polymer composites. In the recent past, there have been serious attempts on the development of more advanced materials by adding nano-fillers on different matrices for improved mechanical and physical properties. Nanocomposites have attracted scientists, engineers, and industrialists with the aim to design and develop nanocomposites having unique combinations of properties, unlike traditional materials. Nanocomposites could have polymeric, metallic or ceramic matrices. Generally, polymer matrix composites yield good specific stiffness, fatigue, corrosion resistance, and specific strength. Still, they exhibit weak residual strength and weak impact energy absorption [152-154]. Studies have been conducted in which nano sized fillers with different diameters have been added to polymeric materials [149], and it was reported that nano sized fillers with smaller diameters have more profound effect on mechanical properties. Also, it is evident from chapter 3, sections 3.3.1 and 3.3.2 that significant improvement in mechanical properties of 3D printed photopolymer was observed with the addition of nano sized silica filler.

An in depth understanding of the mechanical response of polymers over a range of strain rates, temperatures and pressures are required in a wide variety of fields, e.g. aerospace, automotive and medical devices. Researchers have characterised the mechanical response of polymers (specifically stress- strain relationship) over the past 40 years at strain rates between 10^{-4} and 10^{5} s^{-1} [155-158]. Polymers commonly exhibit time dependent mechanical response as shown by rate dependent yield strength, elastic moduli and post yield behaviour. A range of strain rates and temperatures can cause the polymer to change mechanical behaviour from rubbery to ductile plastic to brittle [159-165].

Traditional micromechanical analytical models [73, 166, 167] commonly used for micro-sized reinforcement composites, were recently used to predict the overall stiffness of nanocomposites. These conventional theories are based on the observation that the overall mechanical responses of composite materials are functions of constituent properties, volume fraction, the shape of inclusion and dispersion, but are not dependent on size. Finite element method [168-170] and molecular mechanics [171, 172] have been recently used to study the behaviour of nanocomposite systems.

There are various types of viscoelastic models which are proposed to predict the rate dependent behaviour of polymers. Green and Rivlin proposed the early models for capturing nonlinear response of viscoelastic solids in which stress is expressed as a function of the history of the deformation gradient. For materials with fading memory, Green and Rivlin [173] and Coleman and Noll [174] proposed constitutive models, which demonstrate the point that material response at present time is more strongly dependent on the latest deformations than those happened in the distant past. Pipkin and Rogers [175] used the history of strain rate rather than the history of strain to express the time dependent stress. In addition, they analysed the likelihood that such integral expressions are also effective when the role of stress and strain are switched. Scharphy [176] analysed the nonlinear viscoelastic behaviour of polymers

experiencing small deformations and expressed a nonlinear single integral model. In this model, he presented four nonlinear parameters related to instantaneous (elastic), loading rate, transient and accelerated/decorated time-dependent responses. In addition, he discussed dual representations, in which the roles of stress and strain are switched.

In order to capture the viscoelastic behaviour of biological materials, Fung [177] proposed Quasi Linear Viscoelastic (QLV) model. In the QLV model, stress relaxation function is modelled by separating it into two functions, i.e. reduced (normalised) time function and nonlinear elastic function. The nonlinear elastic function can be derived from strain energy density function [178-180]. The benefit of using the QLV model is that it has mathematical and experimental advantages as it is easy to resolve the constitutive equations and material parameter characterisation. The reduced relaxation function is not special and any function that is continuous, positive and monotonically decreasing with time is acceptable.

Muliana et al. [181] presented a modified form of QLV model in which they expressed strain as an integral of a nonlinear measure of the stress. They predicted the behaviour of elastomers [182] and light activated shape memory polymers using these models [183]. The QLV model is commonly employed nowadays because it provides the simplest way to include both nonlinearity (dependence of properties of load or strain) and time dependence (viscoelasticity) in a simplified integral model. Apart from biomedical applications [184], the QLV model has also been employed to model materials such as elastomeric polymers, rubbers and composites [182, 185].

In this chapter, in order to study the rate dependent mechanical behaviour of the photopolymer and nanocomposite used in this study, tensile tests have been conducted at different loading rates to characterise the rate dependency of the material. Similar to chapter 3, fumed silica is used as the nano filler to enhance the mechanical properties. Different concentrations by weight

have been added in to the polymer and dog-bone samples have been fabricated by casting. QLV model which combines hyper elastic and viscoelastic phenomena have been implemented by developing a MATLAB script to capture the rate dependent mechanical response of the polymer and nanocomposites with different filler concentrations. The QLV model with Yeoh strain energy density function bears good agreement with the experimental results as it adequately captures the behaviour of all four filler concentrations and of the polymer.

5.2 Materials and methods

5.2.1 Preparation of UV curable resin and casting of samples

UV curable resin was prepared and mixed with fumed silica filler in accordance with the methodology discussed in section 3.5 of chapter 3.

Casting of the samples were carried out by following the procedure outlined in section 4.3.2 of chapter 4. Six samples for the polymer, 4%, 8%, 9% and 10% filler concentrations were fabricated.

5.3 Results and discussion

5.3.1 Uniaxial tensile tests at different strain rates

Stress relaxation, creep, and uniaxial tension are different experiments normally conducted to demonstrate the material properties of a rate dependent material. However, the uniaxial tensile test is considered to be the most common mode of deformation. Uniaxial tension tests at different strain rates could provide plausible information about the viscoelastic behaviour of the rate dependent materials [186-188]. Therefore, we considered this mode to study the mechanical behaviour of the photopolymer (UV Dome 58) with four different filler concentrations e.g. 4%, 8% 9% and 10%. Tensile tests were conducted on dog-bone samples with specific dimensions (following ASTM D638 standard type V) as shown in Figure 5.1 at different strain rates of 1.3×10^{-2} s^{-1}, 1.3×10^{-3} s^{-1} and 1.3×10^{-4} s^{-1}. In order to capture the

localised strain in gauge part of the sample, a commercial digital image correlation (DIC) open source software GOM Correlate® was used, and a video camera was mounted in front of the tensile testing machine to record the test. Before the tests, random speckle patterns were created on the samples with the combination of white and black spray paint as shown in Figure 5.3 (c). Strain was measured using a recorded video from start of the experiment till the failure of the specimen. Depending on the deformation rate, the number of pictures per minute is chosen such that the smaller strain increment can be obtained from one image to another using DIC.

(a) (b) (c)

Figure 5.1. Dog-bone specimen of (a) polymer, (b) nanocomposite with silica filler, and (c) with random speckle pattern

After the tests, recorded videos were post processed in GOM to obtain the strain in the gauge part of the specimen. Fig 5.2 (a, b & c) shows the DIC images captured during localised strain measurement at gauge part of the specimen.

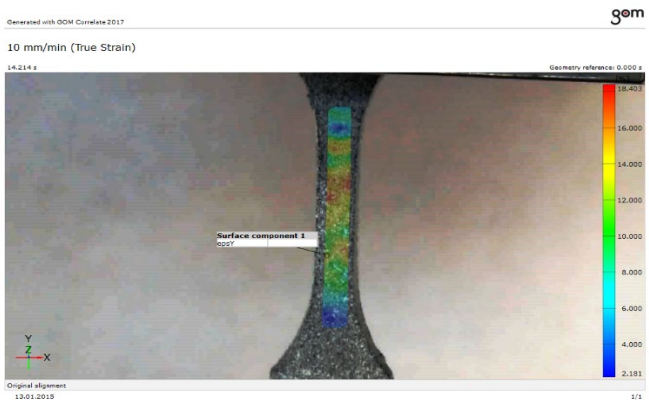

(a)

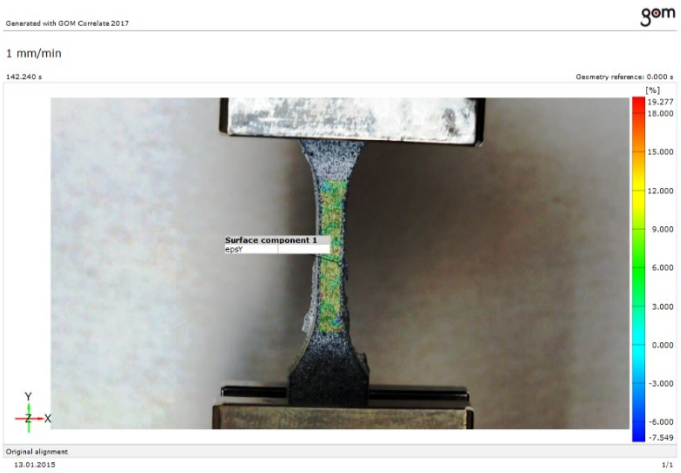

(b)

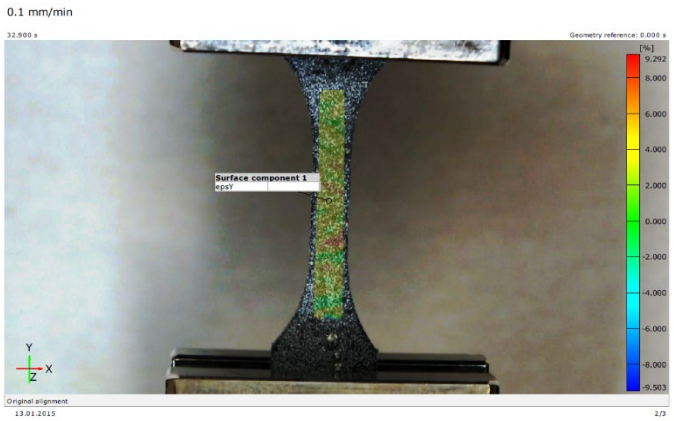

(c)

Figure 5.2. Strain measurement using GOM at gauge part (a) 10 mm/min (b) 5 mm/min (c) 0.1 mm/min

Figure 5.3 (a, b & c) shows the stress-strain curves obtained for the polymer, as well as nanocomposites with 4%, 8%, 9% and 10% filler concentrations with the loading rates discussed above. As most rate dependent materials exhibit a stronger response to faster loading rates, the tensile strengths of the pure photopolymer as well as the nanocomposites with all four filler concentrations increase by increasing the strain rate. At 1.3×10^{-2} s^{-1}, adding filler content decreased the strain to failure of the material except for 4%. At 1.3×10^{-3} s^{-1}, pure polymer is found to exhibit more brittle behaviour compared to all the filler concentrations used, while 4% filler showing high strain to failure demonstrating more ductile behaviour. At 1.3×10^{-4} s^{-1}, pure polymer has low strain to failure compared to all filler concentrations used; 4% and 8% filler contents exhibited almost similar strain to failure demonstrating more ductile behaviour than other filler concentrations.

Tensile strength of polymer is significantly increased by the addition of nano sized silica filler. Tensile strength of nanocomposite with 4% mass fraction of filler concentration is higher than 8%, 9% and 10% at all loading rates, this is because by increasing the filler concentration diameter of the nanoparticles increases and the surface area decreases which leads to poor matrix-particle interfacial adhesion. Nanoparticles with higher surface area provide more enhanced matrix-particle interfacial adhesion. Increasing filler content increases the diameter of the filler and thereby decreasing the surface area, which results in poor matrix-particle interfacial adhesion, the particles are unable to carry any part of the externally applied load. Therefore, the strength of the composite cannot be higher than the neat polymer matrix [189] Nanocomposites could overcome these issues if a suitable processing method is selected for problems such as uniform dispersion of nano fillers in the matrix. Local stress concentration arises within the nanocomposite structure when aggregation is formed in the nano filler. While strength is heavily dependent on the effective stress transfer between particles and matrix. If the bond between the matrix and particle is weak, stress cannot be effectively transferred from

the matrix to the particles. This results in a premature failure of the polymer reducing its strength and strain to failure. To create a strong interface, a suitable nano filler that is compatible with the polymer matrix is essential. A Significant amount of research has been conducted using particulate nanocomposites and promising results have been obtained especially for the improvement of mechanical properties [190, 191].

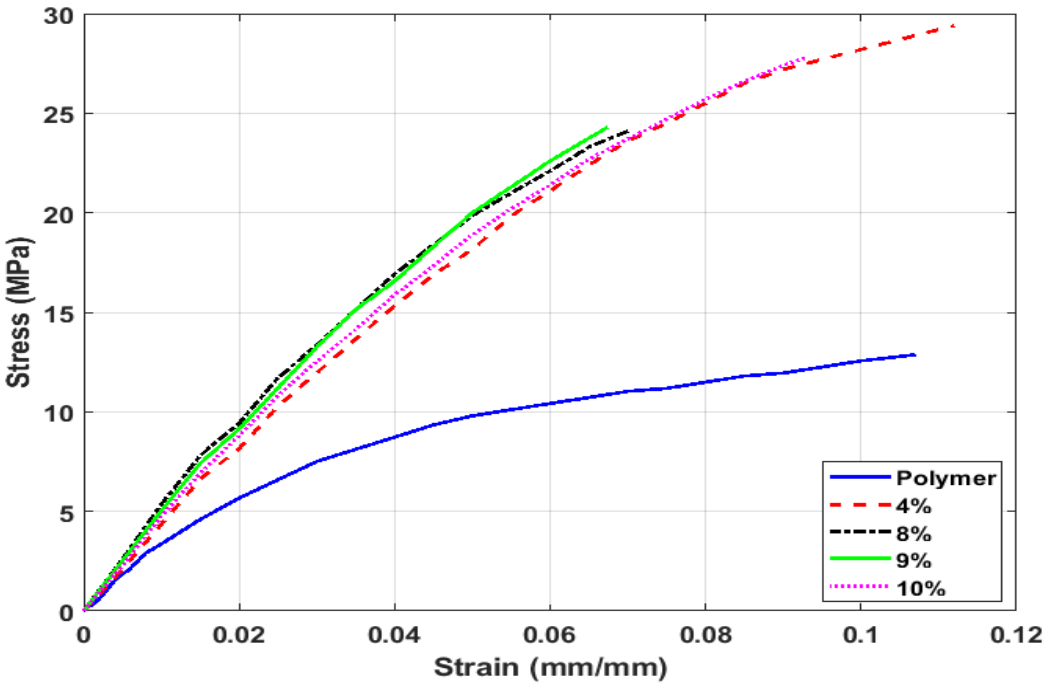

(a)

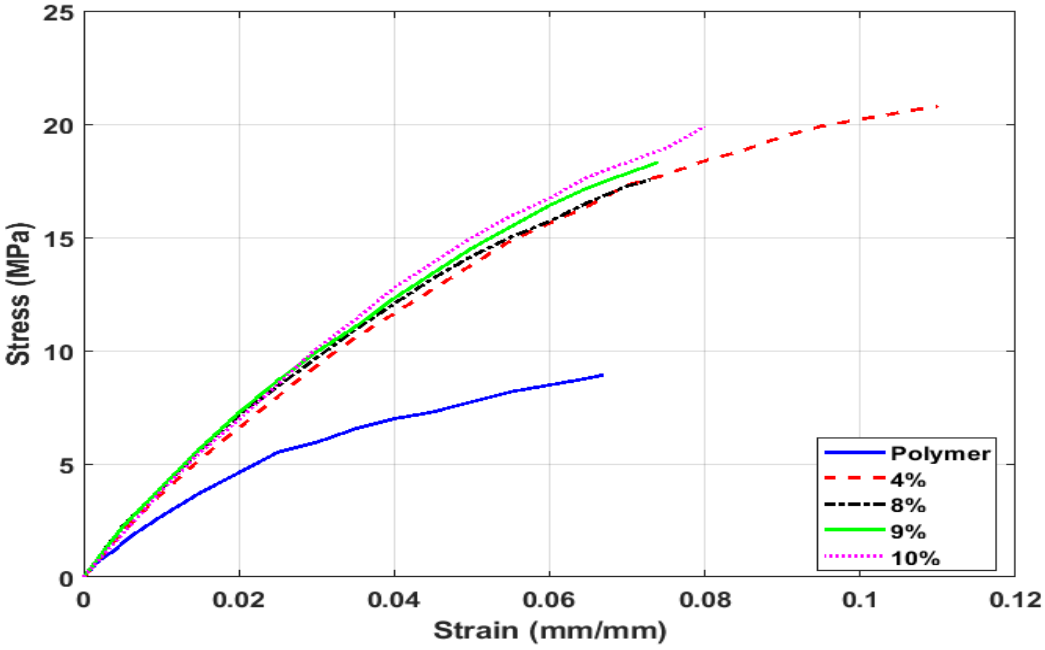
Stress (MPa)
Strain (mm/mm)
Polymer
4%
8%
9%
10%

(b)

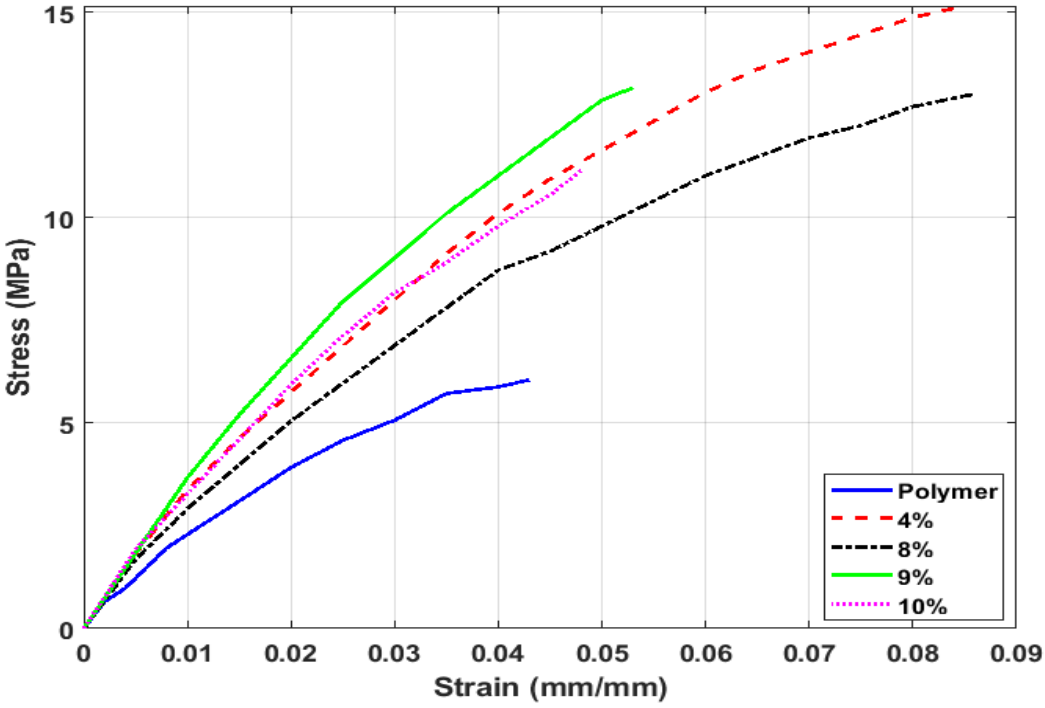
Stress (MPa)
Strain (mm/mm)
Polymer
4%
8%
9%
10%

(c)

Figure 5.3 Stress-strain curves of polymer, and particulate nanocomposites with 4%, 8%, 9% and 10% filler concentrations at strain rates of (a) 10 mm/min (b) 5 mm/min (c) 0.1 mm/min

As seen in Figure 5.3, 4% filler concentration has stronger mechanical properties compared to 8%, 9%, and 10%. Therefore, it can be established that 4% filler content is the maximum amount of filler at which photopolymer (UV Dome 58) exhibits a stronger response.

5.4 Application of QLV model with Yeoh strain energy density function

Viscoelasticity is the property of the materials that exhibits both viscous and elastic characteristics when undergoing deformation. After the load is applied, there is an instantaneous elastic deformation, and the viscous part occurs with respect to time. Fung [177] first proposed the Quasi-Linear Viscoelastic (QLV) model which is frequently used to study the behaviour of soft biological tissues. The QLV is capable of capturing elastic non-linearity of soft tissues. The Cauchy stress for QLV model is represented as

$$\boldsymbol{\sigma}(t) = -p\boldsymbol{I} + F(t)\left\{\boldsymbol{S^e}[\boldsymbol{C}(t)] + \int_0^t \boldsymbol{S^e}[\boldsymbol{C}(t)]\frac{\partial G(t-s)}{\partial(t-s)}\,ds\right\}\boldsymbol{F(t)}^T \qquad (5.1)$$

where, $\boldsymbol{\sigma}(t)$ is the Cauchy stress tensor, $\boldsymbol{F}$ is the deformation gradient, $\boldsymbol{C} = \boldsymbol{F^T F}$ is the right Cauchy-Green tensor, p is Lagrange multiplier and $\boldsymbol{I}$ is identity tensor. The term $\boldsymbol{S^e}[\boldsymbol{C}(t)]$ can be taken as effective (instantaneous) second Piola Kirchhoff elastic stress tensor [192].

Recently, Slesarenko and Rudykh [186] demonstrated QLV model by combining Yeoh strain energy density function and Neo Hooken strain energy density function to study the behaviour of soft rubber-like digital material made by Polyjet multi-material 3D printing. They reported that QLV model with Yeoh strain energy density function successfully captures the behaviour of most of the soft digital materials.

In this study, we employed a similar hyper-viscoelastic approach using QLV model with Yeoh strain energy density function to model the behaviour of our chosen material under uniaxial

tension. Equation (5.3) represents the QLV model with Yeoh strain energy density function, for the detailed theoretical background of the model readers are recommended to read the work of Slesarenko and Rudykh [186] and references therein.

Strain energy density function for classical two-term Yeoh model [193] can be defined as

$$W = \frac{\mu}{2}\left[(I_1 - 3) + \frac{\alpha}{2}(I_1 - 3)^2\right] \tag{5.2}$$

where μ is the instantaneous shear modulus, α is a constant.

The Cauchy stress component for QLV model with Yeoh strain energy density function can be represented as

$$\sigma_{11}(t) = [\alpha\lambda^3(t) + (1-3\alpha)\lambda(t) + 2\alpha][\lambda(t) - \lambda^{-2}(t)] + \mu\int_0^t D'(t-s)[\alpha\lambda^3(s) + (1-3\alpha)\lambda(s) + 2\alpha]\left[\frac{2}{3}\lambda^2(t)\{\lambda^{-1}(s) - \lambda^{-4}(s)\} + \frac{1}{3}\lambda^{-1}(t)\{\lambda^2(s) - \lambda^{-1}(s)\}\right]ds \tag{5.3}$$

Stress relaxation function $D(t)$ defines the influence of current stress state in QLV model, which is represented here by the Prony series as

$$D(t) = 1 - \sum_{i=1}^{n}\gamma_i\left(1 - e^{-\frac{t}{\tau_i}}\right) \tag{5.4}$$

γ_i and τ_i relaxation coefficients and represents relaxation times respectively.

Five term Prony series with relaxation times τ = 0.01, 0.1, 1, 10 and 100 s have been used considering relaxation occurs at different time scales and one term Prony series is normally insufficient to adequately define the material response at different rates. The experimental stress strain curves with different strain rates have been fitted with MATLAB script using trust region reflective algorithm with non-linear least square criterion. Figure 5.4 (a, b, c, d & e) exhibits the fitting results of the QLV model with Yeoh strain energy density function, Eq. (5.3). It can be clearly seen that the model shows very good agreement with experimental

results of pure polymer as well as nanocomposite with 4%, 8%, 9% and 10% filler concentrations. Table 5.1 shows the calibrated material parameters of the QLV model with Yeoh strain energy density function for the polymer, 4%, 8%, 9% and 10% filler concentrations. As seen in Table 5.1, instantaneous shear modulus μ increases with an increase in the filler concentration up to 8%, for 9% and 10% it was found to be decreasing. This is because with higher filler concentration particles tends to form agglomerates, which results in weak matrix-particle interfacial adhesion. Homogenous dispersion of nanoparticles helps to decrease the agglomeration and improve the mechanical properties. However, it is very challenging to homogeneously disperse the nano-filler because of the strong tendency of nanoparticles to agglomeration [194, 195]. In addition, as discussed in section 5.3.1, adding higher filler content decreases the surface area of the particles leading to weak interfacial adhesion, which is also a major contributor to weak mechanical properties.

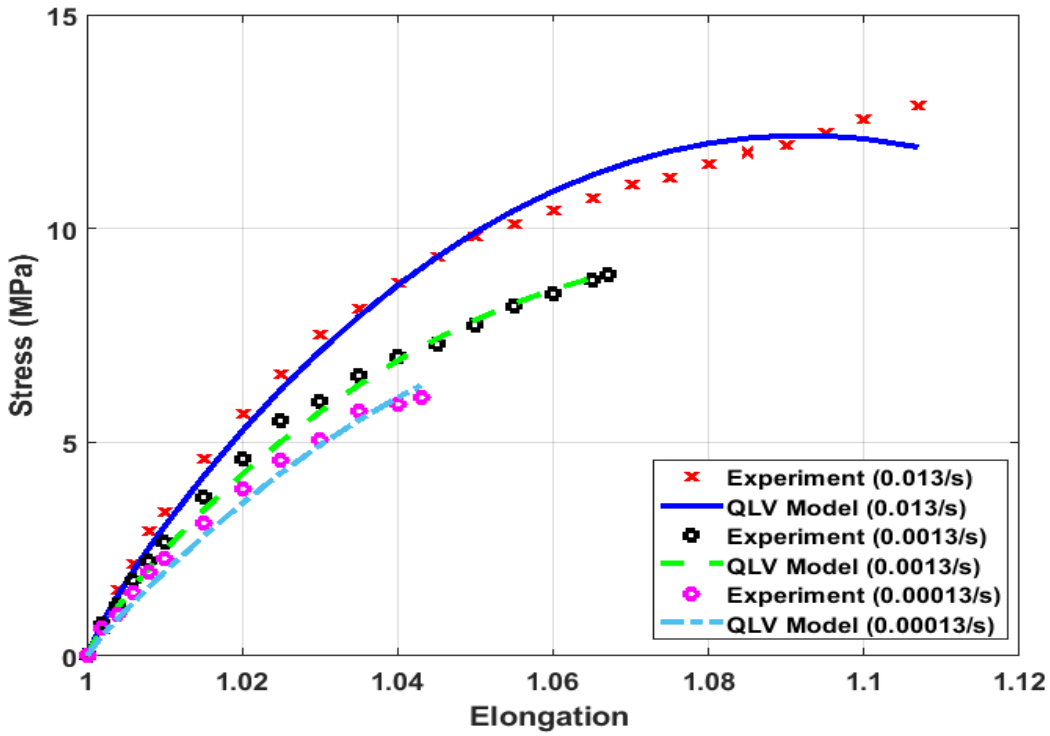

(a)

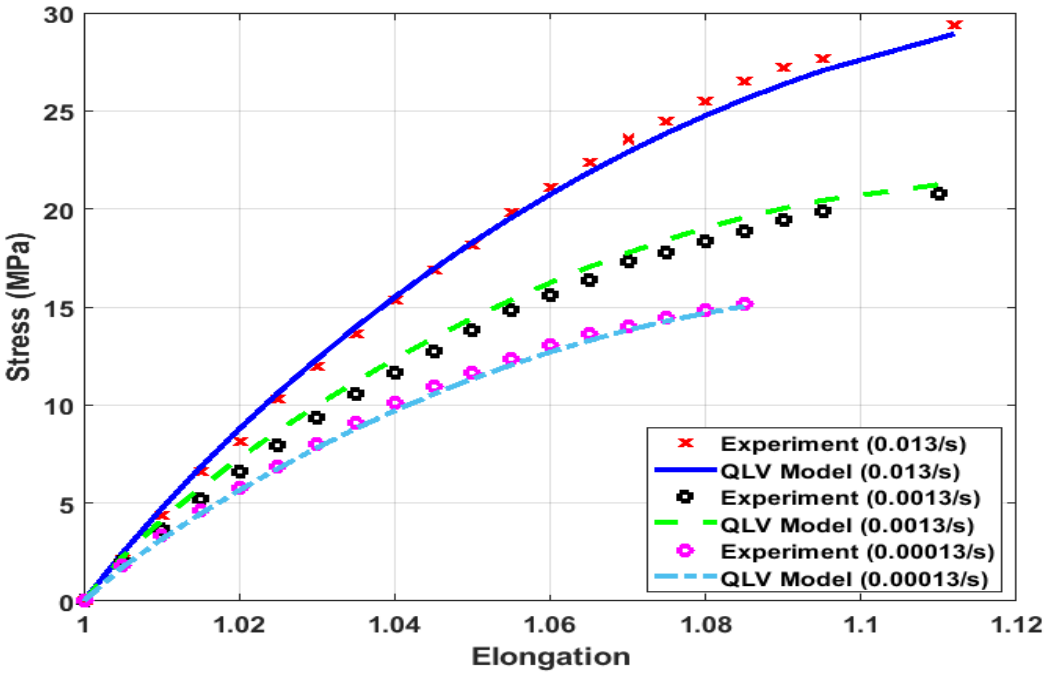
Stress (MPa)
Elongation
Experiment (0.013/s)
QLV Model (0.013/s)
Experiment (0.0013/s)
QLV Model (0.0013/s)
Experiment (0.00013/s)
QLV Model (0.00013/s)

(b)

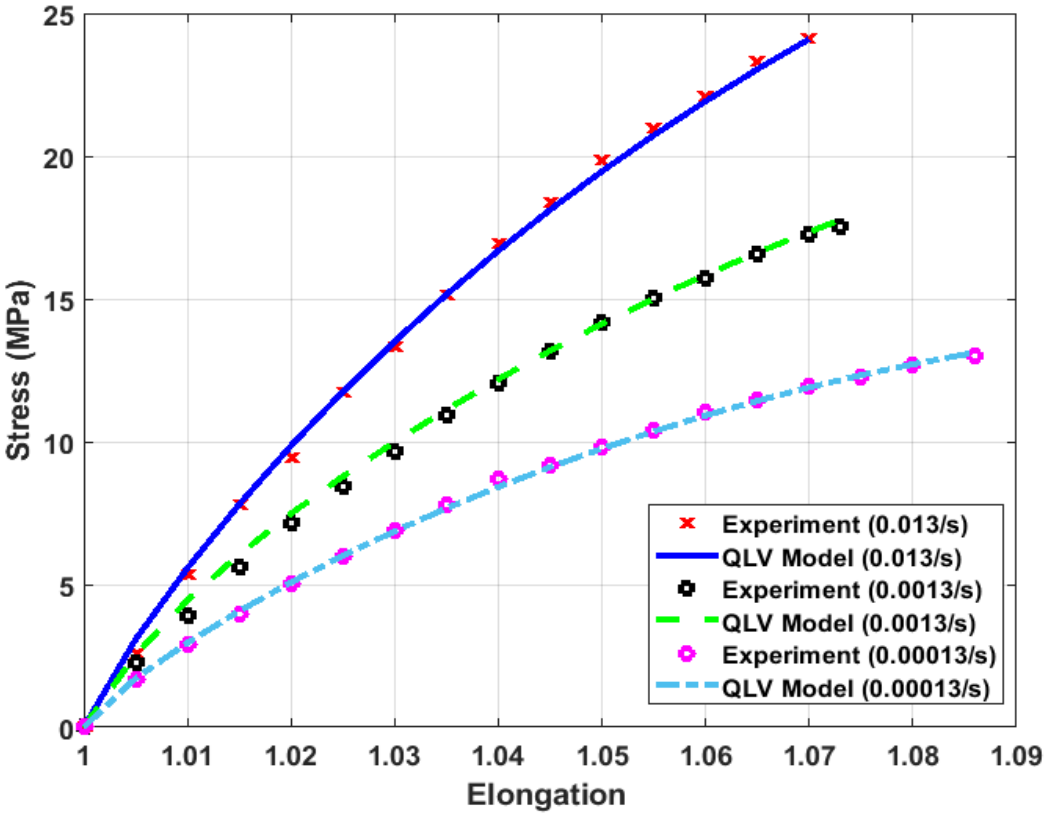
Stress (MPa)
Elongation
Experiment (0.013/s)
QLV Model (0.013/s)
Experiment (0.0013/s)
QLV Model (0.0013/s)
Experiment (0.00013/s)
QLV Model (0.00013/s)

(c)

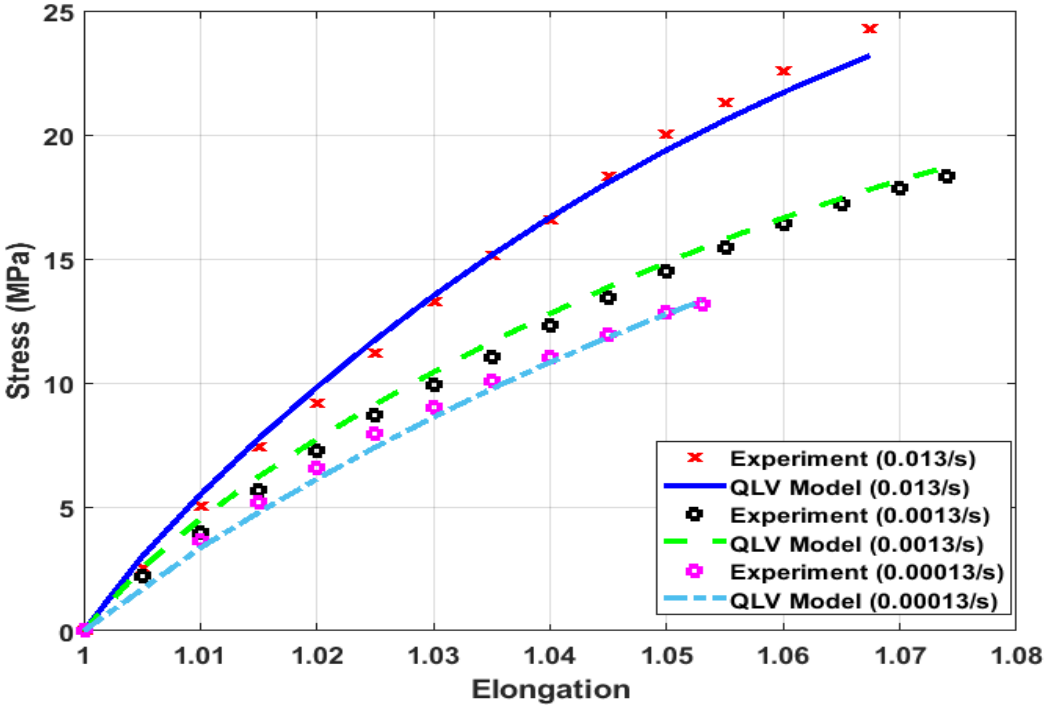

(d)

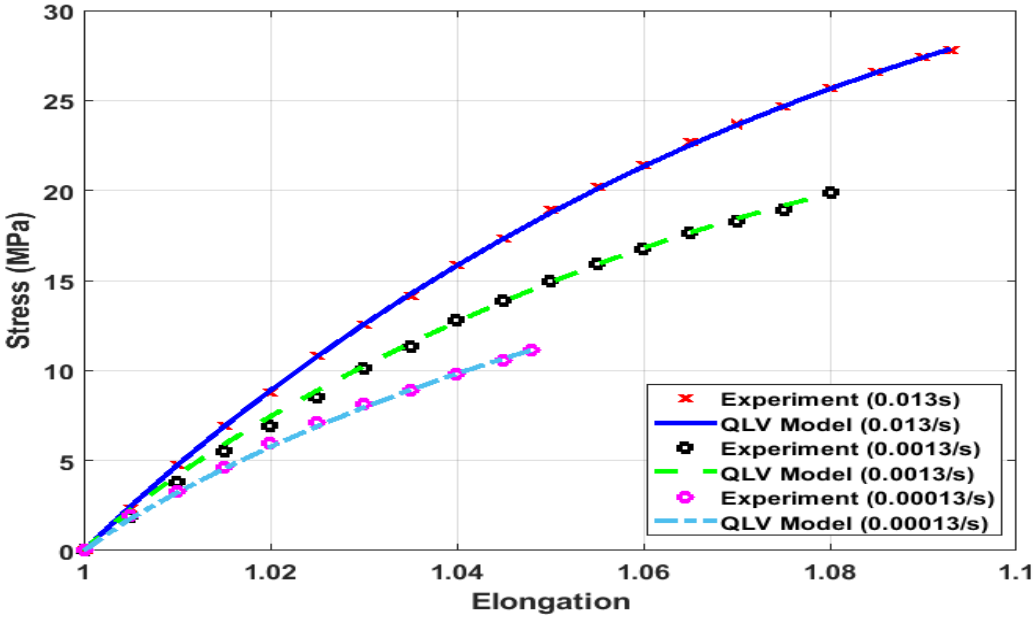

(e)

Figure 5.4. Fitting of experimental results with QLV model with Yeoh strain energy density function (a) polymer (b) nanocomposite with 4% filler concentration (c) nanocomposite with

8% filler concentration (d) nanocomposite with 9% filler concentration (e) nanocomposite with 10% filler concentration

Table 5.1. Material parameters for QLV model with Yeoh strain energy density function

Calibrated parameters of QLV model with Yeoh strain energy density function							
Material	μ **(MPa)**	α	γ_1	γ_2	γ_3	γ_4	γ_5
Polymer	142.90	-1.069	0.999	0.601	0	0	0.742
4%	172.89	-0.9416	0.1025	0.999	0.3334	0	0
8%	245.322	-0.1105	0.7305	0.999	0.3744	0	0.6860
9%	231.45	-0.5989	0.5902	0.999	0.0343	0	0
10%	168.97	-0.9679	0	0.999	0.3768	0.0295	0.999

5.5 Chapter summary

In this chapter, the rate dependent behaviour of pure polymer and polymer reinforced with different concentration of filler have been studied by conducting tensile tests at different strain rates. Similar to chapter 3, fumed silica is used as a reinforcement and different concentrations of filler have been added to enhance the mechanical properties. It was found that the ultimate yield strength is significantly affected by the strain rate; for example, tensile strength of the photopolymer is 2.2 times higher at 1.3×10^{-2} s^{-1} compared to the tensile strength at 1.3×10^{-4} s^{-}

[1]. Adding silica filler enhanced the mechanical properties of the photopolymer; for example with 4% filler content, tensile strength is 2.25, 2.38 and 2.42 times higher than the tensile strength of the polymer at 1.3×10^{-2} s^{-1}, 1.3×10^{-3} s^{-1} and 1.3×10^{-4} s^{-1} respectively. QLV model combining hyper and viscoelastic phenomena have been used to capture the rate dependent non-linear behaviour of the material. Uniaxial tensile tests with three different strain rates have been used to calibrate and capture the viscoelastic parameters and time dependent response respectively. In the end, QLV model with hyper-viscoelastic phenomena successfully demonstrated the capability to capture the rate dependent stress-strain behaviour of the material, as the QLV model with Yeoh strain energy density function bears very good agreement with the experimental results.

In the next chapter, experimental and numerical studies on the effect of silica filler on tensile strength of 3D printed particulate nanocomposite are conducted. The chapter will include FEM model which is used to study the behaviour of the high filler concentrations which were difficult to print using photopolymer extrusion technique.

CHAPTER 6: EXPERIMENTAL AND NUMERICAL STUDY ON THE EFFECT OF SILICA FILLER ON TENSILE STRENGTH OF 3D PRINTED PARTICULATE NANOCOMPOSITE

6.1 Introduction

As discussed in the introductory sections of Chapters 4 and 5, the most common technique to enhance the properties of polymers is the addition of reinforcements elements such as nanoparticles or fibres. Several composites have been manufactured by adding micro sized reinforcements in the past twenty years [196-198]. In this modern age, nano sized reinforcements have attracted a significant interest from scientific and industrial sectors. In fact, the nano sized reinforced composites have proven to show better mechanical behaviour when compared with conventional ones [199, 200]. Especially, significant amount of interest has been dedicated to bi-phase or multiphase systems in which inorganic nano fillers are added to the polymer. These nanometric fillers produce large surface area if homogenously distributed in the matrix; thus, these systems can potentially enhance the interfacial interaction between matrix and filler resulting in an improved mechanical properties of the material [201]. Researchers have reported considerable amount of enhancement in mechanical and tribological properties even at very low volume fractions [202]. Especially, some researchers have reported that ceramic and nano sized silica particles can prominently enhance bulk polymers' mechanical properties [169, 202, 203]. This is true as significant improvement in tensile and flexural properties of the photopolymer after adding silica nanoparticles is evident from Chapter 3, sections 3.6.4.1 and 3.6.4.2.

Finite Element Modelling (FEM) has been successfully implemented by some researchers to model the composites being reinforced with nanometric fillers. For instance, Liu and Chen [10] studied the possibility of applying FEM to composites reinforced with carbon nanotube using

representative volume element (RVE). Other numerical techniques such as 3D FEM and 2D nano scale FEM were also used by other researchers to model the mechanical behaviour of nanocomposite materials [204-206]. It can be noted that such FEM based models are commonly executed by using representative volume elements, thus making the assumption that the nanocomposite microstructure can be replicated by gathering large quantity of these elements. An RVE normally has one or more nanofiller(s) which is surrounded by resin, and adequate loads or boundary conditions are applied to predict the effect of the surrounding materials. It is considered as a building block to accumulate the composite. Until now, majority of the studies focused on linear elastic properties and yielding predictions for the elastic toughness of the nanocomposites with respect to filler concentration, filler properties and in some cases filler orientation.

Zhang et al. [85] utilised the RVE technique to analyse the mechanical behaviour with particular attention to the damage mechanisms of SiCp reinforced Al composites using experiments and FEM. They developed a 3D microstructure FEM model predicting elasto-plastic behaviour and breakage behaviour of 7% volume fraction of SiCp reinforced Al composite. Hua et al. [86] studied the mechanical behaviour of the dental composite resin reinforced with titanium oxide nanoparticles using a 3D nanoscale RVE. They characterised the effect of nano filler concentration, geometrical aspect, toughness and interphase zone among the matrix material and nano filler on bulk properties of the composite. Hua et al. [87] used nanoscale RVE to study interphase property and geometry effect on the mechanical behaviour of the silica-epoxy resin nanocomposite. They found that interphase modulus and interfacial bonding conditions have notable effect on effective stiffness of nanocomposites.

In this chapter, mechanical behaviour of 3D printed silica reinforced nanocomposites have been analysed. Similar to Chapters 3 and 4, nano sized silica filler have been added to enhance the properties of 3D printed photopolymer. Different concentrations of the filler were added and

their effects on mechanical properties were studied by conducting uniaxial tensile tests. Improvement in mechanical properties by the addition of nano sized filler have been observed. In order to observe the tensile strength, dog-bone samples using new photopolymer extrusion printing were prepared. Stress relaxation tests were conducted on photopolymer in order to calibrate the viscoelastic parameters. A numerical model of nano reinforced particulate nanocomposite was developed which takes into account the nanostructure and dispersion of nanoparticles. Hyper and viscoelastic phenomena was employed to validate and analyse the stress-strain relationship of 8%, 9% and 10% filler concentrations. In order to represent the nanostructure, a 3D representative volume element (RVE) was developed on multi-scale material modelling platform DIGIMAT [207] and subsequent simulations were ran in commercial finite element package ABAQUS. The model with hyper and viscoelastic phenomena bears good agreement with experimental results of 8%, 9% and 10% filler concentrations. As part of parametric study, stress relaxation simulations, creep simulations and investigation of the effect of RVE size on tensile strength were carried out after validating the numerical model. In the end, empirical models were developed relating the tensile strength with range of filler concentrations and viscosity at different strain levels. Results acquired in this chapter could lead to better understanding of the mechanical characterisation of the nanoparticle reinforced composite, manufactured using the new photopolymer extrusion 5-axis 3D printing technique.

6.2 Experimental procedure

6.2.1 A new photopolymer extrusion 5-axis 3D printing technique

Samples were printed using a new photopolymer extrusion 3D printing technique the working principle of the technique is discussed in detail in section 3.4 of chapter 3.

6.2.2 Preparation of UV curable resin

UV curable resin was prepared and mixed with fumed silica filler in accordance with the methodology discussed in section 3.5 of chapter 3.

6.2.3 Adequate material viscosity for printing

Methodology of finding the adequate amount of viscosity is discussed in detail in section 3.6.1 of chapter 3. In accordance with the findings observed in section 3.6.1 of chapter 3, only a narrow window of filler concentrations of 8%, 9% and 10% (corresponding to the dynamic viscosities of 15000 cP and 25000 cP) were found to be suitable to print reliably. So, in this chapter, filler concentrations having 8%, 9% and 10% mass fraction were used to print the samples.

6.2.4 Tensile test

In order to observe the tensile strength of the printed parts, dog-bone specimens following the similar standard and procedure as discussed in chapter 3 section 3.6.4 were printed (Figure 6.1) and tensile tests were conducted on each specimen to observe the tensile strength and strain to failure.

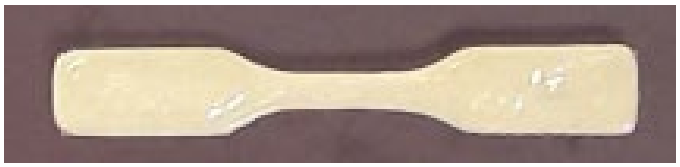

Figure 6.1. ASTM D638 printed specimen

As discussed in section 6.1, fillers are employed to enhance the mechanical properties of the polymers. However, there are certain characteristics on which the overall strength of the nanocomposite rely, e.g. matrix-particle interfacial adhesion, particle size and particle loading [149] . As it is generally understood that adding fillers might increase the mechanical properties of the nanocomposite, but stresses sometimes do not behave as it is expected [189]. Particle

size plays a very important role in increasing the strength of the composite. Also discussed in section 5.3.1 of chapter 5 that Dittanet and Pearson [23] studied the effects of different particle sizes on tensile strength of the composite by increasing the volume fraction and concluded that nano sized particles increase the tensile strength with increasing volume fraction. This is true as smaller particles have larger surface area providing more enhanced matrix-particle interfacial adhesion, which results in effective transfer of the stress from the matrix to particles. Increasing filler content increases the diameter of the filler and thereby decreasing the surface area which sometimes results in poor matrix-particle interfacial adhesion, and as a result, the nanoparticles cannot withstand majority of the externally applied force. Therefore, the mechanical properties of the composite will be similar as that of neat resin.

As shown in Table 6.1, tensile strength of sample with 8% filler concentration is higher than that of 9% and 10%; this is caused by better interfacial adhesion because at lower filler concentration nanoparticles have larger surface area which gives rise to better bond between matrix and nanoparticles. Tensile strength of 10% filler concentration is close to 9% but lower than 8% because higher filler content increases the diameter and decreases the surface area which results in weak interfacial adhesion leading to weak mechanical properties. Figure 6.2 shows the stress-strain curves of the 8%, 9% and 10% filler concentrations, it can been seen that increasing volume fraction made the samples less elastic as strain at break of both 9% and 10% filler concentrations is smaller compared to 8% filler concentration.

Table 6.1. Tensile properties of 8%, 9% and 10% filler concentrations

Filler concentration (%)	**Tensile strength (MPa)**	**Strain at break (%)**
8%	28	11
9%	22.2	5.6
10%	23.6	8.6

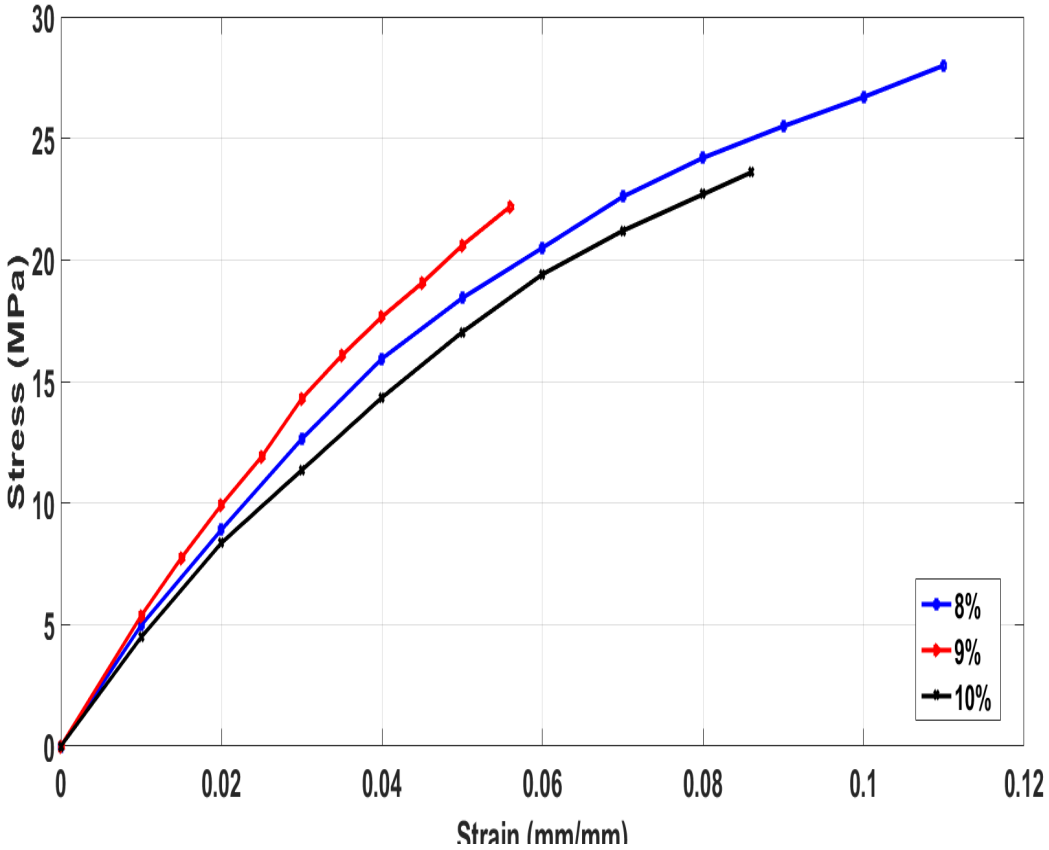

Figure 6.2. Stress-strain curve of 8%, 9% and 10% filler concentrations

6.3 Finite element simulations procedure

6.3.1 Constitutive equations

The experimental stress stain data of polymer (UV Dome 58) was used to calibrate an isotropic hyperelastic strain energy density function (SEDF) in ABAQUS in order to obtain the material constants to be used in FE simulations. After performing the curve fitting procedure in ABAQUS, out of various SEDF available, Yeoh's function captured the behaviour of the photopolymer more accurately as shown in Figure 6.3. Yeoh's model in the form of SEDF can be written as

$$W = \sum_{i=1}^{3} C_{i0}(\bar{I}_1 - 3)^i + \sum_{i=1}^{N} \frac{1}{D_i}(J-1)^{2i} \qquad (6.1)$$

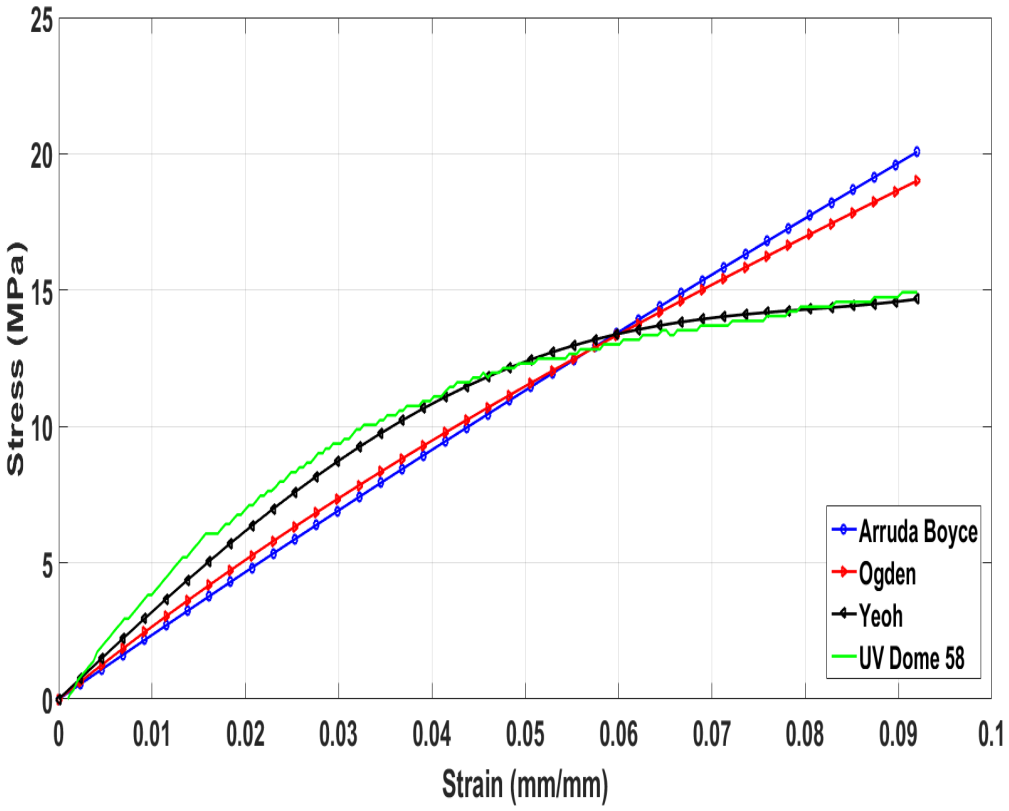

Figure 6.3. Curve fitting using different SEDF in ABAQUS

where $J = \det(F)$ and F is considered as deformation gradient. The term $\bar{I}_1$ is the first invariant of the left Cauchy-Green strain tensor B. ABAQUS employs linear least square fitting in order to calibrate the material constants. The calibrated material constants of the Yeoh's function are shown in Table 6.2.

Table 6.2. Material constants for Yeoh's strain energy density function

C_{10} (MPa)	C_{20} (MPa)	C_{30} (MPa)	D_1	D_2	D_3
76.88	-1225.40	13201.63	6.002e-3	0	0

6.3.2 Stress Relaxation Test

ABAQUS uses Prony series in order to obtain the coefficients of the viscoelastic material as shown in equations 6.2. To calibrate the Prony series coefficients in ABAQUS, stress

relaxation test was conducted at room temperature, sample was subjected to constant strain of 6% applied at the rate of 3 mm/min. Curve fitting procedure was carried out as shown in Figure 6.4, it is quite evident from Figure 6.4 that the normalised shear moduli obtained from ABAQUS are in good agreement with the experimental stress relaxation data. Table 6.3 shows the Prony series coefficients obtained by curve fitting procedure.

$$g_R(t) = 1 - \sum_{i=1}^{N} g_i^{-p}\left(1 - e^{\frac{-t}{\tau_i^G}}\right) \qquad (6.2)$$

Table 6.3. Prony series coefficients

	G(i)	K(i)	Tau(i)
1	0.2950	0	23.90
2	0.4050	0	451.61

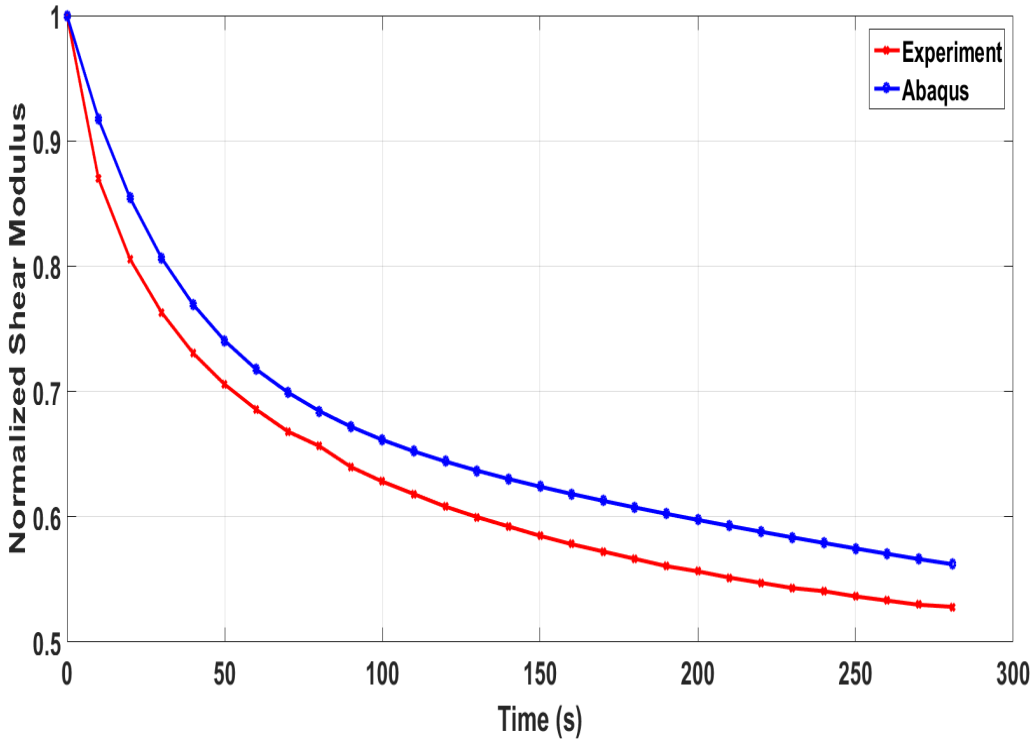

Figure 6.4. Normalised shear modulus vs time

6.3.3 Finite element modelling

The nanostructure of silica reinforced photopolymer matrix nanocomposite is shown by a 3D RVE (220 nm each side) for 8%, 9% and 10% filler concentrations as shown in Figure 6.5 (a, b & c), respectively. 30 similar spherical silica nanoparticles are randomly dispersed in the matrix. Random sequential adsorption algorithm [208] is used to generate nanoparticle centres, in which probability of finding a nanoparticle at a given position is same in all directions. Nanoparticle diameter is dependent on the volume fraction and aspect ratio. Aspect ratio of 1 is chosen for all filler concentrations. As the silica nanoparticles have the diameter of around 30 nm shown in Figure 3.11 of chapter 3, same is used for 8% filler concentration, the diameter increases with an increase in volume fraction. Elastic modulus of fumed silica nanoparticles was taken as E_p= 70 GPa and Poisson's ratio as υ_p= 0.3. For the properties of resin matrix epoxy urethane, calibrated Yeoh's hyperelastic material constants and Prony series coefficients were used as discussed in sections 6.3.1 and 6.3.2. Both phases are meshed with quadratic tetrahedron elements (C3D10M) with initial seed size of 11 nm as shown in Figure 6.6. In order to extend the RVE periodically periodic boundary conditions implemented from a user defined python script and were applied in all directions, i.e. observing the interlinkage among the RVE with its reflecting images. Displacement vector $\boldsymbol{u}$ was used to express the periodic boundary conditions, which relates the displacement among the opposed ends rendering to

$$\boldsymbol{u}(x, y, 0) - \boldsymbol{u_z} = \boldsymbol{u}(x, y, L) \tag{6.3}$$

$$\boldsymbol{u}(x, 0, z) - \boldsymbol{u_y} = \boldsymbol{u}(x, L, z) \tag{6.4}$$

$$\boldsymbol{u}(0, y, z) - \boldsymbol{u_x} = \boldsymbol{u}(L, y, z) \tag{6.5}$$

in which L corresponds to the RVE length and x, y, and z are coordinate axes and $\boldsymbol{u_x}$, $\boldsymbol{u_y}$ and $\boldsymbol{u_z}$ are dependent on the load applied to the RVE. A strain equal to the strain at break observed during uniaxial tensile test for each concentration was applied to the model in x-direction.

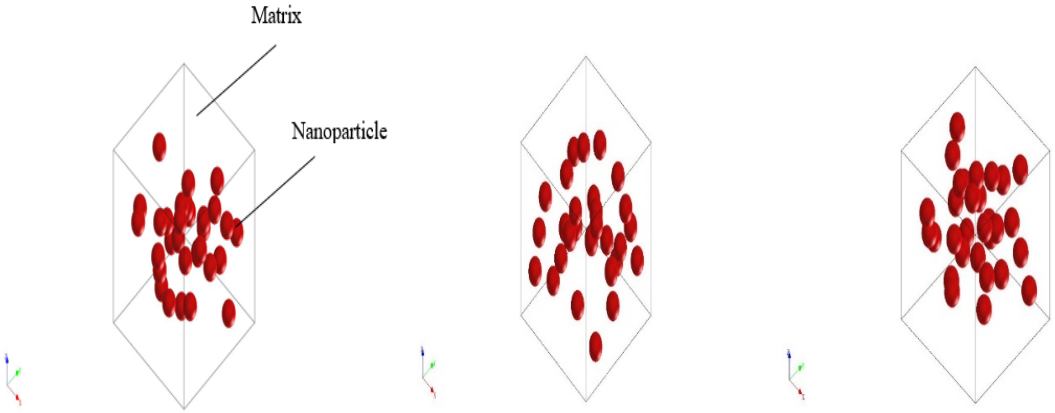

(a) (b) (c)

Figure 6.5. RVE showing (a) 8% filler concentration nanostructure (b) 9% filler concentration nanostructure (c) 10% filler concentration nanostructure

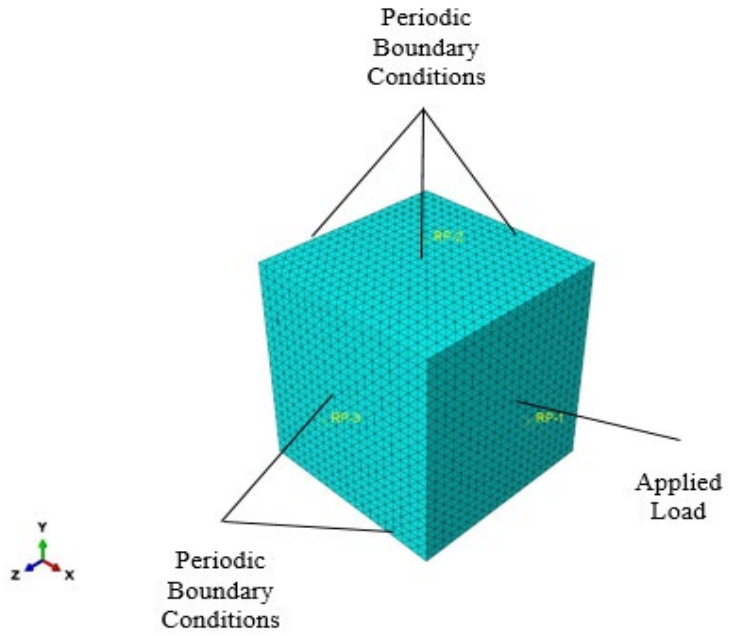

Figure 6.6. RVE showing periodic boundary conditions, applied load and mesh

6.3.4 FE simulations and model verification

A nanoscale RVE reinforced by silica filler with different concentrations was validated in this study, FE simulations were ran on RVE composed of randomly dispersed nanoparticles with proper boundary conditions as discussed in section 6.3.3 and results were compared with experiments. Many researchers have validated the hyperelastic models with experimental data [209-212] using different FE packages. In order to validate the proposed model, Yeoh's hyperelastic coefficients and Prony series coefficients were applied to the FE simulations of samples with filler concentrations of 8%, 9% and 10% and the results were compared with the experimental results.

Comparisons of the output obtained from the experiments and the FE model are depicted in Figures 6.7, 6.9 & 6.11. It is observed that the FE simulation with hyper and viscoelastic model using Yeoh's SEDF has good agreement with the experimental stress-strain curves of samples printed with 8%, 9% and 10% filler concentrations. Figures 7, 9 & 11 show the contour plots of the 8%, 9% and 10% filler concentrations respectively. Figures 6.8 (a), 6.10 (a) & 6.12 (a) show the reaction forces of the respective filler concentrations, stress was obtained by dividing the area of RVE with reaction force. Figures 6.8 (b), 6.10 (b) & 6.12 (b) show the displacement of the respective filler concentration, strain was obtained by dividing the length of the RVE with displacement.

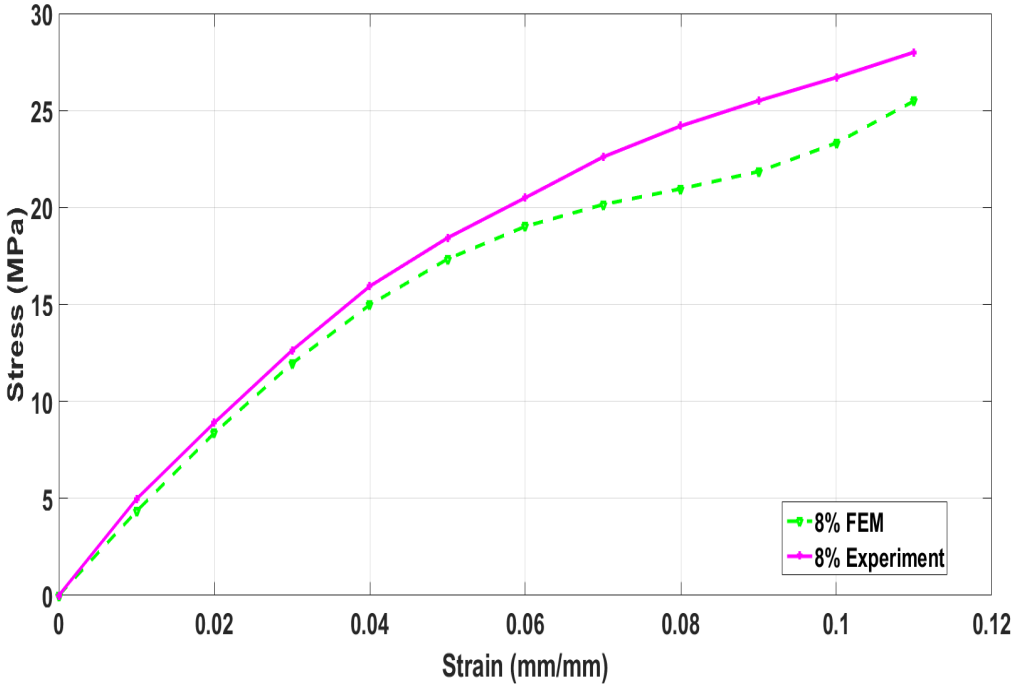

Figure 6.7. Comparison of stress-strain curves obtained from experiments and FEM for 8% filler concentration

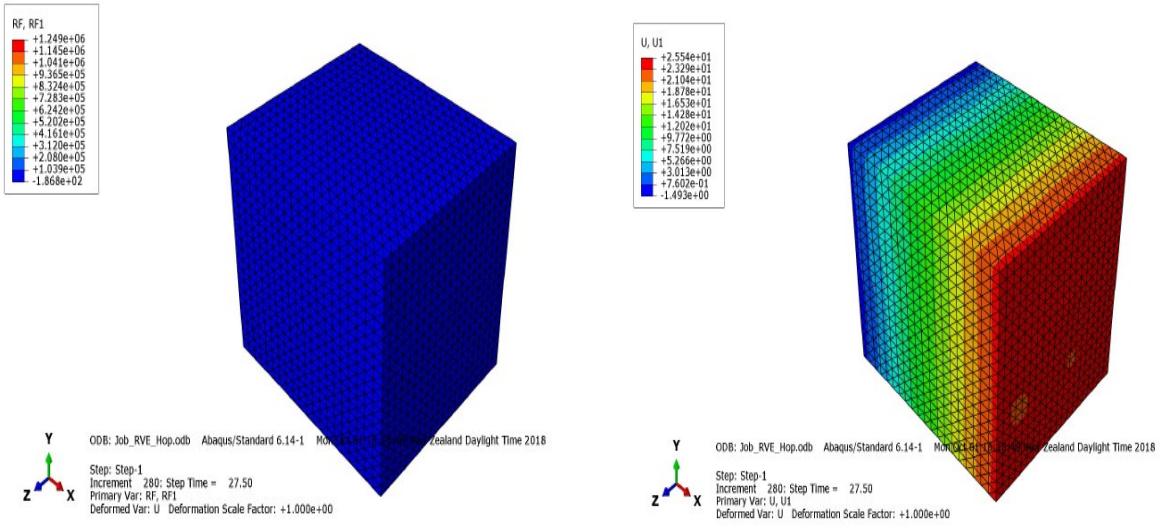

(a) (b)

Figure 6.8. Contour plot showing (a) reaction and (b) displacement for 8% filler concentration

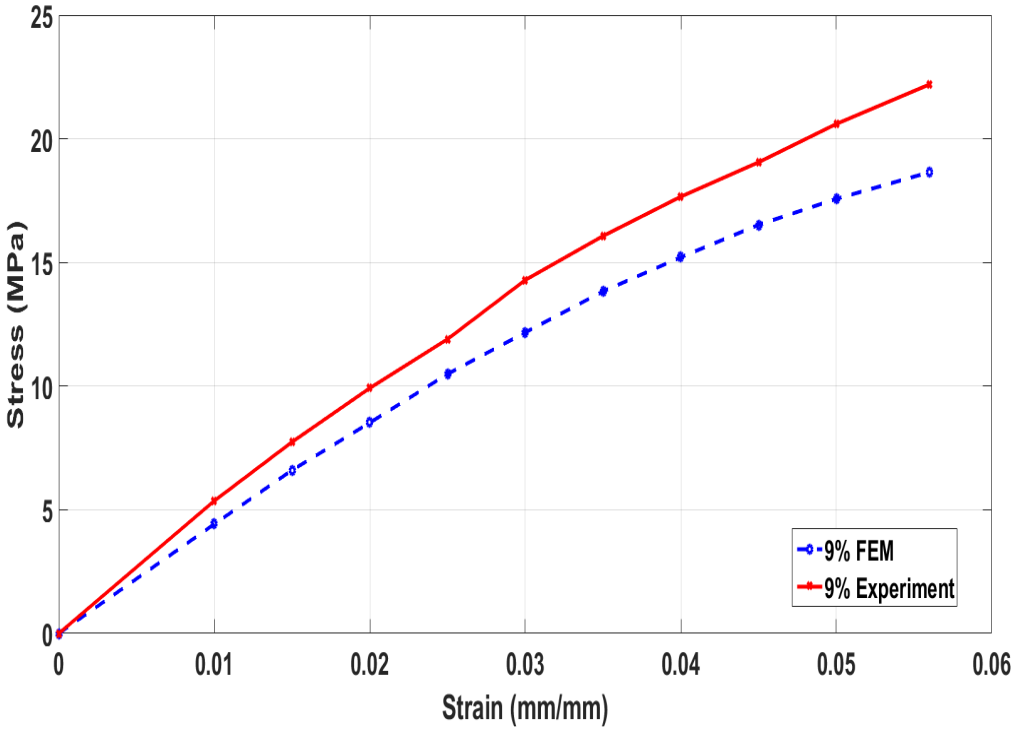

Figure 6.9. Comparison of stress-strain curves obtained from experiments and FEM for 9% filler concentration

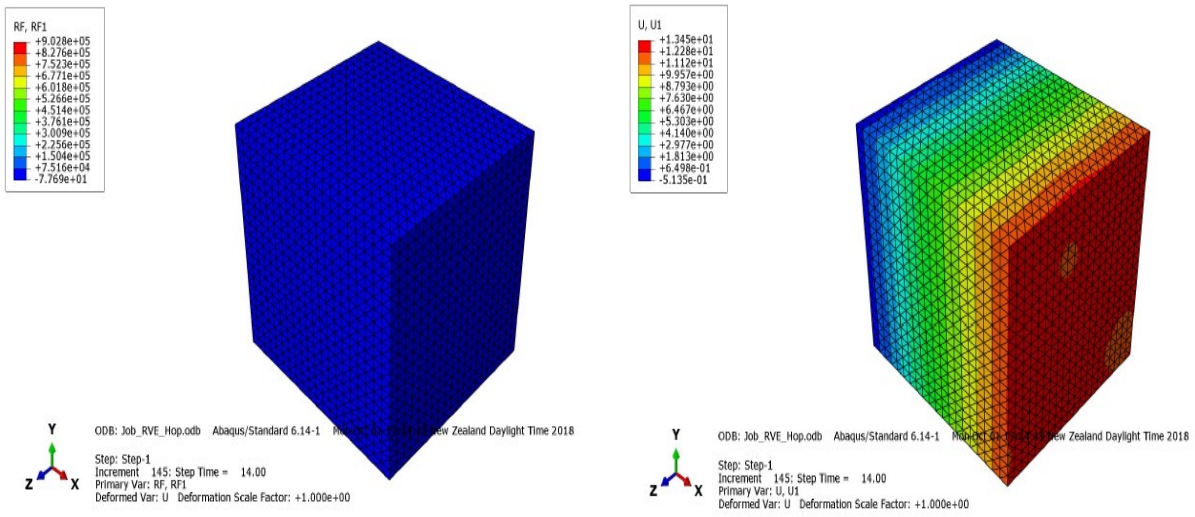

(a) (b)

Figure 6.10. Contour plot showing (a) reaction force and (b) displacement for 9% filler concentration

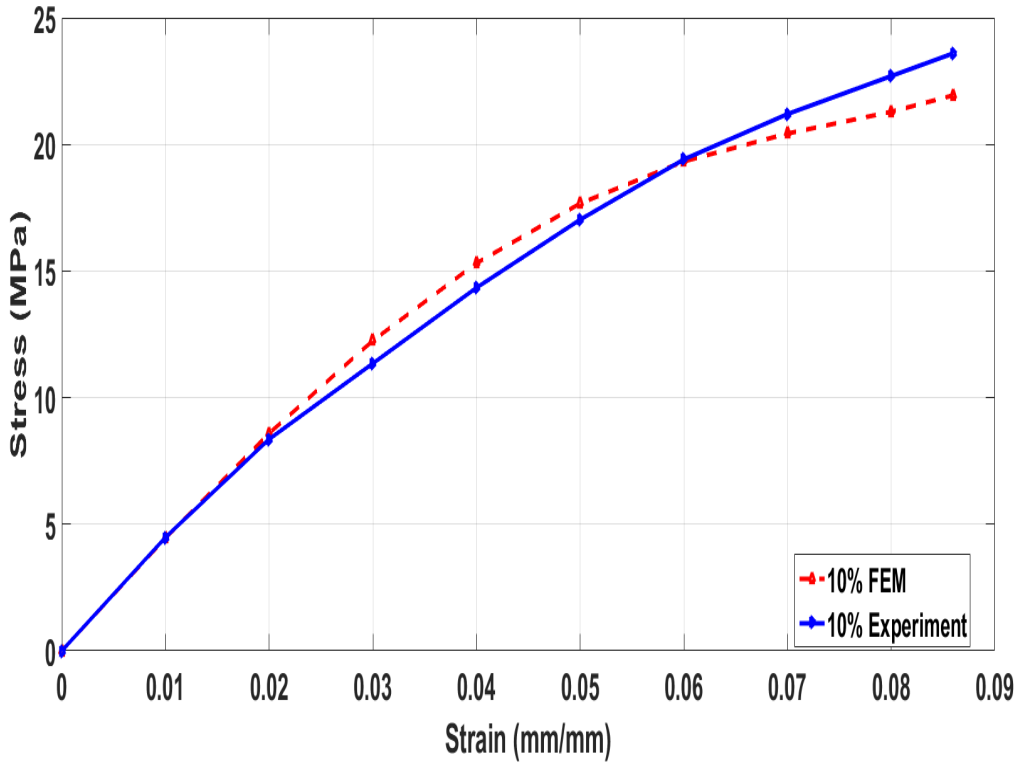

Figure 6.11. Comparison of stress-strain curve obtained from experiments and FEM for 10% filler concentration

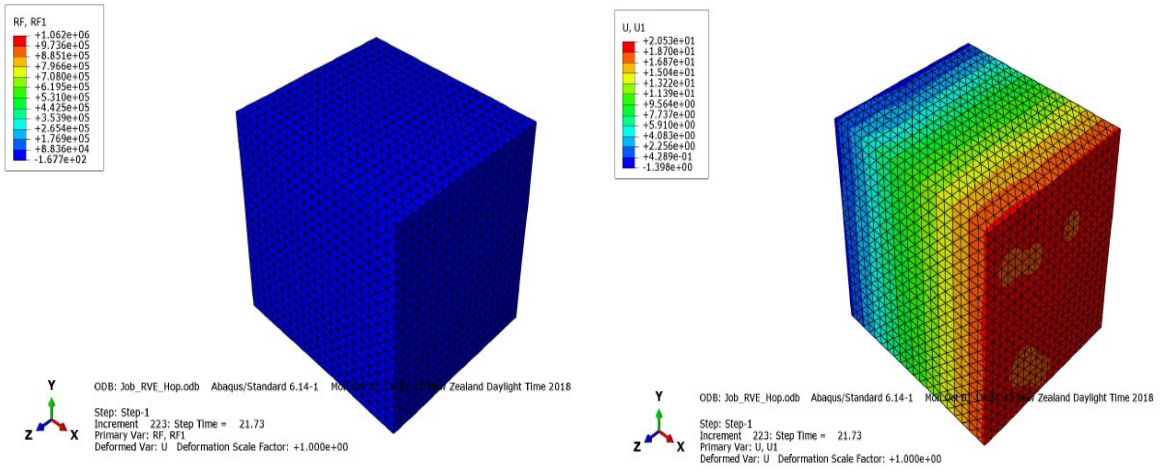

(a) (b)

Figure 6.12. Contour plot showing (a) reaction force and (b) displacement for 10% filler concentration

6.4 Parametric study

After validating the numerical model, parametric study was carried out on 8%, 9% and 10% filler concentrations which included stress relaxation simulations, creep simulations and investigating the effect of RVE size on the tensile strength of nanocomposite.

6.4.1 Stress relaxation

Figure 6.13 represents the stress relaxation diagram of 8%, 9% and 10% filler concentrations. A constant displacement was applied for a very short period of time in all three filler concentrations, initial vertical line shows the stress it took to displace the material. As the material is held at the applied constant displacement, the stress in the material decreases over time as evident from Figure 6.13. At the end, the stress became constant indicating the material has reached equilibrium.

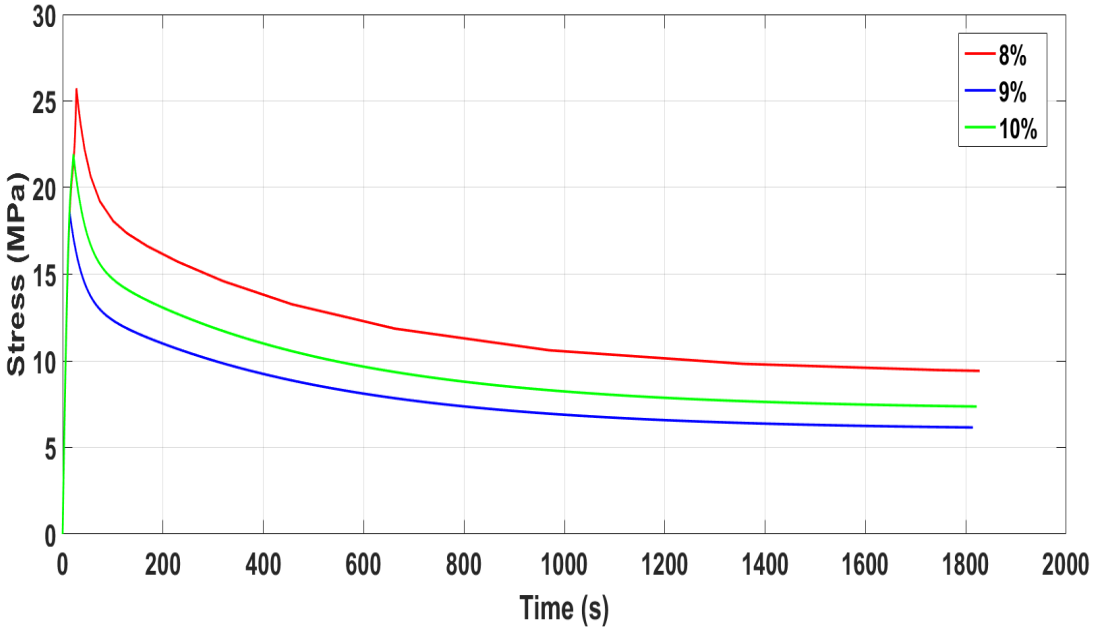

Figure 6.13. Stress relaxation curve of 8%, 9% and 10% filler concentration

6.4.2 Creep

Figure 6.14 shows the creep curve of 8%, 9% and 10% filler concentrations. Instantaneous load equivalent to 5 MPa stress was applied in all three filler concentrations. As seen in Figure 6.14,

initial straight line indicates instantaneous deformation, this deformation is partially elastic. After this, deformation rate decreases with time, this phase is called a transient or primary creep and is not considered to represent damage. Finally, the creep is moving toward stabilisation, where the rate of creep will be nearly constant, this stage is called secondary creep.

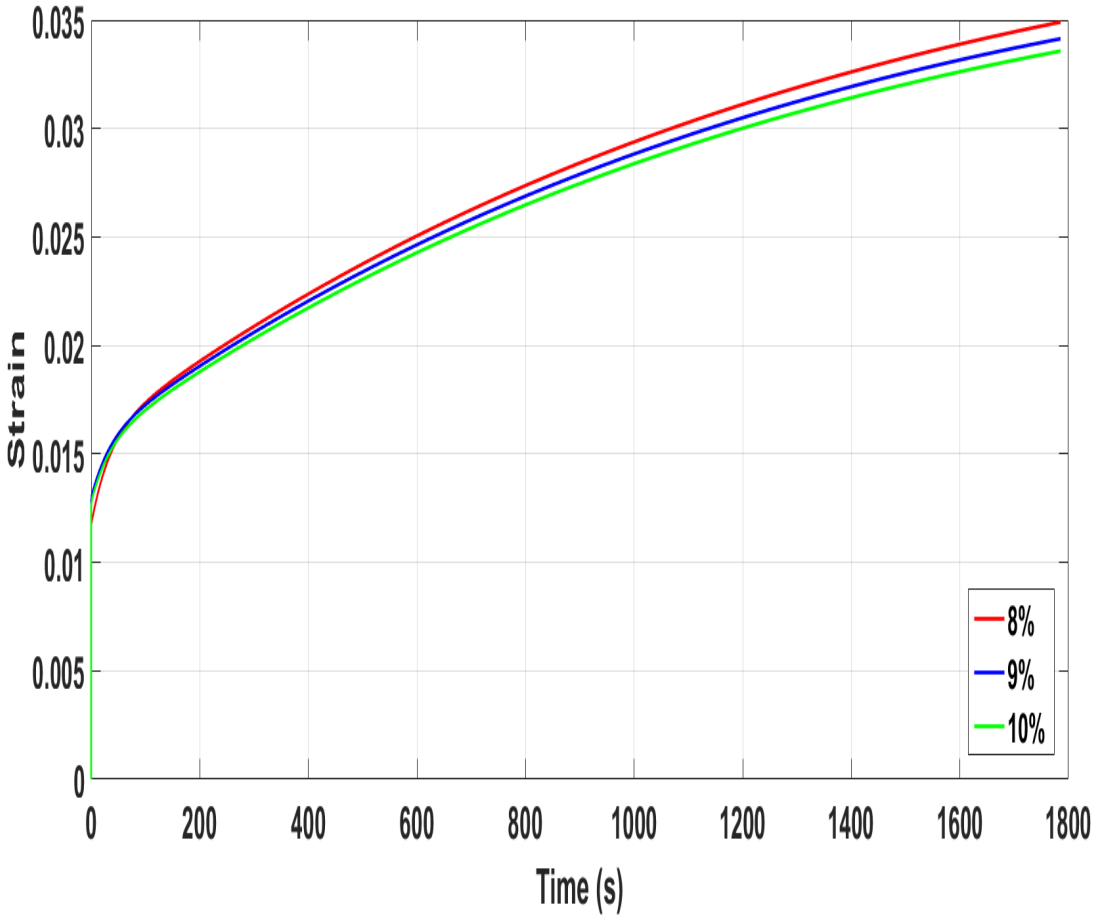

Figure 6.14. Creep curve of 8%, 9% and 10% filler concentrations

6.4.3 Effect of RVE size on tensile strength

In order to study the effect of RVE size on tensile strength, RVE with 3 different sizes were developed. RVE models of 150 nm × 150 nm × 150 nm, 175 nm × 175 nm × 175 nm, and 200 nm × 200 nm × 200 nm sizes were developed for 8%, 9% and 10% filler concentrations. After running the simulations it was found that RVE size does not have any significant effect on the tensile strength of all three filler concentrations used.

6.5 Empirical model

As discussed in section 3.1 of chapter 3, filler concentrations having the viscosity in a range of 15000 cP to 25000 cP were found to be suitable to print reliably. However, after validation of the numerical model, mechanical behaviour of the concentrations that were difficult to print can be simulated. In order to explore the mechanical behaviour at wider range of filler concentrations, the empirical models based on maximum tensile strength versus different filler concentrations and viscosity at different strain levels were developed.

6.5.1 Maximum tensile strength vs filler concentrations at 8%, 10% & 12% strain levels

Figure 6.15, 6.16 & 6.17 and Eq. (6.6), (6.7) & (6.8) represents the polynomial order 3 fit and its equations for the maximum tensile strength at 8%, 10% & 12% strain levels versus range of filler concentrations respectively.

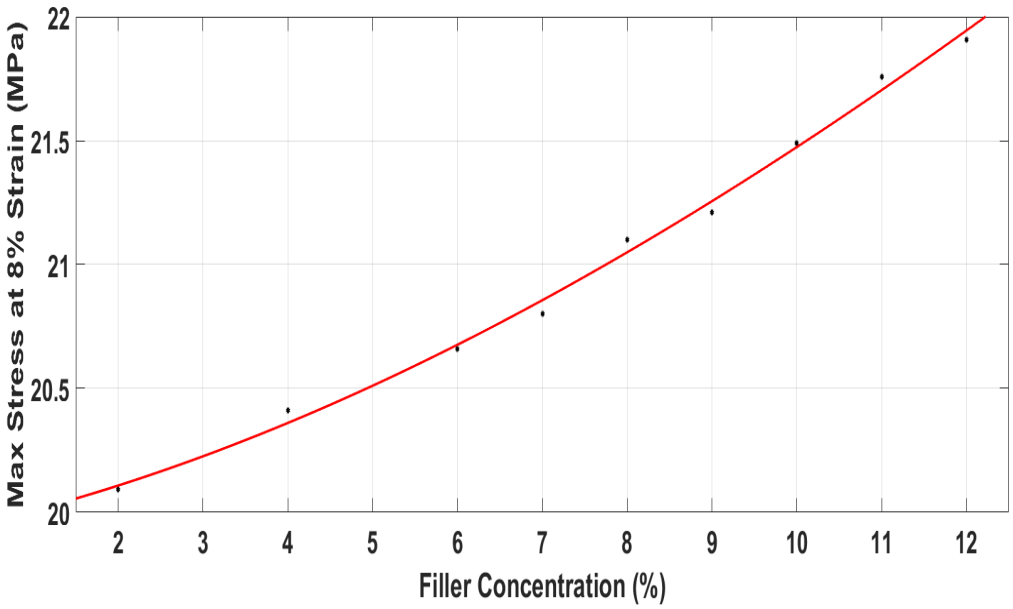

Figure 6.15.Polynomial order 3 fit for maximum stress at 8% strain vs different filler concentrations

$$f(x) = -0.00019x^3 + 0.00932x^2 + 0.07385x + 19.92 \quad (6.6)$$

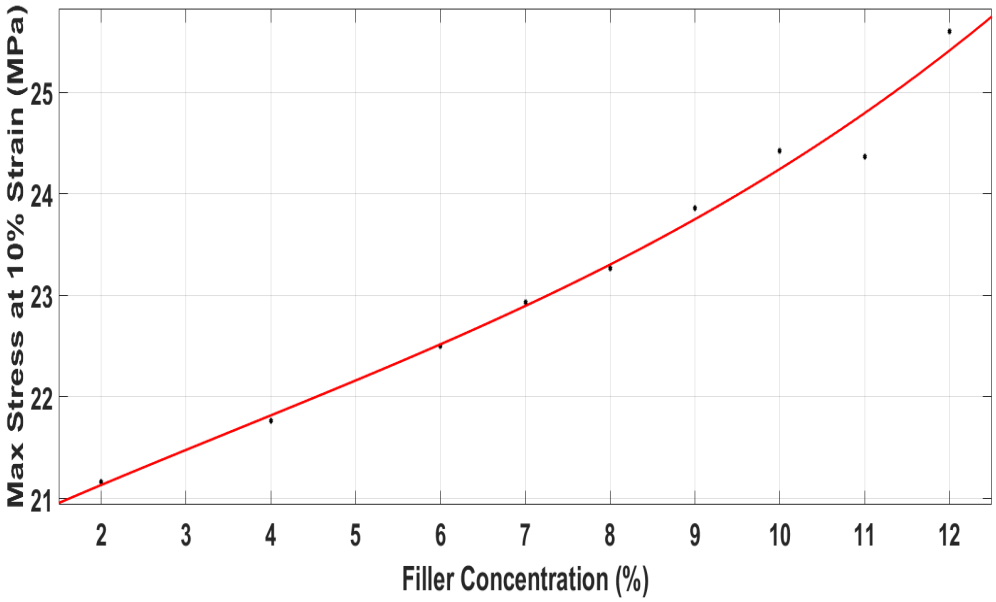

Figure 6.16. Polynomial order 3 fit for maximum stress at 10% strain vs different filler concentrations

$$f(x) = -0.00146x^3 - 0.01576x^2 + 0.3961x + 20.39 \quad (6.7)$$

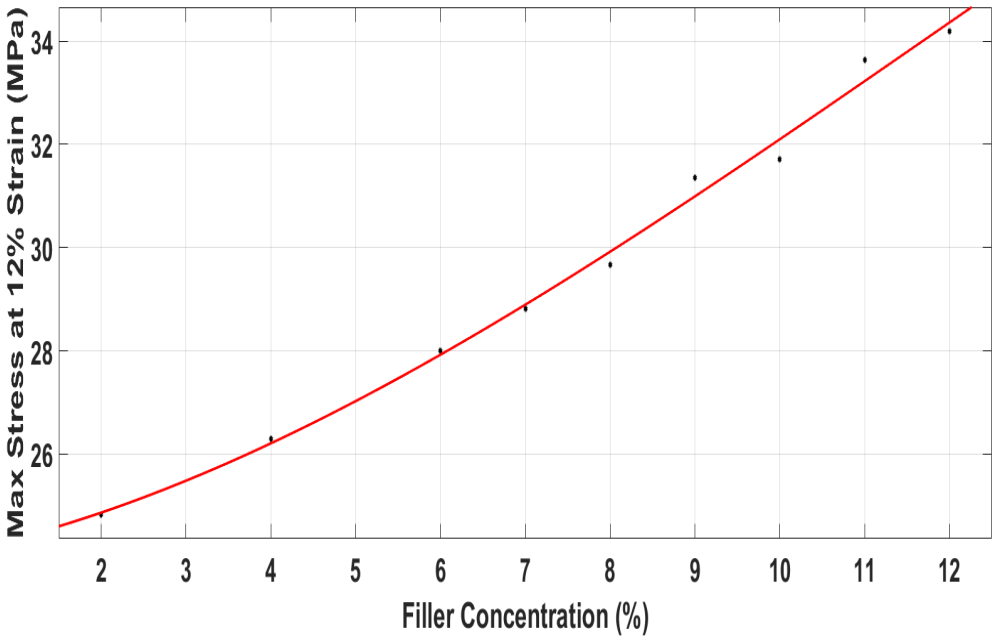

Figure 6.17. Polynomial order 3 fit for maximum stress at 12% strain vs different filler concentrations

$$f(x) = -0.00201x^3 - 0.07113x^2 + 0.3008x + 24 \quad (6.8)$$

6.5.2 Maximum tensile strength vs viscosity at different strain levels

Figures 6.18, 6.19 & 6.20 and Eq. (6.9), (6.10) & (6.11) represent the power term 2 fit and its equations for the maximum tensile strength at 8%, 10% & 12% strain levels versus viscosity respectively.

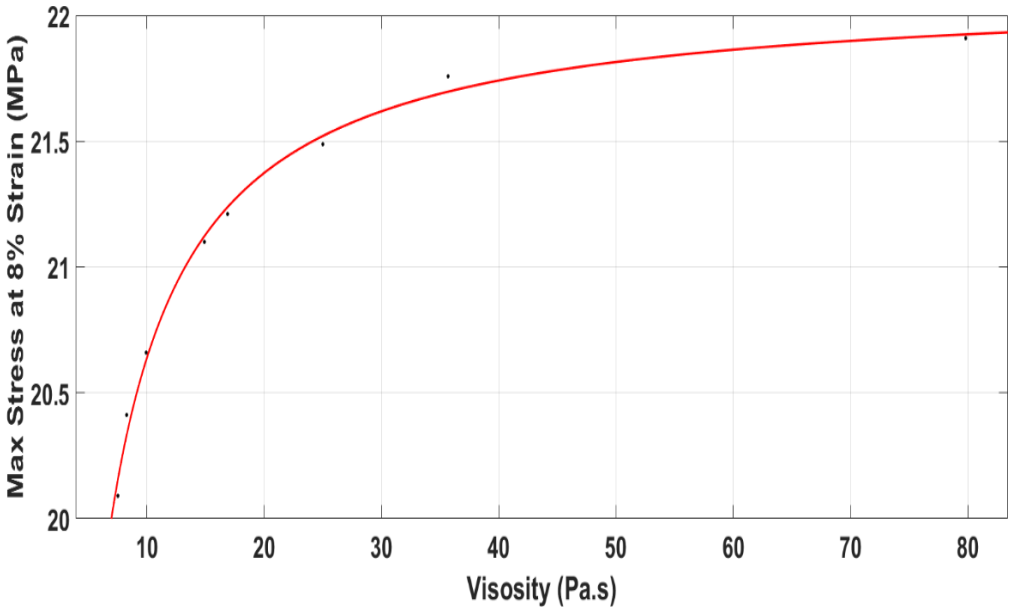

Figure 6.18. Power term 2 fit for maximum stress at 8% strain vs viscosity

$$f(x) = -14.73x^{-1.001} + 22.11 \quad (6.9)$$

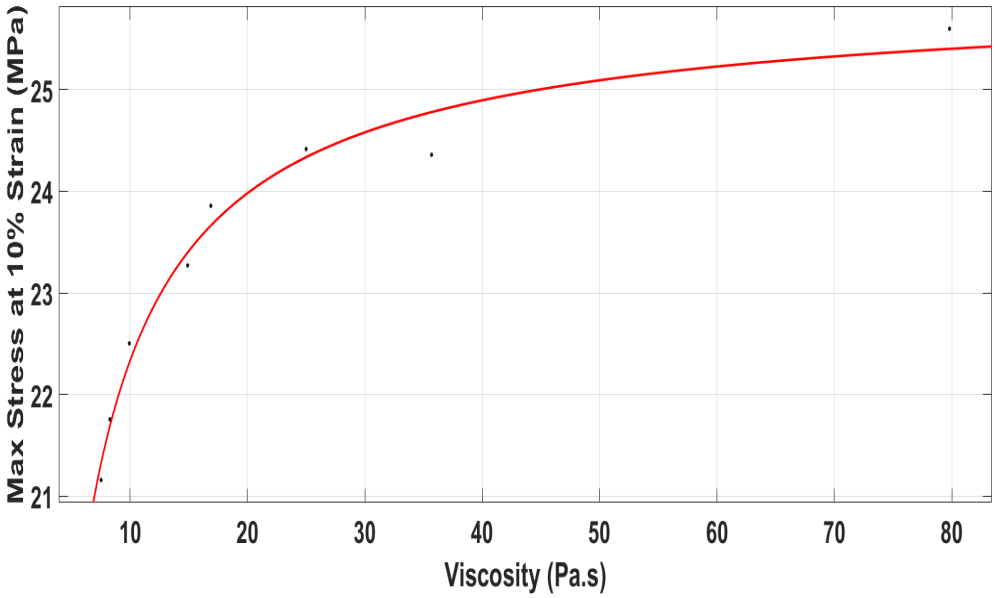

Figure 6.19. Power term 2 fit for maximum stress at 10% strain vs viscosity

$$f(x) = -26.16x^{-0.6493} + 26.04 \quad (6.10)$$

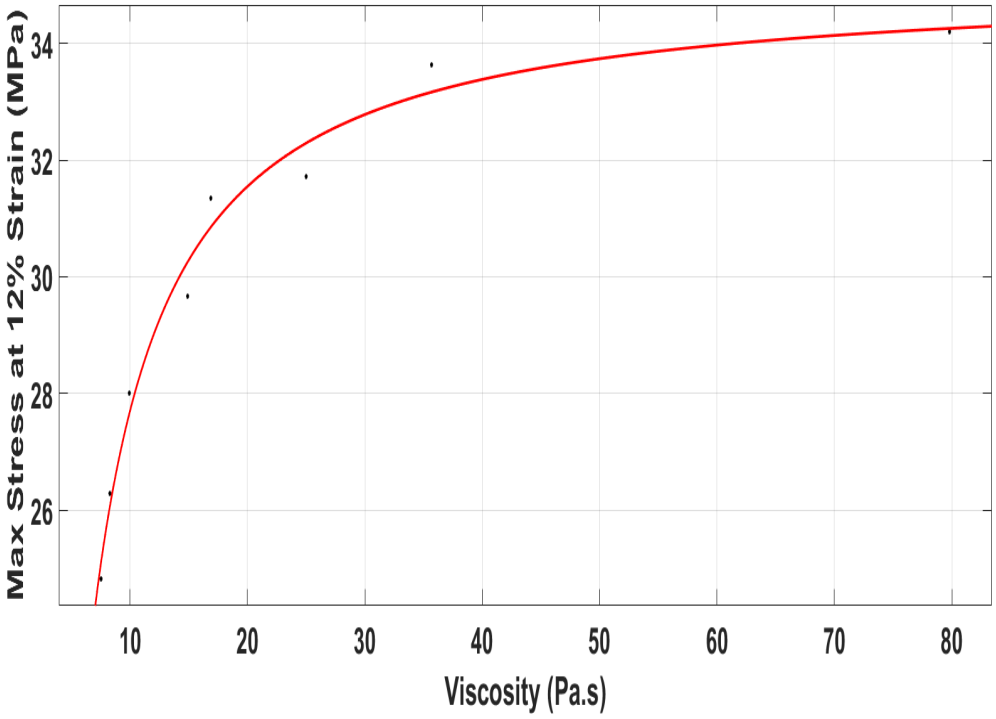

Figure 6.20. Power term 2 fit for maximum stress at 12% strain vs viscosity

$$f(x) = -85.7x^{-1.066} + 35.06 \quad (6.11)$$

6.6 Chapter summary

In this chapter, a detailed experimental and numerical study have been carried out on 3D printed particulate nanocomposites. As mentioned in chapter 1 that photopolymer extrusion is a new 3D printing technique and the mechanical behaviour of the samples printed is yet to be explored, therefore experimental and numerical analysis on the parts manufactured using the novel technique have been successfully carried out. Nano silica filler is used as reinforcement to enhance the mechanical properties of the photopolymer. Different concentrations of fumed silica filler have been added and its effect on mechanical properties have been analysed. A significant improvement in the tensile strength of the photopolymer was observed; for example tensile strength after the addition of 8%, 9% and 10% silica filler was 1.87, 1.48 and 1.57 times the tensile strength of the pure photopolymer respectively. A finite element model using hyper and viscoelastic phenomena have been developed and successfully corroborated with the experimental results. Multi-scale material modelling platform DIGIMAT was used to develop the RVE to represent the nanostructure of the nanocomposite, silica nanoparticles were randomly dispersed and proper boundary conditions were applied. Properties of the matrix were represented by Yeoh's material constant and Prony series coefficients. FE simulations were conducted using ABAQUS after importing the user defined python script. The developed FE model based on hyper and viscoelastic phenomena successfully captured the behaviour of the 3D printed nano silica reinforced particulate nanocomposite. By employing the combination of hyperelasticity and viscoelasticity, the model was found to have good agreement with experimental stress-strain relationship of 8%, 9% and 10% filler concentrations. Stress relaxation and creep behaviour of 8%, 9% and 10% filler concentrations were simulated after validating the numerical model as part of the parametric study. In addition, effect of RVE size on tensile strength was also analysed. As mentioned in section 3.6.1 of chapter 3, only narrow window of 8% to 10% filler concentrations can be reliably printed

because of viscosity. Therefore, in order to explore mechanical properties of wide range of filler concentrations, empirical models were developed. The empirical model provided the tensile strengths of the filler concentrations that were not possible to be printed with the photopolymer extrusion 3D printer at different strain levels, providing the possibility to analyse the mechanical properties at range of filler concentrations.

CHAPTER 7: CONCLUSIONS AND FUTURE WORK

A comprehensive mechanical characterisation, analysis and modelling of particulate nanocomposites made by a new photopolymer extrusion 3D printing technique have been carried out in this work. As the technique is relatively new, the mechanical properties, analysis and modelling of the printed parts have not been investigated yet. Therefore, investigations based on detailed experimentations and modelling approaches were undertaken in order to explore the mechanical behaviour of the 3D printed particulate nanocomposites.

7.1 Conclusions

First, a detailed experimentation was carried out in order to study the mechanical properties of the parts. The photopolymer resin is used as a base material in this technique and in order to reinforce the polymer and make the resin non-Newtonian, fumed silica filler is added. Effect of silica filler on mechanical properties, viscosity and dimensional accuracy have been investigated. As the technique has two additional rotational axes, capability to print free form and self-supported structures have been analysed. This leads to the work carried out in chapter 3.

Results showed that samples bearing viscosity in a range of 15000 cP to 25000 cP corresponding to 8% to 10% filler concentrations can be printed reliably. Fumed silica as filler, enhanced the mechanical properties of the polymer as demonstrated by the significant increase in tensile and flexural strengths. The effect of the filler on dimensional accuracy revealed that higher filler concentrations could lead to more deviated printed dimensions as it is difficult to extrude from the extrusion nozzle. Its capability to print free form and self-supported structures utilising rotational axes have been successfully demonstrated by printing stair case and horizontal U shape objects.

The strength of 3D printed objects heavily rely on interfacial adhesion i.e. bond between matrix and nanoparticles. Therefore, an experimental study was carried out in order to observe the interfacial adhesion of 3D printed particulate nanocomposites. A comparison of interfacial adhesion of 3D printed samples was drawn by fabricating the samples using casting. Tensile tests were conducted on 3D printed and casted samples. Existing theoretical models were used to determine the interfacial adhesion of 3D printed and cast samples. This leads to the work carried out in chapter 4.

Results revealed that 3D printed samples possess stronger tensile strength and Young's modulus compared to the casted samples. In order to find out the reason behind the strong mechanical properties of 3D printed samples, their interfacial adhesion was measured and compared with that of casted samples. It was found that interfacial adhesion in 3D printed samples is stronger compared to casted samples, which led to strong mechanical properties for 3D printed samples. To further elaborate the reason behind this behaviour of 3D printed samples, SEM micrographs were used to study the distribution of silica filler at subsurface of both 3D printed and casted samples. In the case of 3D printed samples, SEM micrographs revealed that the filler is homogenously distributed throughout the sample, where in casted sample, non-homogenous distribution was observed as clear absence of filler was evident. This leads to the strong mechanical properties in 3D printed samples.

Polymers are viscoelastic materials, which exhibit time dependent response. They also possess weak mechanical properties and to enhance the properties, fillers are added. In order to enhance the mechanical properties and study the time dependent response of the photopolymer resin used in this research, a comprehensive study based on experimental and theoretical modelling is carried out. Different concentrations of fillers were added to enhance the properties, and tensile tests were conducted at different strain rates to observe the rate dependent response.

QLV model based on hyper and viscoelastic phenomena was used to capture the rate dependent response and these are reported in chapter 5.

Results show that addition of the reinforcement filler significantly enhanced the mechanical properties of the polymer. 4%, 8%, 9% and 10% filler concentrations were used to enhance the properties of the polymer. However, it was found that 4% filler content had more profound effect on mechanical properties compared to all other filler concentrations used. This is because increasing the filler content decreases the surface area of the nanoparticles, also nanoparticles have the tendency to form agglomerates. This leads to weak interfacial adhesion causing the nanocomposite to exhibit weak mechanical properties. As viscoelastic materials exhibit time dependent response, tensile strength of the polymer and all filler concentrations increased by increasing the strain rate. Three different strain rates of 1.3×10^{-2} s^{-1}, 1.3×10^{-3} s^{-1} and 1.3×10^{-4} s^{-1} were used and stronger response was captured at 1.3×10^{-2} s^{-1}. QLV model combining hyper and viscoelastic phenomena have been used to model the rate dependent behaviour of the material. MATLAB script of the QLV model with Yeoh strain energy density function was developed in optimisation tool box, global fitting procedure was carried out with nonlinear least square criterion and trust region reflective algorithm. It was found that QLV model bears very good agreement with the rate dependent stress-strain response of the pure polymer and nanocomposite with 4%, 8%, 9% and 10% filler concentrations.

Finally, experimental and numerical studies on the effect of filler on mechanical properties were also carried out. Tensile and stress relaxation tests were conducted on the samples. Numerical model combining hyper and viscoelastic phenomena was developed using the 3D RVE. RVE was developed on multi-material modelling platform DIGIMAT© and subsequent simulation were performed in ABAQUS. The results of these studies are reported in chapter 6.

8%, 9% and 10% filler concentrations were used to enhance the mechanical properties of the samples. Results show that fumed silica filler enhanced the mechanical properties of the 3D printed samples. 8% filler found to have more profound effect on tensile strength of 3D printed samples compared to 9% and 10%. Reason behind this behaviour is decrease in surface area of nanoparticles and agglomeration at higher filler content. Numerical model was developed combining hyper and viscoelastic phenomena and it was found that the developed model has good agreement with the experimental stress-strain results of 8%, 9% and 10% filler concentrations. After validating the numerical model, parametric study was carried out, which included stress relaxation behaviour, creep behaviour and the effect of RVE dimensions on tensile strength. In order to study the behaviour of high filler concentrations which were difficult to print due to their high viscosities, empirical models were developed. The developed empirical models could provide prediction of tensile strength of wide range of filler concentration.

7.2 Contributions

- Experimental study carried out in chapter 3 proposed a suitable range of viscosity to print the nanocomposite smoothly using the proposed technique. Different concentrations of the filler were added and their viscosities were measured, based on the viscosity it was proposed that 8% to 10% filler concentrations can be printed reliably. Effect of filler on mechanical properties, dimensional accuracy and surface roughness was also determined which provided plausible information on the addition of the filler for the respective tasks. The capability of the proposed technique for printing free-form and self-supported structures using addition rotational axes is also successfully demonstrated by printed stair case and horizontal U-shape objects.
- Study conducted in chapter 4 outlined a very important property of 3D printed nanocomposite i.e. interfacial adhesion. Interfacial adhesion of 3D printed samples

were compared with cast samples using the existing interfacial adhesion parameter models and the reason behind the superior interfacial adhesion of 3D printed samples was elaborated with the help of SEM micrographs

- In chapter 5 effect of filler on tensile strength was studied, different concentrations of filler were added. Filler concentration which had more profound effect on tensile strength compared to other concentrations was proposed. QLV model with Yeoh strain energy density function was used to calibrate the viscoelastic properties and to capture strain rate dependent mechanical behaviour of the polymer and nanocomposite. Uniaxial tensile tests were conducted at different strain rates. MATLAB script of the QLV model with Yeoh strain energy density function was developed in optimisation tool box, global fitting procedure was carried out with nonlinear least square criterion and trust region reflective algorithm. It was found that QLV model combining hyper and viscoelastic phenomena successfully captured the stress-strain behaviour of the polymer and the nanocomposite with 4%, 8%, 9% and 10% filler concentrations.
- In chapter 6, FE model of 3D printed nanocomposite having 8%, 9% and 10% filler concentrations was developed based on the hyper-viscoelastic material behaviour. FE model was developed using commercial FE package ABAQUS©, the nanostructure of the nanocomposite was imported from multi-material modelling platform DIGIMAT©. After validating the FEM as part of the parametric study stress relaxation behaviour, creep behaviour and effect of RVE size on tensile strength were evaluated. Furthermore, FEM model was used to predict the mechanical behaviour of the filler concentrations having high weight fractions i.e. an empirical model was developed which predicts the mechanical behaviour of the nanocomposite based on filler concentration and viscosity.

7.3 Future work

Based on the findings obtained in this thesis, some potential directions for future research are as follows:

- Experimental study conducted in chapter 3 can be extended by printing and testing type V specimen with 6 mm thickness in order to analyse the effect of thickness on mechanical properties. In addition, fatigue test can be carried out to study the fatigue life of the 3D printed nanocomposite.
- A different filler having diameter in micrometre can be added to reinforce the polymer and results can be compared with the results obtained in this thesis.
- Study on interfacial adhesion of 3D printed nanocomposite conducted in chapter 4 can be extended by adding surfactant or linker with fumed silica filler to avoid agglomeration and have better homogenisation.
- FEM study conducted in chapter 6 can be extended by studying the role of interphase on tensile strength. Furthermore, damage mechanism of the nanocomposite can also be investigated using FEM.
- One of the distinct feature of this hybrid 3D panting technique is the two additional rotational axes, its additional capability to print free-form and freestanding structures have been successfully demonstrated in this research. However, more researches are needed to develop new path generation algorithm that can convert the CAD models into printing path.

References

1. Invernizzi, M., G. Natale, M. Levi, S. Turri and G. Griffini, *UV-Assisted 3D Printing of Glass and Carbon Fiber-Reinforced Dual-Cure Polymer Composites.* Materials, 2016. **9**(7): p. 583.
2. Engelke, R., G. Engelmann, G. Gruetzner, M. Heinrich, M. Kubenz and H. Mischke, *Complete 3D UV microfabrication technology on strongly sloping topography substrates using epoxy photoresist SU-8*. Vol. s 73–74. 2004. 456–462.
3. Ladd, C., J.H. So, J. Muth and M.D. Dickey, *3D printing of free standing liquid metal microstructures.* Adv Mater, 2013. **25**(36): p. 5081-5.
4. Pitts, J.D., P.J. Campagnola, G.A. Epling and S.L. Goodman, *Submicron Multiphoton Free-Form Fabrication of Proteins and Polymers: Studies of Reaction Efficiencies and Applications in Sustained Release.* Macromolecules, 2000. **33**(5): p. 1514-1523.
5. Kaye, R., T. Goldstein, D. Zeltsman, D.A. Grande and L.P. Smith, *Three dimensional printing: A review on the utility within medicine and otolaryngology.* Int J Pediatr Otorhinolaryngol, 2016. **89**: p. 145-8.
6. Rengier, F., A. Mehndiratta, H. von Tengg-Kobligk, C.M. Zechmann, R. Unterhinninghofen, H.U. Kauczor and F.L. Giesel, *3D printing based on imaging data: review of medical applications.* Int J Comput Assist Radiol Surg, 2010. **5**(4): p. 335-41.
7. Kodama, H., *Automatic method for fabricating a three-dimensional plastic model with photo-hardening polymer.* Review of Scientific Instruments, 1981. **52**(11): p. 1770-1773.
8. Murphy, S.V. and A. Atala, *3D bioprinting of tissues and organs.* Nature Biotechnology, 2014. **32**: p. 773.

9. Zhu, W., X. Ma, M. Gou, D. Mei, K. Zhang and S. Chen, *3D printing of functional biomaterials for tissue engineering.* Current Opinion in Biotechnology, 2016. **40**: p. 103-112.

10. Gross, B.C., J.L. Erkal, S.Y. Lockwood, C. Chen and D.M. Spence, *Evaluation of 3D Printing and Its Potential Impact on Biotechnology and the Chemical Sciences.* Analytical Chemistry, 2014. **86**(7): p. 3240-3253.

11. *Additive Manufacturing Research Group*. Available from: https://www.lboro.ac.uk/research/amrg/about/the7categoriesofadditivemanufacturing/binderjetting/.

12. Groth, C., N.D. Kravitz, P.E. Jones, J.W. Graham and W.R. Redmond, *Three-dimensional printing technology.* J Clin Orthod, 2014. **48**(8): p. 475-85.

13. Chia, H.N. and B.M. Wu, *Recent advances in 3D printing of biomaterials.* Journal of biological engineering, 2015. **9**: p. 4-4.

14. Mohammed, J.S., *Applications of 3D printing technologies in oceanography.* Methods in Oceanography, 2016. **17**: p. 97-117.

15. Stansbury, J.W. and M.J. Idacavage, *3D printing with polymers: Challenges among expanding options and opportunities.* Dental Materials, 2016. **32**(1): p. 54-64.

16. Wang, X., M. Jiang, Z. Zhou, J. Gou and D. Hui, *3D printing of polymer matrix composites: A review and prospective.* Composites Part B: Engineering, 2017. **110**: p. 442-458.

17. Smay, J.E., G.M. Gratson, R.F. Shepherd, J. Cesarano and J. Lewis, *Directed Colloidal Assembly of 3D Periodic Structures*. Vol. 14. 2002. 1279-1283.

18. Kumta, S., M. Kumta, L. Jain, S. Purohit and R. Ummul, *A novel 3D template for mandible and maxilla reconstruction: Rapid prototyping using stereolithography.* Indian Journal of Plastic Surgery, 2015. **48**(3): p. 263-273.

19. Cho, Y.H., I.H. Lee and D.-W. Cho, *Laser scanning path generation considering photopolymer solidification in micro-stereolithography.* Microsystem Technologies, 2005. **11**(2): p. 158-167.

20. Heller, C., M. Schwentenwein, G. Russmueller, F. Varga, J. Stampfl and R. Liska, *Vinyl esters: Low cytotoxicity monomers for the fabrication of biocompatible 3D scaffolds by lithography based additive manufacturing.* Journal of Polymer Science Part A: Polymer Chemistry, 2009. **47**(24): p. 6941-6954.

21. Farahani, R.D., K. Chizari and D. Therriault, *Three-dimensional printing of freeform helical microstructures: a review.* Nanoscale, 2014. **6**(18): p. 10470-10485.

22. Schönberger, M. and M. Hoffstetter, *4 - Generative Manufacturing Technologies—The Future?*, in *Emerging Trends in Medical Plastic Engineering and Manufacturing*, M. Schönberger and M. Hoffstetter, Editors. 2016, William Andrew Publishing. p. 107-174.

23. Abdelaal, O., *Review of Rapid Prototyping Techniques for Tissue Engineering Scaffolds Fabrication*. 2013. p. 33-54.

24. Shirazi, S.F.S., S. Gharehkhani, M. Mehrali, H. Yarmand, H.S.C. Metselaar, N. Adib Kadri and N.A.A. Osman, *A review on powder-based additive manufacturing for tissue engineering: selective laser sintering and inkjet 3D printing.* Science and technology of advanced materials, 2015. **16**(3): p. 033502-033502.

25. Goodridge, R.D., M.L. Shofner, R.J.M. Hague, M. McClelland, M.R. Schlea, R.B. Johnson and C.J. Tuck, *Processing of a Polyamide-12/carbon nanofibre composite by laser sintering.* Polymer Testing, 2011. **30**(1): p. 94-100.

26. Do, A.V., B. Khorsand, S.M. Geary and A.K. Salem, *3D Printing of Scaffolds for Tissue Regeneration Applications.* Adv Healthc Mater, 2015. **4**(12): p. 1742-62.

27. Udroiu, R., *Powder bed additive manufacturing systems and its applications*. Vol. 10. 2012. 122-129.

28. Ali, M.N., J.J.C. Busfield and I.U. Rehman, *Auxetic oesophageal stents: structure and mechanical properties.* Journal of Materials Science: Materials in Medicine, 2014. **25**(2): p. 527-553.

29. Singh, S., *Implant Materials and Their Processing Technologies*. 2016.

30. Ge, Q., C.K. Dunn, H.J. Qi and M.L. Dunn, *Active origami by 4D printing.* Smart Materials and Structures, 2014. **23**(9): p. 094007.

31. Cooperstein, I., M. Layani and S. Magdassi, *3D printing of porous structures by UV-curable O/W emulsion for fabrication of conductive objects.* Journal of Materials Chemistry C, 2015. **3**(9): p. 2040-2044.

32. Postiglione, G., G. Natale, G. Griffini, M. Levi and S. Turri, *Conductive 3D microstructures by direct 3D printing of polymer/carbon nanotube nanocomposites via liquid deposition modeling.* Composites Part A: Applied Science and Manufacturing, 2015. **76**: p. 110-114.

33. Tymrak, B.M., M. Kreiger and J.M. Pearce, *Mechanical properties of components fabricated with open-source 3-D printers under realistic environmental conditions.* Materials & Design, 2014. **58**: p. 242-246.

34. Sun, Q., G.M. Rizvi, C.T. Bellehumeur and P. Gu, *Effect of processing conditions on the bonding quality of FDM polymer filaments.* Rapid Prototyping Journal, 2008. **14**(2): p. 72-80.

35. Tran, P., T.D. Ngo, A. Ghazlan and D. Hui, *Bimaterial 3D printing and numerical analysis of bio-inspired composite structures under in-plane and transverse loadings.* Composites Part B: Engineering, 2017. **108**: p. 210-223.

36. Melnikova, R., A. Ehrmann and K. Finsterbusch, *3D printing of textile-based structures by Fused Deposition Modelling (FDM) with different polymer materials.* IOP Conference Series: Materials Science and Engineering, 2014. **62**: p. 012018.

37. Caulfield, B., P.E. McHugh and S. Lohfeld, *Dependence of mechanical properties of polyamide components on build parameters in the SLS process.* Journal of Materials Processing Technology, 2007. **182**(1): p. 477-488.

38. Gu, H., C. Ma, J. Gu, J. Guo, X. Yan, J. Huang, Q. Zhang and Z. Guo, *An overview of multifunctional epoxy nanocomposites.* Journal of Materials Chemistry C, 2016. **4**(25): p. 5890-5906.

39. Gu, J., X. Yang, Z. Lv, N. Li, C. Liang and Q. Zhang, *Functionalized graphite nanoplatelets/epoxy resin nanocomposites with high thermal conductivity.* International Journal of Heat and Mass Transfer, 2016. **92**: p. 15-22.

40. Dou, J., Q. Zhang, M. Ma and J. Gu, *Fast fabrication of epoxy-functionalized magnetic polymer core-shell microspheres using glycidyl methacrylate as monomer via photo-initiated miniemulsion polymerization.* Journal of Magnetism and Magnetic Materials, 2012. **324**(19): p. 3078-3082.

41. Kroll, E. and D. Artzi, *Enhancing aerospace engineering students' learning with 3D printing wind-tunnel models.* Rapid Prototyping Journal, 2011. **17**(5): p. 393-402.

42. Wong, K.V. and A. Hernandez, Int. Sch. Res. Not., 2012: p. 2012.

43. B., S.D., *Use of 3D Printing by Museums: Educational Exhibits, Artifact Education, and Artifact Restoration.* 3D Printing and Additive Manufacturing, 2015. **2**(4): p. 209-215.

44. Huang, S.H., P. Liu, A. Mokasdar and L. Hou, *Additive manufacturing and its societal impact: a literature review.* The International Journal of Advanced Manufacturing Technology, 2013. **67**(5): p. 1191-1203.

45. Isakov, D.V., Q. Lei, F. Castles, C.J. Stevens, C.R.M. Grovenor and P.S. Grant, *3D printed anisotropic dielectric composite with meta-material features.* Materials & Design, 2016. **93**: p. 423-430.

46. Boparai, K., R. Singh and H. Singh, *Comparison of tribological behaviour for Nylon6-Al-Al2O3 and ABS parts fabricated by fused deposition modelling.* Virtual and Physical Prototyping, 2015. **10**(2): p. 59-66.

47. Asif, M., J.H. Lee, M.J. Lin-Yip, S. Chiang, A. Levaslot, T. Giffney, M. Ramezani and K.C. Aw, *A new photopolymer extrusion 5-axis 3D printer.* Additive Manufacturing, 2018. **23**: p. 355-361.

48. Chung, H. and S. Das, *Processing and properties of glass bead particulate-filled functionally graded Nylon-11 composites produced by selective laser sintering.* Materials Science and Engineering: A, 2006. **437**(2): p. 226-234.

49. Nikzad, M., S.H. Masood and I. Sbarski, *Thermo-mechanical properties of a highly filled polymeric composites for Fused Deposition Modeling.* Materials & Design, 2011. **32**(6): p. 3448-3456.

50. Hwang, S., E.I. Reyes, K.-s. Moon, R.C. Rumpf and N.S. Kim, *Thermo-mechanical Characterization of Metal/Polymer Composite Filaments and Printing Parameter Study for Fused Deposition Modeling in the 3D Printing Process.* Journal of Electronic Materials, 2015. **44**(3): p. 771-777.

51. Kokkinis, D., M. Schaffner and A.R. Studart, *Multimaterial magnetically assisted 3D printing of composite materials.* Nature Communications, 2015. **6**: p. 8643.

52. Yugang, D., Z. Yuan, T. Yiping and L. Dichen, *Nano-TiO2-modified photosensitive resin for RP.* Rapid Prototyping Journal, 2011. **17**(4): p. 247-252.

53. Wang, X., F. Liang, Q. Yang, Z. Zhou and J. Gou, *Processing and characterization of helical carbon nanotube paper based thermoplastic nanocomposite films*. 2014.

54. Chen, H., M.B. Müller, K.J. Gilmore, G.G. Wallace and D. Li, *Mechanically Strong, Electrically Conductive, and Biocompatible Graphene Paper.* Advanced Materials, 2008. **20**(18): p. 3557-3561.

55. Gu, J., C. Xie, H. Li, J. Dang, W. Geng and Q. Zhang, *Thermal percolation behavior of graphene nanoplatelets/polyphenylene sulfide thermal conductivity composites.* Polymer Composites, 2014. **35**(6): p. 1087-1092.

56. Lu, H., X. Wang, Y. Yao, J. Gou, D. Hui, B. Xu and Y.Q. Fu, *Synergistic effect of siloxane modified aluminum nanopowders and carbon fiber on electrothermal efficiency of polymeric shape memory nanocomposite.* Composites Part B: Engineering, 2015. **80**: p. 1-6.

57. Liang, F., J. Sparkman, X. Wang, Y. Xu, B. Mabbott and J. Gou, *Polyurethane nanocomposite coatings with enhanced mechanical and thermal properties*. 2014.

58. Liu, H. and L.C. Brinson, *Reinforcing efficiency of nanoparticles: A simple comparison for polymer nanocomposites.* Composites Science and Technology, 2008. **68**(6): p. 1502-1512.

59. Torrado Perez, A.R., D.A. Roberson and R.B. Wicker, *Fracture Surface Analysis of 3D-Printed Tensile Specimens of Novel ABS-Based Materials.* Journal of Failure Analysis and Prevention, 2014. **14**(3): p. 343-353.

60. Shofner, M.L., K. Lozano, F.J. Rodríguez-Macías and E.V. Barrera, *Nanofiber-reinforced polymers prepared by fused deposition modeling.* Journal of Applied Polymer Science, 2003. **89**(11): p. 3081-3090.

61. Hector Sandoval, J. and R.B. Wicker, *Functionalizing stereolithography resins: effects of dispersed multi-walled carbon nanotubes on physical properties.* Rapid Prototyping Journal, 2006. **12**(5): p. 292-303.

62. Lin, D., S. Jin, F. Zhang, C. Wang, Y. Wang, C. Zhou and G.J. Cheng, *3D stereolithography printing of graphene oxide reinforced complex architectures.* Nanotechnology, 2015. **26**(43): p. 434003.

63. Weng, Z., J. Wang, T. Senthil and L. Wu, *Mechanical and thermal properties of ABS/montmorillonite nanocomposites for fused deposition modeling 3D printing.* Materials & Design, 2016. **102**: p. 276-283.

64. Srivastava, D., C. Wei and K. Cho, *Nanomechanics of carbon nanotubes and composites.* Applied Mechanics Reviews, 2003. **56**(2): p. 215-230.

65. Leamy, M.J., *Bulk dynamic response modeling of carbon nanotubes using an intrinsic finite element formulation incorporating interatomic potentials.* International Journal of Solids and Structures, 2007. **44**(3): p. 874-894.

66. Odegard, G.M. and T.S. Gates, *Modeling and Testing of the Viscoelastic Properties of a Graphite Nanoplatelet/Epoxy Composite.* Journal of Intelligent Material Systems and Structures, 2006. **17**(3): p. 239-246.

67. Voigt, W., *Ueber die Beziehung zwischen den beiden Elasticitätsconstanten isotroper Körper.* Annalen der Physik, 1889. **274**(12): p. 573-587.

68. Reuss, A., *Berechnung der Fließgrenze von Mischkristallen auf Grund der Plastizitätsbedingung für Einkristalle.* ZAMM - Journal of Applied Mathematics and Mechanics / Zeitschrift für Angewandte Mathematik und Mechanik, 1929. **9**(1): p. 49-58.

69. Hashin, Z. and S. Shtrikman, *A variational approach to the theory of the elastic behaviour of multiphase materials.* Journal of the Mechanics and Physics of Solids, 1963. **11**(2): p. 127-140.

70. Hashin, Z., *Analysis of Composite Materials—A Survey.* Journal of Applied Mechanics, 1983. **50**(3): p. 481-505.

71. Halpin, J.C. and K.M. Finlayson, *Primer on composite materials analysis, second edition revised*. 2017. 1-227.

72. Hill, R., *Theory of mechanical properties of fibre-strengthened materials: I. Elastic behaviour.* Journal of the Mechanics and Physics of Solids, 1964. **12**(4): p. 199-212.

73. Mori, T. and K. Tanaka, *Average stress in matrix and average elastic energy of materials with misfitting inclusions.* Acta Metallurgica, 1973. **21**(5): p. 571-574.

74. Eshelby, J.D. and R.E. Peierls, *The determination of the elastic field of an ellipsoidal inclusion, and related problems.* Proceedings of the Royal Society of London. Series A. Mathematical and Physical Sciences, 1957. **241**(1226): p. 376-396.

75. J. Broutman, L. and G. Panizza, *Micromechanics Studies of Rubber-reinforced Glassy Polymers*. Vol. 1. 1971. 95-109.

76. Agarwal, B.D. and L.J. Broutman, *Three-dimensional finite element analysis of spherical particle composites.* Fibre Science and Technology, 1974. **7**(1): p. 63-77.

77. Lee, B.J. and M.E. Mear, *Effect of inclusion shape on stiffness of isotropic and transversely isotropic two-phase composites.* International Journal of Solids and Structures, 1991. **28**(8): p. 975-1001.

78. Banks-Sills, L., V. Leiderman and D. Fang, *On the effect of particle shape and orientation on elastic properties of metal matrix composites.* Composites Part B: Engineering, 1997. **28**(4): p. 465-481.

79. Malagù, M., M. Goudarzi, A. Lyulin, E. Benvenuti and A. Simone, *Diameter-dependent elastic properties of carbon nanotube-polymer composites: Emergence of size effects from atomistic-scale simulations.* Composites Part B: Engineering, 2017. **131**: p. 260-281.

80. Arash, B., Q. Wang and V.K. Varadan, *Mechanical properties of carbon nanotube/polymer composites.* Scientific reports, 2014. **4**: p. 6479-6479.

81. Kaseem, G.A., *MICROMECHANICAL MATERIAL MODELS FOR POLYMER COMPOSITES THROUGH ADVANCED NUMERICAL SIMULATION TECHNIQUES*. 2009, RWTH Aachen University

82. Li, C. and T.-W. Chou, *Multiscale modeling of compressive behavior of carbon nanotube/polymer composites.* Composites Science and Technology, 2006. **66**(14): p. 2409-2414.

83. Hyer, M.W. and S.R. White, *Stress Analysis of Fiber-reinforced Composite Materials*. 2009: DEStech Publications, Incorporated.

84. Nemat-Nasser, S. and M. Hori, *Micromechanics: Overall Properties of Heterogeneous Materials*. 1999: Elsevier Science.

85. Zhang, J., Q. Ouyang, Q. Guo, Z. Li, G. Fan, Y. Su, L. Jiang, E.J. Lavernia, J.M. Schoenung and D. Zhang, *3D Microstructure-based finite element modeling of deformation and fracture of SiCp/Al composites.* Composites Science and Technology, 2016. **123**: p. 1-9.

86. Hua, Y., L. Gu and H. Watanabe, *Micromechanical analysis of nanoparticle-reinforced dental composites.* International Journal of Engineering Science, 2013. **69**: p. 69-76.

87. Hua, Y., L. Gu, S. Premaraj and X. Zhang, *Role of Interphase in the Mechanical Behavior of Silica/Epoxy Resin Nanocomposites.* Materials, 2015. **8**(6): p. 3519.

88. Optomec, *Aerosol Jet 5X System* 2016.

89. TWI. Available from: https://www.twi-global.com/media-and-events/insights/revolutionary-development-cuts-manufacturing-times-using-laser-metal-deposition-cuts-manufacturing-time.

90. Zhang, Y., M. Xi, S. Gao and L. Shi, *Characterization of laser direct deposited metallic parts.* Journal of Materials Processing Technology, 2003. **142**(2): p. 582-585.

91. Grutle, O.K., *5-Axis 3D Printer.* 2015.

92. Rafi, H.K., N.V. Karthik, H. Gong, T.L. Starr and B.E. Stucker, *Microstructures and Mechanical Properties of Ti6Al4V Parts Fabricated by Selective Laser Melting and Electron Beam Melting.* Journal of Materials Engineering and Performance, 2013. **22**(12): p. 3872-3883.

93. Frazier, W.E., *Metal Additive Manufacturing: A Review.* Journal of Materials Engineering and Performance, 2014. **23**(6): p. 1917-1928.

94. Zein, I., D.W. Hutmacher, K.C. Tan and S.H. Teoh, *Fused deposition modeling of novel scaffold architectures for tissue engineering applications.* Biomaterials, 2002. **23**(4): p. 1169-1185.

95. N Chia, H. and B. Wu, *Recent advances in 3D printing of biomaterials*. Vol. 9. 2015.

96. Abdelaal, O.A.M. and S.M.H. Darwish, *Review of Rapid Prototyping Techniques for Tissue Engineering Scaffolds Fabrication*, in *Characterization and Development of Biosystems and Biomaterials*, A. Öchsner, L.F.M. da Silva, and H. Altenbach, Editors. 2013, Springer Berlin Heidelberg: Berlin, Heidelberg. p. 33-54.

97. Chae, M.P., W.M. Rozen, P.G. McMenamin, M.W. Findlay, R.T. Spychal and D.J. Hunter-Smith, *Emerging Applications of Bedside 3D Printing in Plastic Surgery.* Front Surg, 2015. **2**: p. 25.

98. Rossiter, J., P. Walters and B. Stoimenov, *Printing 3D dielectric elastomer actuators for soft robotics*. 2009. 72870H-72870H.

99. Raviv, D., W. Zhao, C. McKnelly, A. Papadopoulou, A. Kadambi, B. Shi, S. Hirsch, D. Dikovsky, M. Zyracki, C. Olguin, R. Raskar and S. Tibbits, *Active Printed Materials for Complex Self-Evolving Deformations.* Scientific Reports, 2014. **4**: p. 7422.

100. Leong, K.F., C.M. Cheah and C.K. Chua, *Solid freeform fabrication of three-dimensional scaffolds for engineering replacement tissues and organs.* Biomaterials, 2003. **24**(13): p. 2363-2378.

101. Ladd, C., J.-H. So, J. Muth and M.D. Dickey, *3D Printing of Free Standing Liquid Metal Microstructures.* Advanced Materials, 2013. **25**(36): p. 5081-5085.

102. Engelke, R., G. Engelmann, G. Gruetzner, M. Heinrich, M. Kubenz and H. Mischke, *Complete 3D UV microfabrication technology on strongly sloping topography substrates using epoxy photoresist SU-8.* Microelectronic Engineering, 2004. **73-74**: p. 456-462.

103. Yamada, A., F. Niikura and K. Ikuta, *A three-dimensional microfabrication system for biodegradable polymers with high resolution and biocompatibility.* Journal of Micromechanics and Microengineering, 2008. **18**(2): p. 025035.

104. Vlasea, M. and E. Toyserkani, *Experimental characterization and numerical modeling of a micro-syringe deposition system for dispensing sacrificial photopolymers on particulate ceramic substrates.* Journal of Materials Processing Technology, 2013. **213**(11): p. 1970-1977.

105. Vozzi, G., A. Previti, D. De Rossi and A. Ahluwalia, *Microsyringe-based deposition of two-dimensional and three-dimensional polymer scaffolds with a well-defined geometry for application to tissue engineering.* Tissue Eng, 2002. **8**(6): p. 1089-98.

106. *Arduino Microcontroller* Available from: https://store.arduino.cc/usa/arduino-uno-rev3.

107. *Pronterface*. Available from: http://www.pronterface.com/.

108. *Thorlabs*. Available from: https://www.thorlabs.com/thorproduct.cfm?partnumber=DL5146-101S.

109. Zhang, Y., S. Ge, B. Tang, T. Koga, M. Rafailovich, J. Sokolov, D. G. Peiffer, Z. Li, A. Dias, K. O. McElrath, M.Y. Lin, S. K. Satija, S. Urquhart, H. Ade and D. Nguyen, *Effect of Carbon Black and Silica Fillers in Elastomer Blends*. Vol. 34. 2001.

110. *Fumed Silica Powder* Available from: https://www.reade.com/products/fumed-silica-powder-sio2.

111. *Sonics and Materials Inc Ultrasonic Homogenizer* Available from: https://www.sonics.com/.

112. Mahrholz, T., J. Stängle and M. Sinapius, *Quantitation of the reinforcement effect of silica nanoparticles in epoxy resins used in liquid composite moulding processes.* Composites Part A: Applied Science and Manufacturing, 2009. **40**(3): p. 235-243.

113. Liu, H.-Y., G.-T. Wang, Y.-W. Mai and Y. Zeng, *On fracture toughness of nano-particle modified epoxy.* Composites Part B: Engineering, 2011. **42**(8): p. 2170-2175.

114. Ahmad, F.N., M. Jaafar, S. Palaniandy and K.A.M. Azizli, *Effect of particle shape of silica mineral on the properties of epoxy composites.* Composites Science and Technology, 2008. **68**(2): p. 346-353.

115. Sun, S., C. Li, L. Zhang, H.L. Du and J.S. Burnell-Gray, *Effects of surface modification of fumed silica on interfacial structures and mechanical properties of poly(vinyl chloride) composites.* European Polymer Journal, 2006. **42**(7): p. 1643-1652.

116. Uddin, M.F. and C.T. Sun, *Strength of unidirectional glass/epoxy composite with silica nanoparticle-enhanced matrix.* Composites Science and Technology, 2008. **68**(7): p. 1637-1643.

117. Jiao, J., X. Sun and T.J. Pinnavaia, *Mesostructured silica for the reinforcement and toughening of rubbery and glassy epoxy polymers.* Polymer, 2009. **50**(4): p. 983-989.

118. Chen, C., R.S. Justice, D.W. Schaefer and J.W. Baur, *Highly dispersed nanosilica–epoxy resins with enhanced mechanical properties.* Polymer, 2008. **49**(17): p. 3805-3815.

119. Tsai, J.-L., H. Hsiao and Y.-L. Cheng, *Investigating Mechanical Behaviors of Silica Nanoparticle Reinforced Composites.* Journal of Composite Materials, 2010. **44**(4): p. 505-524.

120. Zhu, Z.-K., Y. Yang, J. Yin and Z.-N. Qi, *Preparation and properties of organosoluble polyimide/silica hybrid materials by sol–gel process.* Journal of Applied Polymer Science, 1999. **73**(14): p. 2977-2984.

121. Dekkers, M.E.J. and D. Heikens, *The effect of interfacial adhesion on the tensile behavior of polystyrene–glass-bead composites.* Journal of Applied Polymer Science, 1983. **28**(12): p. 3809-3815.

122. Fu, S.-Y. and B. Lauke, *Characterization of tensile behaviour of hybrid short glass fibre/calcite particle/ABS composites.* Composites Part A: Applied Science and Manufacturing, 1998. **29**(5): p. 575-583.

123. Fu, S.Y. and B. Lauke, *Analysis of mechanical properties of injection molded short glass fibre (SGF)/calcite/ABS composites*. Vol. 13. 1997. 389-396.

124. Eirich, F.R., *Some mechanical and molecular aspects of the performance of composites.* Applied polymer symposia, 1984. **39**(1): p. 93-102.

125. Radford, K.C., *The mechanical properties of an epoxy resin with a second phase dispersion.* Journal of Materials Science, 1971. **6**(10): p. 1286-1291.

126. Spanoudakis, J. and R.J. Young, *Crack propagation in a glass particle-filled epoxy resin.* Journal of Materials Science, 1984. **19**(2): p. 473-486.

127. Amdouni, N., H. Sautereau and J.-F. Gerard, *Epoxy composites based on glass beads. I. Viscoelastic properties*. Vol. 45. 1992. 1799-1810.

128. Wang, M., C. Berry, M. Braden and W. Bonfield, *Young's and shear moduli of ceramic particle filled polyethylene*. Vol. 9. 1998. 621-4.

129. Young, R.J. and P.W.R. Beaumont, *Failure of brittle polymers by slow crack growth.* Journal of Materials Science, 1977. **12**(4): p. 684-692.

130. Pukanszky, B. and G. VÖRÖS, *Mechanism of interfacial interactions in particulate filled composites*. Vol. 1. 1993.

131. Nakamura, Y., M. Yamaguchi, M. Okubo and T. Matsumoto, *Effects of particle size on mechanical and impact properties of epoxy resin filled with spherical silica.* Journal of Applied Polymer Science, 1992. **45**(7): p. 1281-1289.

132. Reynaud, E., T. Jouen, C. Gauthier, G. Vigier and J. Varlet, *Nanofillers in polymeric matrix: a study on silica reinforced PA6.* Polymer, 2001. **42**(21): p. 8759-8768.

133. Ou, Y., F. Yang and Z.-Z. Yu, *A new conception on the toughness of nylon 6/silica nanocomposite prepared via in situ polymerization.* Journal of Polymer Science Part B: Polymer Physics, 1998. **36**(5): p. 789-795.

134. Liang, J.Z., R.K.Y. Li and S.C. Tjong, *Tensile fracture behaviour and morphological analysis of glass bead filled low density polyethylene composites*. Vol. 26. 1997. 278-282.

135. Tjong, S.C. and S.A. Xu, *Ternary polymer composites: PA6,6/maleated SEBS/glass beads.* Journal of Applied Polymer Science, 2001. **81**(13): p. 3231-3237.

136. Danusso, F. and G. Tieghi, *Strength versus composition of rigid matrix particulate composites.* Polymer, 1986. **27**(9): p. 1385-1390.

137. Levita, G., A. Marchetti and A. Lazzeri, *Fracture of ultrafine calcium carbonate/polypropylene composites.* Polymer Composites, 1989. **10**(1): p. 39-43.

138. Nicolais, L. and M. Narkis, *Stress-strain behavior of styrene-acrylonitrile/glass bead composites in the glassy region*. Vol. 11. 1971. 194-199.

139. Moloney, A.C., H.H. Kausch, T. Kaiser and H.R. Beer, *Parameters determining the strength and toughness of particulate filled epoxide resins.* Journal of Materials Science, 1987. **22**(2): p. 381-393.

140. Spanoudakis, J. and R. J. Young, *Crack propagation in a glass particle-filled epoxy resin - Part 1 Effect of particle volume fraction and size*. Vol. 19. 1984. 473-486.

141. Broutman, L.J. and S. Sahu, *The effect of interfacial bonding on the toughness of glass filled polymers.* Materials Science and Engineering, 1971. **8**(2): p. 98-107.

142. C. Roulin-Moloney, A., W. J. Cantwell and H. Kausch, *Parameters determining the strength and toughness of particulate-filled epoxy resins*. Vol. 8. 1987. 314-323.

143. Jancar, J. and J. Kucera, *Yield behavior of polypropylene filled with CaCO3 and Mg(OH)2. I. 'Zero' interfacial adhesion*. Vol. 30. 2004. 707-713.

144. Jančář, J. and J. Kučera, *Yield behavior of PP/CaC03 and PP/Mg(OH)2 composites. II: Enhanced interfacial adhesion.* Polymer Engineering & Science, 1990. **30**(12): p. 714-720.

145. Collino, R.R., T.R. Ray, R.C. Fleming, J.D. Cornell, B.G. Compton and M.R. Begley, *Deposition of ordered two-phase materials using microfluidic print nozzles with acoustic focusing.* Extreme Mechanics Letters, 2016. **8**: p. 96-106.

146. Compton, B.G., N.S. Hmeidat, R.C. Pack, M.F. Heres and J.R. Sangoro, *Electrical and Mechanical Properties of 3D-Printed Graphene-Reinforced Epoxy.* JOM, 2018. **70**(3): p. 292-297.

147. Lewicki, J.P., J.N. Rodriguez, C. Zhu, M.A. Worsley, A.S. Wu, Y. Kanarska, J.D. Horn, E.B. Duoss, J.M. Ortega, W. Elmer, R. Hensleigh, R.A. Fellini and M.J. King, *3D-Printing of Meso-structurally Ordered Carbon Fiber/Polymer Composites with Unprecedented Orthotropic Physical Properties.* Scientific Reports, 2017. **7**: p. 43401.

148. Malek, S., J.R. Raney, J.A. Lewis and L.J. Gibson, *Lightweight 3D cellular composites inspired by balsa.* Bioinspiration & Biomimetics, 2017. **12**(2): p. 026014.

149. Fu, S.-Y., X.-Q. Feng, B. Lauke and Y.-W. Mai, *Effects of particle size, particle/matrix interface adhesion and particle loading on mechanical properties of particulate–polymer composites.* Composites Part B: Engineering, 2008. **39**(6): p. 933-961.

150. Kunori, T. and P.H. Geil, *Morphology-property relationships in polycarbonate-based blends. II. Tensile and impact strength.* Journal of Macromolecular Science, Part B, 1980. **18**(1): p. 135-175.

151. Demjén, Z., B. Pukánszky and J. Nagy, *Evaluation of interfacial interaction in polypropylene/surface treated CaCO3 composites.* Composites Part A: Applied Science and Manufacturing, 1998. **29**(3): p. 323-329.

152. Berketis, K., D. Tzetzis and P.J. Hogg, *The influence of long term water immersion ageing on impact damage behaviour and residual compression strength of glass fibre reinforced polymer (GFRP).* Materials & Design, 2008. **29**(7): p. 1300-1310.

153. Berketis, K., D. Tzetzis and P. Hogg, *Impact Damage Detection and Degradation Monitoring of Wet GFRP Composites Using Noncontact Ultrasonics*. Vol. 30. 2009. 1043-1049.

154. Berketis, K. and D. Tzetzis, *The compression-after-impact strength of woven and non-crimp fabric reinforced composites subjected to long-term water immersion ageing*. Vol. 45. 2010. 5611-5623.

155. Walley, S., J. Field, R. Pope and N. Safford, *The rapid deformation behaviour of various polymers.* Journal de Physique III, 1991. **1**(12): p. 1889-1925.

156. *A study of the rapid deformation behaviour of a range of polymers.* Philosophical Transactions of the Royal Society of London. Series A,

Mathematical and Physical Sciences, 1989. **328**(1597): p. 1-33.

157. Walley, S.M. and J.E. Field, *Strain rate sensitivity of polymers in compression from low to high rates*. Vol. 1. 1994. 211-227.

158. Khan, K.A., H. Wafai and T.E. Sayed, *A variational constitutive framework for the nonlinear viscoelastic response of a dielectric elastomer.* Computational Mechanics, 2013. **52**(2): p. 345-360.

159. Rae, P.J. and D.M. Dattelbaum, *The Properties of Poly(tetrauoroethylene) (PTFE) in Compression*. Vol. 2035. 2004.

160. Brown, E.N., P.J. Rae and E.B. Orler, *The influence of temperature and strain rate on the constitutive and damage responses of polychlorotrifluoroethylene (PCTFE, Kel-F 81).* Polymer, 2006. **47**(21): p. 7506-7518.

161. Brown, E.N., P.J. Rae, E. Bruce Orler, G.T. Gray and D.M. Dattelbaum, *The effect of crystallinity on the fracture of polytetrafluoroethylene (PTFE).* Materials Science and Engineering: C, 2006. **26**(8): p. 1338-1343.

162. Brown, E.N., C.P. Trujillo, G.T.G. III, P.J. Rae and N.K. Bourne, *Soft recovery of polytetrafluoroethylene shocked through the crystalline phase II-III transition.* Journal of Applied Physics, 2007. **101**(2): p. 024916.

163. Rae, P.J. and E. Brown, *The Properties of Poly(tetrauoroethylene) (PTFE) in Tension*. Vol. 46. 2005. 8128-8140.

164. Rae, P.J., E.N. Brown, B.E. Clements and D.M. Dattelbaum, *Pressure-induced phase change in poly(tetrafluoroethylene) at modest impact velocities.* Journal of Applied Physics, 2005. **98**(6): p. 063521.

165. Bourne, N.K., E.N. Brown, J.C.F. Millett and G.T.G. III, *Shock, release and Taylor impact of the semicrystalline thermoplastic polytetrafluoroethylene.* Journal of Applied Physics, 2008. **103**(7): p. 074902.

166. Halpin, J.C. and J.L. Kardos, *The Halpin-Tsai equations: A review*. Vol. 16. 1976. 344-352.

167. Khan, K.A. and A.H. Muliana, *Effective thermal properties of viscoelastic composites having field-dependent constituent properties.* Acta Mechanica, 2009. **209**(1): p. 153.

168. Bondioli, F., V. Cannillo, E. Fabbri and M. Messori, *Epoxy-silica nanocomposites: Preparation, experimental characterization, and modeling*. Vol. 97. 2005. 2382-2386.

169. Cannillo, V., F. Bondioli, L. Lusvarghi, M. Monia, M. Avella, M. Errico and M. Malinconico, *Modeling of ceramic particles filled polymer–matrix nanocomposites*. Vol. 66. 2006. 1030-1037.

170. Saber-Samandari, S. and A. Khatibi, *Evaluation of elastic modulus of polymer matrix nanocomposites*. Vol. 28. 2007. 405-411.

171. Smith, J.S., D. Bedrov and G.D. Smith, *A molecular dynamics simulation study of nanoparticle interactions in a model polymer-nanoparticle composite.* Composites Science and Technology, 2003. **63**(11): p. 1599-1605.

172. Odegard, G.M., T.C. Clancy and T.S. Gates, *Modeling of the mechanical properties of nanoparticle/polymer composites.* Polymer, 2005. **46**(2): p. 553-562.

173. Green, A.E., R.S. Rivlin and A.J.M. Spencer, *The Mechanics of Non-Linear Materials with Memory*, in *Collected Papers of R.S. Rivlin: Volume I and II*, G.I. Barenblatt and D.D. Joseph, Editors. 1997, Springer New York: New York, NY. p. 1127-1136.

174. Coleman, B.D. and W. Noll, *Foundations of Linear Viscoelasticity.* Reviews of Modern Physics, 1961. **33**(2): p. 239-249.

175. Pipkin, A.C. and T.G. Rogers, *A non-linear integral representation for viscoelastic behaviour.* Journal of the Mechanics and Physics of Solids, 1968. **16**(1): p. 59-72.

176. Schapery, R.A., *On the characterization of nonlinear viscoelastic materials.* Polymer Engineering & Science, 1969. **9**(4): p. 295-310.

177. Fung, Y.-C., *Biomechanics Mechanical Properties of Living Tissues*, ed. Second. 1993, New York: Springer.

178. Dai, F., K.R. Rajagopal and A.S. Wineman, *Non-uniform extension of a non-linear viscoelastic slab.* International Journal of Solids and Structures, 1992. **29**(7): p. 911-930.

179. Johnson, G.A., G.A. Livesay, S.L. Woo and K.R. Rajagopal, *A single integral finite strain viscoelastic model of ligaments and tendons.* J Biomech Eng, 1996. **118**(2): p. 221-6.

180. Puso, M.A. and J.A. Weiss, *Finite element implementation of anisotropic quasi-linear viscoelasticity using a discrete spectrum approximation.* J Biomech Eng, 1998. **120**(1): p. 62-70.

181. Muliana, A., K. R. Rajagopal and A. S. Wineman, *A new class of quasi-linear models for describing the nonlinear viscoelastic response of materials*. Vol. 224. 2013.

182. Muliana, A., K.R. Rajagopal and D. Tscharnuter, *A Nonlinear Integral Model for Describing Responses of Viscoelastic Solids*. Vol. 58. 2015.

183. Yuan, Z., A. Muliana and K. Ramamani Rajagopal, *Modeling the response of light-activated shape memory polymers*. Vol. 22. 2016.

184. Abramowitch, S.D., S.L.-Y. Woo, T.D. Clineff and R.E. Debski, *An Evaluation of the Quasi-Linear Viscoelastic Properties of the Healing Medial Collateral Ligament in a Goat Model.* Annals of Biomedical Engineering, 2004. **32**(3): p. 329-335.

185. Suchocki, C., *A quasi-linear viscoelastic rheological model for thermoplastics and resins*. Vol. 51. 2013. 117-129.

186. Slesarenko, V. and S. Rudykh, *Towards mechanical characterization of soft digital materials for multimaterial 3D-printing.* International Journal of Engineering Science, 2018. **123**: p. 62-72.

187. Hussein, M., *Effects of strain rate and temperature on the mechanical behavior of carbon black reinforced elastomers based on butyl rubber and high molecular weight polyethylene.* Results in Physics, 2018. **9**: p. 511-517.

188. Yang, B.J., B.R. Kim and H.K. Lee, *Predictions of viscoelastic strain rate dependent behavior of fiber-reinforced polymeric composites.* Composite Structures, 2012. **94**(4): p. 1420-1429.

189. Dittanet, P. and R.A. Pearson, *Effect of silica nanoparticle size on toughening mechanisms of filled epoxy.* Polymer, 2012. **53**(9): p. 1890-1905.

190. Hsieh, T.H., A.J. Kinloch, K. Masania, A.C. Taylor and S. Sprenger, *The mechanisms and mechanics of the toughening of epoxy polymers modified with silica nanoparticles.* Polymer, 2010. **51**(26): p. 6284-6294.

191. Hsieh, T.H., A.J. Kinloch, K. Masania, J. Sohn Lee, A.C. Taylor and S. Sprenger, *The toughness of epoxy polymers and fibre composites modified with rubber microparticles and silica nanoparticles.* Journal of Materials Science, 2010. **45**(5): p. 1193-1210.

192. De Pascalis, R., I.D. Abrahams and W.J. Parnell, *On nonlinear viscoelastic deformations: a reappraisal of Fung's quasi-linear viscoelastic model.* Proceedings of the Royal Society A: Mathematical, Physical and Engineering Science, 2014. **470**(2166).

193. Yeoh, O.H., *Some Forms of the Strain Energy Function for Rubber.* Rubber Chemistry and Technology, 1993. **66**(5): p. 754-771.

194. Oberdisse, J., *Aggregation of colloidal nanoparticles in polymer matrices.* Soft Matter, 2006. **2**(1): p. 29-36.

195. Li, D. and R.B. Kaner, *How nucleation affects the aggregation of nanoparticles.* Journal of Materials Chemistry, 2007. **17**(22): p. 2279-2282.

196. Zhang, Q., M. Tian, Y. Wu, G. Lin and L. Zhang, *Effect of particle size on the properties of Mg(OH)2-filled rubber composites.* Journal of Applied Polymer Science, 2004. **94**(6): p. 2341-2346.

197. Lazzeri, A., Y.S. Thio and R.E. Cohen, *Volume strain measurements on CACO3/polypropylene particulate composites: The effect of particle size.* Journal of Applied Polymer Science, 2004. **91**(2): p. 925-935.

198. Nakamura, Y., M. Yamaguchi, M. Okubo and T. Matsumoto, *Effect of particle size on mechanical properties of epoxy resin filled with angular-shaped silica.* Journal of Applied Polymer Science, 1992. **44**(1): p. 151-158.

199. Ling Ji, X., J. Kai Jing, W. Jiang and B. Zheng Jiang, *Tensile modulus of polymer nanocomposites*. Vol. 42. 2002. 983-993.

200. Mishra, S., S.H. Sonawane and R.P. Singh, *Studies on characterization of nano CaCO3 prepared by the in situ deposition technique and its application in PP-nano CaCO3 composites.* Journal of Polymer Science Part B: Polymer Physics, 2005. **43**(1): p. 107-113.

201. Schmidt, D., D. Shah and E.P. Giannelis, *New advances in polymer/layered silicate nanocomposites.* Current Opinion in Solid State and Materials Science, 2002. **6**(3): p. 205-212.

202. Wetzel, B., F. Haupert and M.Q. Zhang, *Epoxy nanocomposites with high mechanical and tribological performance.* Composites Science and Technology, 2003. **63**(14): p. 2055-2067.

203. Wang, H., Y. Bai, S. Liu, J. Wu and C.P. Wong, *Combined effects of silica filler and its interface in epoxy resin.* Acta Materialia, 2002. **50**(17): p. 4369-4377.

204. Katti, D.R., K.S. Katti, J.M. Sopp and M. Sarikaya, *3D finite element modeling of mechanical response in nacre-based hybrid nanocomposites.* Computational and Theoretical Polymer Science, 2001. **11**(5): p. 397-404.

205. Wang, X.Y. and X. Wang, *Numerical simulation for bending modulus of carbon nanotubes and some explanations for experiment.* Composites Part B: Engineering, 2004. **35**(2): p. 79-86.

206. Wang, Y., C. Sun, X. Sun, J. Hinkley, G.M. Odegard and T.S. Gates, *2-D nano-scale finite element analysis of a polymer field.* Composites Science and Technology, 2003. **63**(11): p. 1581-1590.

207. *Digimat - muli-scale material modelling platform* Available from: https://www.e-xstream.com/products/digimat/about-digimat.

208. Widom, B., *Random Sequential Addition of Hard Spheres to a Volume.* The Journal of Chemical Physics, 1966. **44**(10): p. 3888-3894.

209. Sasso, M., G. Palmieri, G. Chiappini and D. Amodio, *Characterization of hyperelastic rubber-like materials by biaxial and uniaxial stretching tests based on optical methods.* Polymer Testing, 2008. **27**(8): p. 995-1004.

210. Charlton, D.J., J. Yang and K.K. Teh, *A Review of Methods to Characterize Rubber Elastic Behavior for Use in Finite Element Analysis.* Rubber Chemistry and Technology, 1994. **67**(3): p. 481-503.

211. Yeoh, O.H., *Some benchmark problems for FEA from torsional behavior of rubber.* Rubber Chemistry and Technology, 2003. **76**(5): p. 1212-1227.

212. Mohan, C.V.R., J. Ramanathan, S. Kumar and A.V.S.S.K.S. Gupta, *Characterisation of materials used in flex bearings of large solid rocket motors.* Defence Science Journal, 2011. **61**(3): p. 264-269.